UNIVERSITÀ DEGLI STUDI DI PALERMO

DEPARTMENT OF ENERGY, INFORMATION TECHNOLOGY ENGINEERING AND MATHEMATICAL MODELING

PHD COURSE IN: Electric, Electronic and Telecommunication Engineering, Mathematics and Automation

SPECIALISM IN: Mathematics and automation for scientific and technological innovation

S.S.D. ***ING-INF/04***

Innovative Observers for Induction Motor Control

Phd Candidate

Ing. Tonino Scaffidi

TUTOR

Prof. Filippo D'Ippolito

PhD Course Coordinator

Prof. Francesco Alonge

XXV CYCLE OF STUDY - YEAR 2015

DOTTORATO

to my parents

Acknowledgment

Sometimes in our life we have to deal with difficult moments, when all values seem to vacillate and does not seem to find the solution. The difference is made by someone who love you. My special thanks to: my tutor prof. Filippo d'Ippolito, prof. Francesco Alonge, ing. Antonino Sferlazza, prof. Adriano Fagiolini, who made the difference in a bad period of my life. This work wouldn't have existed without them.

colophon
made with LaTeX 2ε e BibTeX.

Contents

List of Figures

List of Tables

Introduction

Maximum efficiency asynchronous motor control

0.1 preface

This work aims to evaluate the dynamic performance of state rotor observers applied to a control system for rotary asynchronous motor.

The huge amount of induction motors installed in industrial field, the continuous improvement of the cost or the instruction cycle of modern microcontroller and DSP and the increasingly reduced dimensions of the IGBT power inverter, has allowed designers to improve the quality of the control system realized, together with a decrease in the cost of implementation.

The evolution of the field oriented control (FOC) and the development of hybrid control systems have resulted in units reliable and high-performance AC, which have been conveniently employed in applications which, previously, were domain DC. It seems natural to use this technique with modules AC controlled conveniently in automotive.

The type of drives controlled by inverters suffered, over time, constant but radical changes. The latest developments of the construction technique of induction machines drives led to the creation of voltage source inverter (VSI) and generation mode of the control variables, realized in PWM mode. The devices of IGBT power (*Insulated Gate Bipolar Transistor*) achieved by switching speed comprised between 5 and 10 $kV/\mu sec$. In this way today it is possible to realize a control system with carrier frequency higher than the audible band.

This work deals with the problem of choosing the model of the observer of the rotor state evaluating the performance of various types, pointing out strengths and weaknesses of each.

These evaluations will be supported by experimental evidence.

0.2 Object

While dealing with the development of this work are going to design a control system for a drive of asynchronous machines that uses a voltage source inverter and necessary to generate the currents and voltages which carry the drive by making use of an observer from the state rotor.

Such observer of the status rotor can be designed according to various theoretical results that have been made over the years. Each of these studies has solved various problems and exacerbated some side effects that affect the problem, because the system to control is non-linear.

In the present work we used reduced, stochastic, sliding and deterministic observer through the Luenberger and Kalman techniques. The result is the development of control algorithms, which maximize the performance in the various load conditions.

0.3 Control Mode

Various control algorithms were taken into account, such as *field oriented control* (FOC) and *direct torque control* is with *switching table* (ST-DTC) that with *vector modulation* (SVM-DTC).

All three control techniques are based on a suitable decoupling of the components of flux and torque, according to a rotating reference system, of the stator current in such a way that a component acting solely on the flow of the rotor, while the other is proportional to the torque generated.

This can be achieved by orienting the axes of reference according to the direction of the field rotor and, in particular, by choosing the direction of the direct axis (d axis) which coincides with that of the representative vector of the rotor flux and the direction of the axis in quadrature (axis q) orthogonal to the axis and directed in advance.

By means of the decoupling between the effects of the two components of the stator current the control of mechanical variables of the drive is simplified and it can, thus, realize a closed-chain control of the rotor flux.

Initially both ST-DTC and DTC-SVM controls were realized.

Both gave he best results with respect to the FOC as regards the dynamics corresponding to both flow variations and torque, but showed considerable drawbacks in the operation at low speeds. It was therefore established to use the FOC because the dynamic requirements are not so as stringent in practical applications.

However, what is important in the field of application is the conversion efficiency from electrical to mechanical energy. This is obtained by regulating the flow in function of the required torque, the voltage of DC bus and the actual speed.

This adjustment takes place through the implementation of some algorithms that will be used in the control system.

0.4 Model of the asynchronous motor

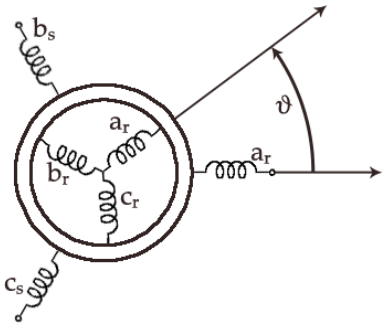

Figure 1: *Electric Diagram of a Induction Motor*

The three-phase asynchronous electric motor is structurally very simple.

This actuation is realized by a fixed part, the stator, and by a mobile part, the rotor. The stator is constituted by a stack of laminations in the shape of a circular crown. The conductors (enamelled copper wire) stator winding phase or two-phase stator (in the case of using single phase alternating current) are collected in the grooves inside the pack of stator laminations.

The rotor is constructed in order to allow the circulation of induced current. The simplest and most robust rotor is realized by inserting in the channels as many bars die-cast of copper or aluminum, each of which fills a channel completely. The heads of the bars protruding from the lamellar pack are directly connected to each other, on both sides, by means of a big ring of copper. The rotor thus constructed is indicated with the name of "rotor squirrel

cage" or "short circuit rotor" (these engines owe their name to the similarity of the rotor to the wheels present in the cages for squirrels and where they are used to run).

These engines are widely used in industry because they are reliable and economic.

The three-phase asynchronous electric motor is constituted by two circuits, one fixed to the stator, and the other, with induced currents, rotating with the rotor. They are electrically separate, and magnetically coupled (cfr. fig. 1); the rotor is usually a squirrel cage.

In this work, will be taken into account the electromechanical model of the asynchronous engine.

By means of coordinate transformations it is possible to simplify the discussion, as far as the study of the induction motor is regarded.

They are the Clark and Park transform.

The Clarke transform modifies a three-phase system (x_a, x_b, x_c) into a two-phase orthogonal system (x_α, x_β).

Assuming the homopolar component equal to zero:

$$x_a + x_b + x_c = 0 \tag{0.4.1}$$

the Clarke transform results to be given by:

$$\begin{cases} x_\alpha = x_a \\ x_\beta = \dfrac{1}{\sqrt{3}} x_a + \dfrac{2}{\sqrt{3}} x_b \end{cases} \tag{0.4.2}$$

With reference to the system of orthogonal axes ($alpha,\ beta$) integral with the stator, the mathematical model that describes the induction motor is transformed into the following:

$$\frac{d}{dt} i_\alpha = -\mathrm{a}_{11} i_\alpha + \frac{1}{\mathrm{L_e}} \left(\frac{1}{\mathrm{T_r}} \hat{\varphi}_\alpha + \omega\, \hat{\varphi}_\beta \right) + \frac{1}{\mathrm{L_e}} v_\alpha \tag{0.4.3}$$

$$\frac{d}{dt} i_\beta = -\mathrm{a}_{11} i_\beta + \frac{1}{\mathrm{L_e}} \left(\frac{1}{\mathrm{T_r}} \hat{\varphi}_\beta - \omega\, \hat{\varphi}_\alpha \right) + \frac{1}{\mathrm{L_e}} v_\beta \tag{0.4.4}$$

$$\frac{d}{dt} \hat{\varphi}_\alpha = \mathrm{a}_{31} i_\alpha - \frac{1}{\mathrm{T_r}} \hat{\varphi}_\alpha - \omega \hat{\varphi}_\beta \tag{0.4.5}$$

$$\frac{d}{dt}\hat{\varphi}_\beta = \mathrm{a}_{31} i_\beta - \frac{1}{\mathrm{T_r}}\hat{\varphi}_\beta + \omega\hat{\varphi}_\alpha \tag{0.4.6}$$

$$\frac{d}{dt}\omega = -a_w\omega + K_m\left(i_\beta\hat{\varphi}_\alpha - i_\alpha\hat{\varphi}_\beta\right) - b_m c_d - \frac{1}{T_c}\mathrm{sgn}\left(\omega\right) \tag{0.4.7}$$

$$c_m = pK_m\left(i_\beta\hat{\varphi}_\alpha - i_\alpha\hat{\varphi}_\beta\right) \tag{0.4.8}$$

considering the parameters listed in Table 1 and in Table 2.

$R_s(L_s)$	: stator resistance (inductance);
L_e	: equivalent stator inductance;
T_r	: rotor time constant;
J	: inertia moment;
p	: number of pole pairs;
F	: coefficient of viscous friction;
c_d	: torque disturbance;
c_m	: torque;
f_c	: coefficient of coulomb friction;
$\hat{\varphi}_\beta = \frac{L_m}{L_r}\varphi_\beta$	: component of the flow vector scaled along the axis β;
$\hat{\varphi}_\alpha = \frac{L_m}{L_r}\varphi_\alpha$	: component of the flow vector scaled along the axis α;
$i_\alpha(i_\beta)$	: stator current referred to axis $\alpha(\beta)$;
$v_\alpha(v_\beta)$	: stator tension referred to axis $\alpha(\beta)$;

Table 1: *Electric Parameter of a Induction Motor*

$a_{11} = \frac{1}{L_e}\left(R_s + \frac{L_s - L_e}{T_r}\right)$	$a_w = \frac{F}{J}$	$T_r = \frac{L_r}{R_r}$
$b_m = \frac{p}{J}$	$a_{33} = \frac{1}{T_r}$	
$a_{31} = \frac{L_s - L_e}{T_r}$	$K_m = \frac{2p^2}{3J}$	$a_{13} = \frac{1}{T_r L_e}$

Table 2: *Minimum Parameters Identifiable of a Induction Motor Model*

Considering now a two-phase orthogonal reference system (d, q) that rotates with respect to the system (α, β) previously described with an angular velocity $\dot{\rho}$, the components x_α and x_β projecting q axis using the following Park transform:

$$\begin{cases} x_d = x_\alpha \cos\rho + x_\beta \sin\rho \\ x_q = -x_\alpha \sin\rho + x_\beta \cos\rho \end{cases} \tag{0.4.9}$$

The model of the induction motor disclosed above, can then be reported to the system dq by applying to electrical values expressed in the axes $\alpha - \beta$ the Park's transformation (see. Eq. 0.4.2).

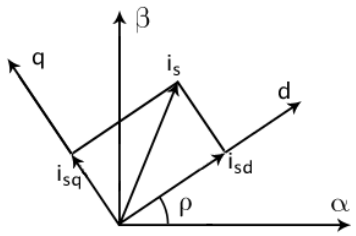

Figure 2: *System of axes fixed $\alpha - \beta$ and rotary $d - q$.*

0.5 Steinmetz equivalent electrical circuit

The relationships between time, current, voltage, speed, power factor and torque can be obtained from analysis of the Steinmetz equivalent circuit. From this equivalent electrical circuit (also termed T-equivalent circuit or IEEE recommended equivalent circuit) is possible to derive a mathematical model used to describe how an induction motor's electrical input is transformed into useful mechanical energy output. The equivalent circuit is a single-phase representation of a multiphase induction motor that is valid in steady-state balanced-load conditions.

The Steinmetz equivalent circuit is expressed in terms of the Stator Resistance and the Leakage Reactance (R_s, X_s), the Rotor Resistance, the Leakage Reactance,the slip frequency (R_r, X_r, $X_{r'}$, and ω_s) and the Magnetizing Reactance (X_m).

An induction motor we can compare with an electrical transformer. The magnetic circuit is separated by an air gap between the stator winding and the moving rotor winding. The equivalent circuit can accordingly be shown either with equivalent circuit components of

respective windings separated by an ideal transformer or with rotor components referred to the stator side.

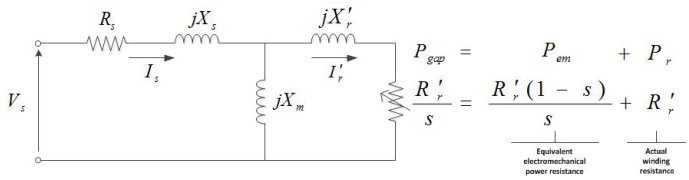

Figure 3: *Steinmetz Equivalent Magnetic - Electric Circuit of a Induction Motor*

0.6 State Model of Asynchronous Motor

The formulation of the mathematical model of the induction motor, in the $d-q$ representation, may be given, in the form of the state vector, as follows:

$$\mathbf{x} = \begin{bmatrix} i_{ds} & i_{qs} & \phi_{dr} & \phi_{qr} \end{bmatrix}^{\mathbf{T}} \tag{0.6.1}$$

The system has, as input variables, the projections of the supply voltage vector v_s on the axes $d-q$. The value of this projection is given by:

$$\mathbf{u} = \begin{bmatrix} v_{ds} & v_{qs} \end{bmatrix} \tag{0.6.2}$$

and the slip frequency is given by the difference between the synchronous speed and the angular speed:

$$u_3 = \omega_s = \omega_a - \omega \tag{0.6.3}$$

The torque produced by the motor is given by a non-linear relationship between the projections of the stator current and the rotor flux along the axes d and q. For high power motors, for which the criterion of minimum energy consumption is important, the variations of the mechanical speed is sufficiently slow compared to the electrical variations during transient torque, and therefore it can be considered that the speed of the motor is constant with respect to the components of the state vector. Assuming ω as constant, the model can be reformulated in the form of state as follows:

$$\begin{cases} \dot{\mathbf{x}} = [\mathbf{A} + \mathbf{G}u_3]\mathbf{x} + \mathbf{B}\mathbf{u} \\ y = h(\mathbf{x}) = p(x_2x_3 - x_1x_4) \end{cases} \tag{0.6.4}$$

where:

$$\mathbf{A} = \begin{pmatrix} -(\alpha+\beta) & \omega & \frac{\beta}{L_S} & \frac{\omega}{\sigma L_S} \\ -\omega & -(\alpha+\beta) & \frac{-\omega}{\sigma L_S} & \frac{\beta}{L_S} \\ -a_{31} & 0 & 0 & \omega \\ 0 & -a_{31} & -\omega & 0 \end{pmatrix}$$

$$\mathbf{B} = \begin{pmatrix} \frac{1}{\sigma L_s} & 0 \\ 0 & \frac{1}{\sigma L_s} \\ 0 & 0 \\ 0 & 0 \end{pmatrix} \tag{0.6.5}$$

$$\mathbf{G} = \begin{pmatrix} 0 & 1 & 0 & 0 \\ -1 & 0 & 0 & 0 \\ 0 & 0 & 0 & 1 \\ 0 & 0 & -1 & 0 \end{pmatrix}$$

having established that:

$$\alpha = \frac{R_s}{\sigma L_s}, \beta = \frac{R_r}{\sigma L_r}, \sigma = 1 - \frac{M^2}{L_s L_r}$$

0.7 Matematical Model of the Asynchronous Motor

If we don't take into consideration (as it usually done) the losses in the iron, the saturation of the electromagnetic circuits and the anisotropy of the geometrical structure. If we consider the changes in resistance of the rotor and stator, the mathematical model of the electromagnetic circuit of the induction motor, reported (α, β) axes, fixed the stator, is described by the following equations (cfr. [38]):

$$\dot{\mathbf{x}} = \mathbf{A}(\omega)\mathbf{x} + \mathbf{Bm} + \mathbf{Gd} \tag{0.7.1}$$

where:

$$\mathbf{x} = \begin{bmatrix} \mathbf{x}_1 & \mathbf{x}_2 \end{bmatrix}^{\mathrm{T}}, \quad \mathbf{x}_1 = \begin{bmatrix} i_a & i_b \end{bmatrix}^{\mathrm{T}}, \quad \mathbf{x}_2 = \begin{bmatrix} \hat{\phi}_a & \hat{\phi}_b \end{bmatrix}^{\mathrm{T}},$$

$$\mathbf{m} = \begin{bmatrix} m_a & m_b \end{bmatrix}^{\mathrm{T}}, \quad \mathbf{d} = \begin{bmatrix} d_1 & d_2 & d_3 & d_4 \end{bmatrix}^{\mathrm{T}},$$

$$d_1 = c_1\delta_s i_a, \quad d_2 = c_1\delta_s i_b, \quad d_3 = \frac{\hat{\phi}_a}{\delta_{\tau r} L_e}, \quad d_4 = \frac{\hat{\phi}_{\omega b}}{\delta_{\tau r} L_e}$$

$$\mathbf{A}(\omega) = \begin{bmatrix} \mathbf{A}_{11} & \mathbf{A}_{12} \\ \mathbf{A}_{21} & \mathbf{A}_{22} \end{bmatrix}, \quad \mathbf{B} = \begin{bmatrix} c_1\mathbf{I} \\ 0 \end{bmatrix}, \quad \mathbf{G} = \begin{bmatrix} -\mathbf{I} & -\mathbf{I} \\ 0 & l\mathbf{I} \end{bmatrix}$$

$$\mathbf{A}_{11} = -a_{11}\mathbf{I}, \quad \mathbf{A}_{12} = a_{13}\mathbf{I} - c_1\omega\mathbf{J}, \quad \mathbf{A}_{21} = a_{31}\mathbf{I}, \quad \mathbf{A}_{22} = -a_{33}\mathbf{I} + \omega\mathbf{J} \tag{0.7.2}$$

$$l = \frac{1}{c_1}, \quad \mathrm{c}_1 = \frac{1}{L_e},$$

$$\mathrm{a}_{11} = \frac{1}{L_e}\left(R_s + \frac{L_s - L_e}{\tau_r}\right), \quad \mathrm{a}_{13} = \frac{1}{\tau_r L_e}, \quad \mathrm{a}_{31} = \frac{L_s - L_e}{\tau_r}, \quad \mathrm{a}_{33} = \frac{1}{\tau_r}$$

$$\mathbf{I} = \begin{bmatrix} 1 & 0 \\ 0 & 1 \end{bmatrix}, \mathbf{J} = \begin{bmatrix} 0 & -1 \\ 1 & 0 \end{bmatrix}$$

where $\hat{\phi}_a$ and $\hat{\phi}_b$ are the components of the vector of rotor flux scaled according to the equation $\hat{\phi} = \frac{L_m}{L_r}\phi$ having ϕ the flux vector of the rotor, while δ_s and δ_r are, respectively, the changes of the rotor and stator resistance, $\delta_{\tau r} = \frac{L_r}{\delta_r}$. It is convenient to note that $\mathbf{d}$ is a perturbation due solely to variations in the rotor and stator resistance.

The problem, now, is to estimate the rotor flux vector of scaled $\mathbf{x}_2$ this is effected by means of a reduced order observer. For this purpose, you can notice that the velocity ω varies

slowly compared to the electromagnetic variables and consequently it can be considered as an additional input.

For this reason we do not consider the equation for the mechanical design of the observer. In this case the mathematical model of the electromagnetic circuit of the motor (0.7.1) can be considered as a bilinear model. It follows that the bilinear and low order observers of the components of the rotor flux can be designed according to the methods Hara and Furuta ([38]) or Funahashi ([31]).

With the aim of simplifying the formulation of the model (0.7.1), we can take advantage of the symmetries of the model. Let us define the following complex state and input vectors:

$$\mathbf{x} = (\mathbf{x}_1, \mathbf{x}_2, \mathbf{x}_3)^T = (\mathbf{i}_{s,\alpha} + j\,\mathbf{i}_{s,\beta},\, \psi_{r,\alpha} + j\,\psi_{r,\beta},\, \omega)^T\,, \tag{0.7.3}$$

and

$$\mathbf{u} = \mathbf{u}_{s,\alpha} + j\,\mathbf{u}_{s,\beta}\,, \tag{0.7.4}$$

where j is the imaginary unit. Then, in terms of the new complex state variables, choosing (0.7.3) as complex state vector and (0.7.4) as complex input vector, the dynamic model (0.7.1) is:

$$\dot{x}_1 = -a_{11}\,x_1 + f_1\,(a_{22} - j\,x_3)\;x_2 + f_1\,u\,, \tag{0.7.5}$$

$$\dot{x}_2 = a_{21}\,x_1 - (a_{22} - j\,x_3)\;x_2\,, \tag{0.7.6}$$

$$\dot{x}_3 = -a_{33}x_3 + f_3\Im[x_1\bar{x}_2] - g_5 t_l\,, \tag{0.7.7}$$

0.7.1 Discrete time mathematical model

A discrete-time model corresponding to (0.7.1) can be obtained by using a first order Euler discretization. By choosing the stator current components as the system output, the discrete-time model is given by:

$$\begin{aligned} \mathbf{x}_{k+1} &= \mathbf{A}_d\,\mathbf{x}_k + \mathbf{f}_d(\mathbf{x}_k) + \mathbf{B}_d\,\mathbf{u}_{s,k}\,, \\ \mathbf{y}_k &= \mathbf{C}_d x_k\,, \end{aligned} \tag{0.7.8}$$

where matrices $\mathbf{A}_d$, $\mathbf{B}_d$, $\mathbf{C}_d$ and vector field $\mathbf{f}_d(\mathbf{x}_k)$ are:

$$\begin{aligned} \mathbf{A}_d = (\mathbf{I}_6 + T_s\,\mathbf{A}_c)\,, \quad \mathbf{f}_d(\mathbf{x}_k) = T_s\,\mathbf{f}_c(\mathbf{x}_k)\,, \\ B_d = T_s\,B_c\,, \quad \mathbf{C}_d = (\mathbf{I}_2, 0_{2\times 3}). \end{aligned} \tag{0.7.9}$$

T_s is the sampling time, and matrices $\mathbf{A}_c$, $\mathbf{B}_c$ and vector field $\mathbf{f}_c$ are defined in (0.6.5). An equivalent complex model is obtained by applying the first-order Euler approximation to the continuous-time dynamics:

$$\begin{aligned} x_1(k+1) &= \tilde{a}_{11}\,x_1(k) + \tilde{f}_1\,(a_{22} - j\,x_3(k))\,x_2(k) + \tilde{f}_1\,u(k)\,, \\ x_2(k+1) &= \tilde{a}_{21}\,x_1(k) + (1 - T_s\,(a_{22} - j\,x_3(k)))\,x_2(k)\,, \\ x_3(k+1) &= x_3(k)\,, \end{aligned} \tag{0.7.10}$$

where:

$$\tilde{a}_{11} = 1 - a_{11}\,T_s\,, \tilde{f}_1 = f_1\,T_s\,, \tilde{a}_{21} = a_{21}\,T_s\,,$$

where $\tilde{a}_{11} = 1 - a_{11}\,T_s$, $\tilde{f}_1 = f_1\,T_s$, $\tilde{a}_{21} = a_{21}\,T_s$, with system output given by:

$$y(k) = h(x(k)) = x_1(k)\,.$$

0.8 Complete scheme of the control system

The diagram of the control system is shown in Figure 2.1. The proposed scheme is FOC (field-oriented control) in which the control variable is the torque. Moreover, the limitation of the voltage and the references of flux and torque are established in function of the bus-bar voltage.

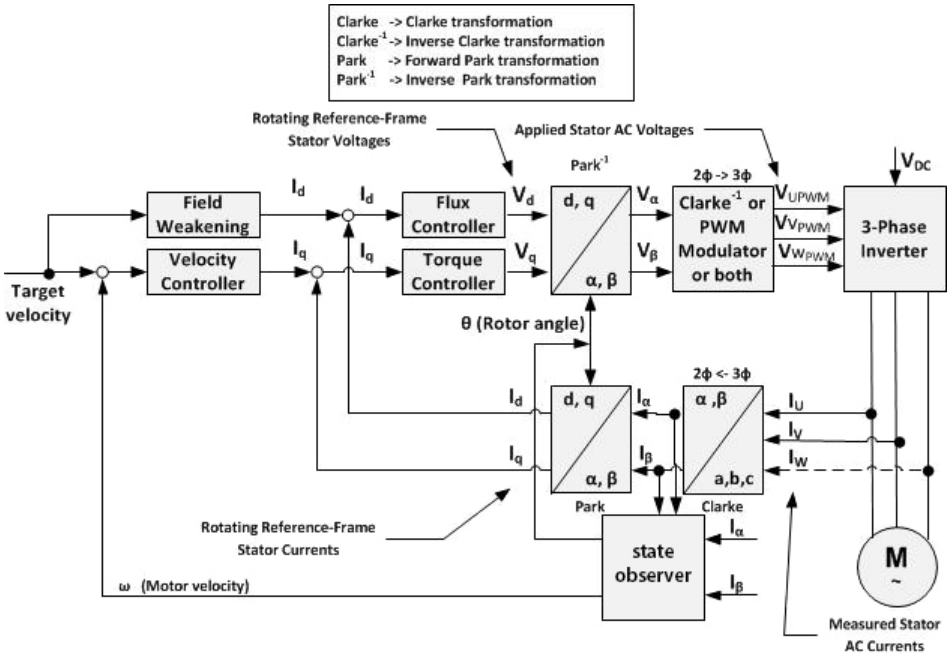

Figure 4: *Scheme of the Control System*

Chapter 1

Rotor Flux Observers for Induction Motors

1.1 Introduction

The implementation of a control law based on the control of the rotor flux for asynchronous motors, requires the estimation of the magnitude and phase of the rotor flux vector, in a reference system integral with the stator. In order to estimate the components of the rotor flux in the desired reference can be made observers of integer and reduced order by taking the speed of rotation of the motor as a free variable.

The reduced order observers are dynamic systems of fourth order. They allow to estimate both the stator current and the rotor flux through measurements of stator voltages and currents. One of the major benefits brought by the use of these observers is that the stator currents are estimated without the noise of the measurement. Therefore you don't have to filter these quantities to purge them from the noise. The use of filters introduces undesired phase delays.

Observers are reduced order dynamic systems of the second order. They allow to estimate only the components of the rotor flux through the measurements of voltage and stator current. In general filters of adequate bandwidth must be employed in order to reproduce the output signals affected by negligible delays.

There are different structures of the rotor flux observers of reduced order obtained by

various methods with the hypothesis that the motor parameters assume their nominal values.

Several scientific articles ([1], [6], [29], [81]) demonstrate that the behavior of the system is sufficiently approximated during the transient stage, even in the presence of considerable deviations of the motor parameters from the nominal values.

In these articles, the tests, executed in simulation, have shown that observers of reduced order may be far less sensitive to variations of the resistance of the rotor and stator and may have a convergence rate better than those based on the realization of the mathematical model of the rotor circuit ([32], [65]),

This is due to the existence of a feedback loop around the system that describes the dynamics of the error of observation of the rotor flux. The use of such observers requires estimation in line of the constant time of the rotor circuit ([65], [26]).

This paper examines the behavior of the reduced order observer. The ultimate goal is the implementation of the observer in digital systems. The voltages and currents acquired have to be filtered by the noise sampling. They are used for this purpose antialiasing filters with an adequate bandwidth. The observer used must meet the following specifications on the error of flow calculation:

a) convergence rate;

b) low sensitivity to variations in the stator resistance and rotor;

c) low sensitivity to approximation errors due to the implementation of observers on microprocessor-based systems.

The requirement c) is necessary because the control system must be necessarily implemented in digital processing systems. Inevitably, the sampling period is finished. According to the calculation method, in certain time intervals, the voltages that power the motor can be also very different than those placed in input to the observer. It follows that there may be additional fluctuations in the error of estimation of the rotor flux.

In order to reduce these additional erroneous oscillations, it is taken in consideration a further disturbance given by the difference between the voltages that feed the engine and the ones supplying the observer. This perturbation is present in the mathematical model of the observer.

Even the deviations of the resistance values of the rotor and stator resistance are modeled as a disturbance that appears in the mathematical model of the electromagnetic circuit of the motor. This is to meet the requirement b).

All of the requirements a) - c) are thus satisfied by the minimization of a suitable cost function that takes into account explicitly the requirement a).

1.2 Full Order Luenberger Observer

Definition 1. *A square matrix is defined* ***Hurwitz matrix*** *if all the eigenvalues have negative real part. For each eigenvalue λ_i of the Hurwitz matrix* $\mathbf{A}$ *the differential equation:*

$$\dot{x} = \mathbf{A}x$$

is stable.

Assumption 1. *Gain* $\mathbf{L} \in \mathbb{R}^2$ *is such that matrix* $\mathbf{A} - \mathbf{LC}$ *is Hurwitz.*

Let us consider the linear time-varying (LTV) equations of the electromagnetic part of an induction motor.

The results given below are based on the following two dimensional LTI dynamics, naturally arising from the four-dimensional model, and satisfying the result given next.

$$\begin{aligned} \dot{\mathbf{x}} &= \mathbf{A}\mathbf{x} + \mathbf{B}u, \\ \mathbf{y} &= \mathbf{C}\mathbf{x}. \end{aligned} \tag{1.2.1}$$

Lemma 1. *For any value of the physical parameters satisfying (0.7.2), matrix* $\mathbf{A}$ *is Hurwitz and the triple (*$\mathbf{A}$, $\mathbf{B}$, $\mathbf{C}$*) is controllable and observable.*

Exploiting the symmetries in the structure of model representation (1.2.1), in the form that uses the Kronecker product (1.2.2),

$$\begin{aligned} \dot{x} &= \overbrace{\left[\mathbf{A} \otimes I + \Omega(t) \otimes J\right]}^{:=A(t)} x + \overbrace{\left(\mathbf{B} \otimes I\right)}^{:=B} u, \\ y &= \overbrace{\left(\mathbf{C} \otimes I\right)}^{:=C} x, \end{aligned}$$

and the properties of Lemma 1, we can construct a full order dynamic observer having the same rate of convergence of the error comparable to that induced by a linear Luenberger gain $\bar{L}$ designed for the dynamics system (1.2.1), in fact:

Assumption 2. *Gain* $\mathbf{L} \in \mathbb{R}^2$ *is such that matrix* $\mathbf{A} - \mathbf{LC}$ *is Hurwitz.*

Note that from Lemma 1, there is no restriction in Assumption 2, because pair $(\mathbf{C}, \mathbf{A})$ is observable.

According to any gain $\mathbf{L}$ that satisfies the Assumption 2, consider the following LTV dynamics observers:

$$\dot{\hat{x}} = [\mathbf{A} \otimes I + \Omega(t) \otimes J]\, \hat{x} + [\mathbf{L} \otimes I]\, (y - \hat{y}) + (\mathbf{B} \otimes I)\, u. \tag{1.2.2}$$

The following theorem establishes that the LTV observer (1.2.2) inherit the convergence properties induced by $\mathbf{L}$ on the LTI closed loop $\mathbf{A} - \mathbf{LC}$ of Assumption 2. It is associated at the error dynamics essendo il sistema uniformly globally exponentially stable.

First let us state the following lemma:

Lemma 2. *Given two square matrices* $\mathbf{E}$ *and* $\mathbf{F}$, $\mathbf{E} \otimes \mathbf{F}$ *is skew-symmetric if either* $\mathbf{E}$ *is skew-symmetric and* $\mathbf{F}$ *is symmetric or vice-versa.*

Theorem 1. *Consider any gain* $\mathbf{L}$ *satisfying Assumption 2 and any pair*[1] *of positive definite matrices* $(\mathbf{P},\ \mathbf{Q})$ *such that:*

$$\mathrm{He}\,(\mathbf{P}(\mathbf{A} - \mathbf{LC})) = -\mathbf{Q} < 0. \tag{1.2.3}$$

Then, denoting the estimation error as $e = x - \hat{x}$, *the quadratic positive definite Lyapunov function* $V(e) = \frac{1}{2} e^T\, (\mathbf{P} \otimes I)\, e$ *satisfies:*

$$\dot{V}(e) = \langle \nabla V(e), \dot{e} \rangle = -e^T\, (\mathbf{Q} \otimes I)\, e, \tag{1.2.4}$$

along all solutions to (1.2.2), (1.2.2).

The result in Theorem 1 is interesting because it exploits the structure of the 4-dimensional LTV dynamics (1.2.2) to design an observer inducing error dynamics quadratically stable. Moreover, this design can be performed by looking at a lower dimensional LTI dynamical system, joining the useful properties established in Lemma 1.

[1] Note that an infinite number such pairs exist because $\mathbf{A} - \mathbf{LC}$ is Hurwitz by design.

Clearly, the error variables depend on ω and exhibit a peculiar time-varying transient. Moreover, the upper bound on their norm is a time-invariant function. Note that once a gain $\mathbf{L}$ satisfying the Assumption 2 has been chosen, one can compute $\alpha_l = -\max_i \left(\mathrm{Re}\{\lambda_i(\mathbf{A}-\mathbf{LC})\}\right)$ and then solve the convex optimization:

$$\begin{gathered}\min_{k,\mathbf{P}=\mathbf{P}^T} k, \qquad \text{subject to:}\\ \mathrm{He}\left(\mathbf{P}(\mathbf{A}-\mathbf{LC})\right) \leq -2\alpha_l \mathbf{P},\\ I \leq \mathbf{P} \leq kI,\end{gathered}$$

to obtain the tight bound:

$$|e(t)| \leq \sqrt{k} e^{-\alpha_l t}|e(0)|, \tag{1.2.5}$$

which follows from straightforward Lyapunov results obtained from Theorem 1 applied with $\bar{Q} = 2\alpha_l \mathbf{P}$.

An other way to exploit the results of Theorem 1 is to solve a suitable disturbance attenuation problem, for example designing gain $\mathbf{L}$ to reduce as much as possible the $\mathcal{L}_2$ gain between an unmeasured disturbance d acting on the current measurement and the estimation error e, subject to a prescribed desired convergence rate $\alpha_l > 0$ for the error dynamics. Using the well known LMI derivations associated with the bounded real lemma for the case $\mu = 1$), this is accomplished by solving the following LMI optimization:

$$\begin{gathered}\min_{\mu,\bar{P},\bar{X}} \mu, \qquad \text{subject to:}\\ \bar{P} = \bar{P}^T > 0,\\ \mathrm{He}\begin{bmatrix} \bar{P}\bar{A} - \bar{X}\bar{C} & -\bar{X} & 0 \\ 0 & -\mu I & 0 \\ I & 0 & -\mu I \end{bmatrix} < 0,\\ \mathrm{He}\left(\bar{P}\bar{A} - \bar{X}\bar{C}\right) \leq -2\alpha_l \bar{P},\end{gathered}$$

and then selecting $\mathbf{L} = \mathbf{P}^{-1}\mathbf{X}$. With this selection, Theorem 1 can be applied to conclude that the $\mathcal{L}_2$ gain from d to e for the error dynamics (see (1.2.2) and (1.2.2)):

$$\dot{e} = \left((\mathbf{A}-\mathbf{LC}) \otimes I + \Omega(t) \otimes J\right) e + (\mathbf{L} \otimes I)\, d, \tag{1.2.6}$$

is upper bounded by μ (which is minimized by design).

In addition to the above numerical solutions, a few relevant explicit selections of $\mathbf{L}$ ensuring Assumption 2 can also be given. Below we provide three relevant cases corresponding to different trade-offs between convergence speed and computational complexity.

Proposition 1. *Considering model (1.2.2) with parameters satisfying (0.7.2), the following holds:*

1 *(Open loop observer) Selection:*

$$\bar{L} = \begin{bmatrix} 0 \\ 0 \end{bmatrix}, \tag{1.2.7}$$

satisfies Assumption 2 and selection $\mathbf{P} = \left[\begin{smallmatrix} \frac{L_r}{f_1} & 0 \\ 0 & 1 \end{smallmatrix}\right] > 0$ *and* $\mathbf{Q} = 2\left[\begin{smallmatrix} a_{11}\frac{L_r}{f_1} & -a_{21} \\ -a_{21} & a_{22} \end{smallmatrix}\right] > 0$ *satisfies (1.2.3).*

2 *(Speed of convergence a_{22}) Selection:*

$$\bar{L} = \begin{bmatrix} a_{22} - a_{11} \\ a_{21} \end{bmatrix}, \tag{1.2.8}$$

satisfies Assumption 2 and assigns both eigenvalues of $\mathbf{A} - \mathbf{LC}$ *in* $-a_{22}$*. Moreover selection* $\mathbf{P} = \left[\begin{smallmatrix} \frac{1}{a_{22}f_1} & 0 \\ 0 & \frac{f_1}{a_{22}} \end{smallmatrix}\right] > 0$ *and* $\bar{Q} = \left[\begin{smallmatrix} \frac{2}{f_1} & -1 \\ -1 & 2f_1 \end{smallmatrix}\right] > 0$ *satisfies (1.2.3).*

3 *(Arbitrary speed of convergence $(a_{22} + \eta)$). Given any scalar $\eta > 0$, selection:*

$$\bar{L} = \begin{bmatrix} a_{22} - a_{11} + 2\eta \\ a_{21} + \frac{\eta}{f_1}\left(1 + 2\frac{\eta}{a_{22}}\right) \end{bmatrix}, \tag{1.2.9}$$

satisfies Assumption 2. Moreover, selection:

$$\mathbf{P} = \begin{bmatrix} \frac{\eta}{a_{22}}\left(1 + 2\frac{\eta}{a_{22}}\right) & -\frac{f_1}{a_{22}}\eta \\ -\frac{f_1}{a_{22}}\eta & f_1^2 \end{bmatrix}, \tag{1.2.10}$$

is definite positive and satisfies (1.2.3) with $\bar{Q} = 2(a_{22} + \eta)\mathbf{P}$*.*

1.3 Reduced Order Luenberger Observer

The structure of a reduced order observer, for system A, is given by:

$$\dot{\mathbf{p}} = \mathbf{L}(\omega)\mathbf{p} + \mathbf{K}(\omega)\mathbf{x}_1 + \mathbf{B}(\omega)\tilde{\mathbf{m}} \tag{1.3.1}$$

$$\mathbf{q} = \mathbf{p} + \mathbf{K}_0\mathbf{x}_1 \tag{1.3.2}$$

$\mathbf{q}$ is the estimation of vector of the rotor flux and

$$\tilde{\mathbf{m}} = \mathbf{m} + \delta\mathbf{m}, \delta\mathbf{m} = \begin{bmatrix} \delta m_a & \delta m_b \end{bmatrix}^{\mathrm{T}}$$

being:

$$\begin{aligned} \mathbf{L}(\omega) &= \mathbf{L}_0 + \mathbf{L}_1\omega \\ \mathbf{K}(\omega) &= [\mathbf{L}(\omega) - \mathbf{A}_{11}]\,\mathbf{K}_0 + \mathbf{A}_{21} - \dot{\mathbf{K}}_0 \\ \mathbf{B}(\omega) &= -c_1\mathbf{K}_0 \end{aligned} \tag{1.3.3}$$

in which:

$$\begin{aligned} \mathbf{L}_0 &= -a_{33}\mathbf{I} - a_{13}\mathbf{K}_0 \\ \mathbf{L}_1 &= (\mathbf{I} + c_1\mathbf{K}_0)\,\mathbf{J} \end{aligned}$$

Demonstration: At first, I determine the equation that describes the dynamics of the error of the survey defined by the equation:

$$\mathbf{e}(t) = \mathbf{x}_2(t) - \mathbf{q}(t)$$

Deriving the previous expression and taking into account the equations (1.3.1) and (1.3.3), get:

$$\dot{\mathbf{e}}(t) = \mathbf{L}(\omega)\mathbf{e}(t) + c_1\mathbf{K}_0\delta\mathbf{m} + \mathbf{K}_0\mathbf{d}_1 + (l\mathbf{I} + \mathbf{K}_0)\mathbf{d}_2 \tag{1.3.4}$$

with $\delta\mathbf{m} = \tilde{\mathbf{m}} - \mathbf{m}$.

The (1.3.4) shows that the dynamics of the error of observation contain the forcing terms that arise because of the variation in the resistances rotor and stator and of the difference between the actual supply voltage of the motor and the observer. Such forcing terms prevent the same error of zero asymptotically. However, in the absence of such terms, the dynamic

error of observation is expressed by an equation in free mode that converges to zero by appropriately selecting $\mathbf{L}(\omega)$

Assuming as constant the elements of the matrix $\mathbf{K}_0$ and the observer (1.3.1) - (1.3.3), as described in [29], we can use a synthesis method based on the criterion of Popov hyper stability. Or better, assuming that $\delta\mathbf{m} = \mathbf{0}$, $\mathbf{d}_1 = \mathbf{0}$ e $\mathbf{d}_2 = \mathbf{0}$, the dynamic of observation error (1.3.4) can be described by equations:

$$\begin{aligned} \dot{\mathbf{e}} &= \mathbf{L}_0\mathbf{e} + \mathbf{u} \\ \mathbf{u} &= \mathbf{L}_1\omega \end{aligned} \tag{1.3.5}$$

which can be interpreted as the interconnection of a linear system and stationary described by the first of (1.3.5) and by a non-linear system described by the second equation of (1.3.5), as shown in fig. (1.1).

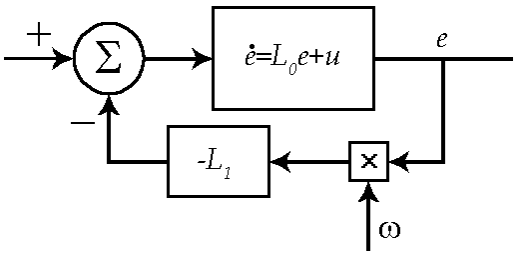

Figure 1.1: *Interconnection of a linear and nonlinear systems.*

Assuming that the non-linear system of the feedback line satisfies Popov's theb integral inequality given by:

$$-\int_0^T -\mathbf{e}^T\mathbf{L}_1\mathbf{e}\omega dt \geq -\gamma^2, \qquad \forall T > 0 \tag{1.3.6}$$

The system of fig.(1.1) is asymptotically iperstabile if and only if the transfer function of the linear and stationary line of direct action is real and strictly positive. As it is known, the transfer function of the linear system and the stationary line of direct action is real ad strictly positive if exists a matrix $\mathbf{Q}$ symmetric and definite positive, like that:

$$\mathbf{L}_0 + \mathbf{L}_0^{\mathrm{T}} = -\mathbf{Q} \tag{1.3.7}$$

Note that from (1.3.6) you can design different observers of reduced order.

a) $\mathbf{L}_1 = \mathbf{0}$

From (1.3.3) we have:

$$\mathbf{K}_0 = -\frac{1}{c_1}\mathbf{I}, \quad \mathbf{L}_0 = \mathbf{0}$$

It follows that there is an observer because the transfer function of the line of direct action can not be strictly positive real.

b) $\mathbf{e}^{\mathrm{T}}\mathbf{L}_1\mathbf{e} = 0, \quad \mathbf{L}_1 \neq 0$

As it is easily verified, it can get $\mathbf{e}^{\mathrm{T}}\mathbf{L}_1\mathbf{e} = 0$ choosing $\mathbf{L}_1 = \gamma\mathbf{J}, \quad \gamma \neq 0$. The correspondent matrix $\mathbf{K}_0$ is given by:

$$\mathbf{K}_0 = \frac{1}{c_1}(\gamma - 1)\mathbf{I}$$

from this, it happens that the first member of (1.3.7) becomes:

$$\mathbf{L}_0 + \mathbf{L}_0^{\mathrm{T}} = -a_{33}\gamma\mathbf{I}$$

The matrix $\mathbf{K_0}$ is definite negative for $\gamma \neq 0$. The diagram of fig.(1.1) can be obtained using the **method of Lyapunov** choosing $\mathbf{e}^T\mathbf{e}$ as the "Lyapunov function". The eigenvalues of the dynamics matrix of the observer are given by:

$$\lambda_{1,2} = (-a_{33} \pm j\omega)\gamma$$

and, consequently, the observer in question has the same characteristics of the observer described in [81]. For $l = 1$ these observers lead back to the one based on the integration of the mathematical model of the motor.

b) $\mathbf{e}^{\mathrm{T}}\mathbf{L}_1\mathbf{e} \neq 0$

In this case the (1.3.6) is satisfied if the quadratic form $\mathbf{e}^{\mathrm{T}}\mathbf{L}_1\mathbf{e}$ is positive definite for $\omega > 0$ and negative definite for $\omega < 0$. According to the criterion of Sylvester it is known that the above-mentioned quadratic form is defined positive or negative depending on what is defined positive or negative, the following matrix $\mathbf{H}$:

$$\mathbf{H} = \frac{1}{2}(\mathbf{L}_1 + \mathbf{L}_1^{\mathrm{T}}) \tag{1.3.8}$$

Setting $\mathbf{Q} = 2q\mathbf{I}$, the matrix $\mathbf{K}_0$, obtained starting from (1.3.7) is given by:

$$\mathbf{K}_0 = \frac{(q - a_{33})}{a_{13}}\mathbf{I} + h\mathbf{J}$$

corresponding the matrix $\mathbf{H} = -\mathbf{c_1}h\mathbf{I}$. It follows that, in according to the positive definite matrix H, result for $\omega > 0$ and negative definite for $\omega < 0$ is necessary and just choose h as follows:

$$h = r\text{sgn}(\omega), \text{r} > 0 \tag{1.3.9}$$

The eigenvalues of the dynamic matrix of the observer are given by:

$$\lambda_{1,2} = -\left(q + c_1 r\left|\omega\right|\right) \pm j\left(a_{13} r\text{sgn}\left(\omega\right) - \left(\frac{q}{a_{33}}\right)\omega\right)$$

which shows that both the real and imaginary part are a function of ω and so it is possible to obtain a value of the damping coefficient suitable even at high speed.

The dynamic error of observation of the rotor flux (1.3.4) can be written as follows:

$$\dot{\mathbf{e}} = \mathbf{L}(\omega)\mathbf{e} + \mathbf{G}_2\mathbf{d} + \mathbf{T}_2\mathbf{v} \tag{1.3.10}$$

where:

$$\begin{aligned} \mathbf{G}_2 &= \mathbf{G}_b - \mathbf{K}_0\mathbf{G}_a \\ \mathbf{T}_2 &= \mathbf{T}_b - \mathbf{K}_0\mathbf{T}_a \end{aligned} \tag{1.3.11}$$

being:

$$\mathbf{G}_a = \begin{bmatrix} -\mathbf{I} & -\mathbf{I} \end{bmatrix}, \quad \mathbf{G}_a = \begin{bmatrix} \mathbf{0} & l\mathbf{I} \end{bmatrix}, \quad \mathbf{T}_a = -\mathbf{I}, \quad \mathbf{T}_b = \mathbf{0}, \quad \mathbf{v} = c_1\delta\mathbf{m}$$

The model (1.3.10), which expresses the dynamic error of observation, can be represented graphically as shown in fig.(1.2).

An examination of this figure shows that the observer model is considered a feedback scheme for $\mathbf{K}_0 \neq 0$, subject to interference $\mathbf{d}$ e $\mathbf{v}$. The only problem is to determine the matrix $\mathbf{K}_0$ in order to minimize the effects of disturbances $\mathbf{d}$ and $\mathbf{v}$ on error of the observation. To do this, consider the following positive-definite function:

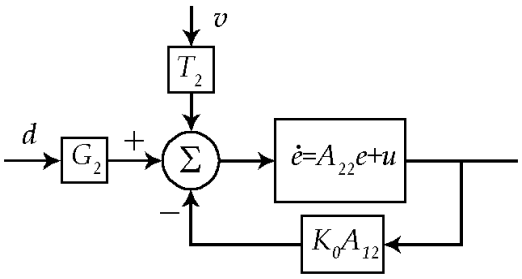

Figure 1.2: *Block diagram of the observer.*

$$V(\mathbf{e}) = \frac{1}{2}\mathbf{e}^{\mathrm{T}}\mathbf{e} \tag{1.3.12}$$

Taking into consideration the (1.3.10), the derivative related to the time of this function is:

$$\dot{V}(\mathbf{e}) = V_q + \mathbf{d}^{\mathrm{T}}\mathbf{G}_2^{\mathrm{T}}\mathbf{e} + \mathbf{v}^{\mathrm{T}}\mathbf{T}_2^{\mathrm{T}}\mathbf{e} \tag{1.3.13}$$

where V_{q} is given by:

$$V_{\mathrm{q}} = \frac{1}{2}\mathbf{e}^{\mathrm{T}}\left[\mathbf{L}(\omega) + \mathbf{L}^{\mathrm{T}}(\omega)\right]\mathbf{e} \tag{1.3.14}$$

Substituting in (1.3.14) the expression of $\mathbf{L}(\omega)$ given by (**??**) is obtained:

$$V_{\mathrm{q}} = \mathbf{e}^{\mathrm{T}}(\mathbf{F}_0 + \mathbf{F}_1\omega)\mathbf{e} \tag{1.3.15}$$

where:

$$\begin{aligned}\mathbf{F}_0 &= \tfrac{1}{2}\left(\mathbf{L}_0 + \mathbf{L}_0^T\right)\\ \mathbf{F}_1 &= \tfrac{1}{2}\left(\mathbf{L}_1 + \mathbf{L}_1^T\right)\end{aligned} \tag{1.3.16}$$

Note now that for $\mathbf{d} = 0$ and $\mathbf{v} = 0$ we have $\dot{V}(\mathbf{e}) = V_q$ and therefore the function V_q must be negative definite. For this to happen it is sufficient that $\mathbf{F}_0$ is definite negative and that $\mathbf{F}_1$ is negative definite for $\omega > 0$ and definite positive for $\omega < 0$. Assuming:

$$\mathbf{F}_0 = -a\mathbf{I}, \quad a > 0 \tag{1.3.17}$$

and using the expression of $\mathbf{L}_0$ shown earlier, we obtain the following expression of the

matrix $\mathbf{K}_0$:

$$\mathbf{K}_0 = k_i\mathbf{I} + k_\mathbf{j}\mathbf{J} \tag{1.3.18}$$

where k_j is subsequently calculated and:

$$k_i = \frac{a - a_{33}}{a_{13}} \tag{1.3.19}$$

From (1.3.18), from the expression of $\mathbf{L}_1$ and from (1.3.16), we obtain the following expression of $\mathbf{F}_1$:

$$\mathbf{F}_1 = -c_1 k_j \mathbf{I} \tag{1.3.20}$$

that highlights that the conditions previously set forth in the matrix $\mathbf{F}_1$ are satisfied if we choose k_j as follows:

$$k_j = r \cdot \text{sgn}(\omega), \quad r \geq 0 \tag{1.3.21}$$

Now, replacing (1.3.21) in (1.3.20) and taking into consideration the (1.3.17), the (1.3.14) become:

$$V_q = -f \left\|\mathbf{e}\right\|^2 \tag{1.3.22}$$

where $\|\cdot\|$ is the Euclidean norm and:

$$f = a + c_1 \left|\omega\right|$$

Consequently:

$$\dot{V}(\mathbf{e}) = -f \left\|\mathbf{e}\right\|^2 + \mathbf{d}^{\mathrm{T}}\mathbf{G}_2^{\mathrm{T}}\mathbf{e} + \mathbf{v}^{\mathrm{T}}\mathbf{T}_2^{\mathrm{T}}\mathbf{e}$$

which, taking into account the properties of the operator norm, we obtain:

$$\begin{gathered}\dot{V}(e) \leq -f \left\|e\right\| \left[\left\|e\right\| - \tfrac{1}{f}\left(\left\|d\right\| \tfrac{\left\|G_2^T e\right\|}{\left\|e\right\|} + \left\|v\right\| \tfrac{\left\|T_2^T e\right\|}{\left\|e\right\|}\right)\right] \leq \\ -f \left\|e\right\| \left[\left\|e\right\| - \tfrac{1}{f}\left(\left\|d\right\|_x \sigma\left(G_2^T\right) + \left\|v\right\|_x \sigma(T_2^T)\right)\right]\end{gathered} \tag{1.3.23}$$

where $\|\mathbf{d}\|_x$ and $\|\mathbf{v}\|_x$ are the maximum values of norms of $\mathbf{d}$ and $\mathbf{v}$ respectively, and $\sigma\left(\mathbf{G}_2^{\mathrm{T}}\right)$ and $\sigma\left(\mathbf{T}_2^{\mathrm{T}}\right)$ are the maximum singular values of the matrices $\mathbf{G}_2^T$ e $\mathbf{T}_2^T$.

The (1.3.23) and the constraints on a and r (cfr. (1.3.17) and (1.3.21)), show that the function $V(\mathbf{e})$ is a Lyapunov function in the region:

$$\|\mathbf{e}\| > \frac{1}{f}\left(\|\mathbf{d}\|_x \sigma\left(\mathbf{G}_2^{\mathrm{T}}\right) + \|\mathbf{v}\|_x \sigma(\mathbf{T}_2^{\mathrm{T}})\right) \tag{1.3.24}$$

La (1.3.24) shows that the choice of the candidate Lyapunov function (**??**) ensures the convergence of the error of observation to a finite value expressed by (1.3.24).

In order to reduce this lower limit, should determine a and r in order to minimize the following cost function:

$$J_c = p_1 \frac{\sigma^2(\mathbf{G}_2^{\mathrm{T}})}{f^2} + p_2 \frac{\sigma^2(\mathbf{T}_2^{\mathrm{T}})}{f^2} \tag{1.3.25}$$

subject to the constraints:

$$\begin{aligned} a &\geq a_0 > 0, \\ r &\geq r_0 \geq 0. \end{aligned} \tag{1.3.26}$$

Obviously, choosing $p_1 = 1$ and $p_2 = 0$ is only minimize the effects of the disturbance $\boldsymbol{d}$, while assuming $p_1 = 0$ and $p_2 = 1$ is only minimize the effects of $\boldsymbol{v}$.

The solutions of the above mentioned problem of constrained minimum are obtained using the sufficient conditions of Kuhn-Tucker [84].

Assuming $a > a_0 > 0$ and $r > r_0 > 0$, we obtain the following solution:

$$\begin{aligned} a &= a_{33} \\ r &= \tfrac{\rho}{a_{13}} |\omega| \end{aligned} \tag{1.3.27}$$

where:

$$\rho = \frac{p_1}{p_2 + 2p_1}$$

1.3.1 Conclusion

The dynamic behavior of the observer Luenberger proved unsatisfactory because the elements of the matrices $\mathbf{G}_2$ e $\mathbf{T}_2$ are very high even at low speeds.

Assuming $a = a_0$ e $r > r_0 > 0$, we obtain:

$$\begin{aligned} a &= a_0 \\ r &= \tfrac{c_1}{a_0}\left(k_{i0}^2 + 2\rho k_{i0} l + \rho l^2\right)|\omega| \end{aligned} \tag{1.3.28}$$

where:

$$k_{i0} = \frac{a_0 - a_{33}}{a_{13}}$$

The dynamic behavior expected from the use of such a solution is unsatisfactory for the reasons outlined in the previous case.

Assuming $a > a_0$ e $r = 0$, we obtain $\mathbf{F}_1 = 0$ and the solution become:

$$\begin{aligned} a &= a_{33} \\ r &= 0 \end{aligned} \tag{1.3.29}$$

This solution involves $\mathbf{K}_0 = 0$ which corresponds to an observer based on the simulation of the rotor circuit whose benefits have been considered previously.

Finally, assuming $a > a_0$ e $r = r_0 > 0$, we obtain the following solution:

$$\begin{aligned} a &= a_{33}(1-\rho)\tfrac{a_{33}+c_1 r_0|\omega|}{a_{33}(1-\rho)+c_1 r_0|\omega|} \\ r &= r_0 \end{aligned} \tag{1.3.30}$$

This solution implies that $|k_i|$ increases with ω and assume the values $\rho \cdot a_{33}$ at high speed, when k_j is independent of ω.

Consequently, the elements of $\mathbf{G}_2$ and $\mathbf{T}_2$ do not grow at high speeds. This solution seems to be the best among those obtained.

Remark 1. It is emphasized that although the reduced order observers described in this section may be desirable due to their lower computational complexity (2 states instead of 4), it is often desirable to adopt a full order strictly proper observer so that high frequency measurement noise is suitably filtered out in the feedback signal. This is accomplished, for

example, by designing $\bar{L}$ according to optimization (**??**) as illustrated by the simulations of Figure 2.4.

1.4 Sliding Observer

Various structures of reduced order rotor flux observers were obtained using different approaches and assuming that the motor parameters assume nominal values. In this context, there is a trend towards the choice of adjustable observer parameters. This in order to obtain a satisfactory dynamic behavior and steady state even in the presence of motor parameters variation.

The use of the observer requires the on-line estimation of the rotor circuit time constant. In reference to sliding observers exists a method ([27]) based on the minimization of a cost function, in which both the convergence rate and the sensitivity to rotor and stator resistance variations of the rotor flux estimation error are considered explicitly. Exist the possibility of extending these methods to design reduced order observers.

There has as its objective the design of an sliding and reduced order observer for meeting the following requirements relating the rotor flux observation error:

a) convergence rate;

b) low sensitivity to rotor and stator resistance variations;

c) low sensitivity to errors due to the implementation of the observer on μ-processor-based systems.

The requirement *c)* is required in order to take into account the finite processing time of the μ-processor-based systems, which implies a finite sampling period for the observer implementation. Regarding the sliding observer, the finite sampling period implies that the real sliding motion occurs whose amplitude and frequency increase and diminishes, respectively, as the sampling period increases. This causes oscillation in the rotor flux observation error.

For both the sliding and reduced order observers, the finite sampling period, causes that the voltages supplying the motor can be very different from those providing the observer in certain intervals of time, depending on the implementation method employed. This involves that additional oscillations occur in the rotor flux estimation error.

To minimize these additional oscillations, the differences between the supply voltages of the motor and those supplying the observer are modeled as a noise appearing in the mathematical model of the observer himself.

In order to take into account explicitly the requirement *b)* the variation of rotor and stator resistance are modeled as a noise which appears in the mathematical model of the electromagnetic circuit of the motor.

All requirements *a), b), c)* are satisfied, therefore, by minimization of a suitable cost function to minimize the effects of the two above disturbances on the rotor flux observation error, in presence of a constraints which takes into account explicitly the requirement *a)*.

The structure of the sliding observer is presumed to have the following form:

$$\dot{\mathbf{z}} = \mathbf{A}(\omega)\mathbf{z} + \mathbf{B}\tilde{\mathbf{m}} - \mathbf{H}\mathbf{u} \tag{1.4.1}$$

where:

$$\mathbf{H} = \begin{vmatrix} \mathbf{H}_\alpha \\ \mathbf{H}_\beta \end{vmatrix} \quad \mathbf{z} = \begin{vmatrix} \mathbf{z}_1 \\ \mathbf{z}_2 \end{vmatrix} \quad \mathbf{z_1} = [z_{11} \quad z_{12}]' \quad \mathbf{z_2} = [z_{21} \quad z_{22}]' \quad \mathbf{s} = [\mathbf{s_1} \quad \mathbf{s_2}]' = \mathbf{x_1} - \mathbf{z_1}$$

$$\mathbf{u} = sgn(\mathbf{s}) \tag{1.4.2}$$

The vectors $\mathbf{z_1}$ and $\mathbf{z_2}$ are, respectively, the estimation of $\mathbf{x_1}$ and $\mathbf{x_2}$. $\mathbf{B}\tilde{\mathbf{m}}$ is the vector effective voltage supplied to the observer, which, as previously mentioned, is different from that which feeds the motor.

Establishing that:

$$\tilde{\mathbf{m}} = \mathbf{m} + \delta\mathbf{m}; \qquad \delta\mathbf{m} = [\delta m_\alpha \quad \delta m_\beta]' \tag{1.4.3}$$

$$\mathbf{v} = [v_1 \quad v_2]' = c_1\delta\mathbf{m} \tag{1.4.4}$$

then the equation 1.4.1 becomes:

$$\dot{\mathbf{z}} = \mathbf{A}(\omega)\mathbf{z} + \mathbf{B}\mathbf{m} - \mathbf{H}\mathbf{u} - \mathbf{T}\mathbf{v} \tag{1.4.5}$$

$$\mathbf{T} = \begin{vmatrix} \mathbf{T}_\alpha \\ \mathbf{T}_\beta \end{vmatrix} = \begin{vmatrix} -\mathbf{I} \\ \mathbf{0} \end{vmatrix} \tag{1.4.6}$$

The vector $\mathbf{v}$ is proportional to the difference between the motor supply voltage and which feeds the observer, and can be regarded as a disturbance agent on the observer.

The observer error dynamics $\mathbf{e}$ is represented by the equation:

$$\dot{\mathbf{e}} = \mathbf{A}(\omega)\mathbf{e} + \mathbf{H}u + \mathbf{G}\mathbf{d} + \mathbf{T}\mathbf{v} \tag{1.4.7}$$

$$\mathbf{e} = \mathbf{x} - \mathbf{z} = \begin{bmatrix} \mathbf{e}_1{}' & \mathbf{e}_2{}' \end{bmatrix}; \quad \mathbf{e}_1 = \mathbf{x}_1 - \mathbf{z}_1 = \begin{bmatrix} \mathbf{e}_{11} & \mathbf{e}_{12} \end{bmatrix}'; \quad \mathbf{e}_2 = \mathbf{x}_2 - \mathbf{z}_2 = \begin{bmatrix} \mathbf{e}_{21} & \mathbf{e}_{22} \end{bmatrix}'$$

Now, suppose there exists an ideal sliding motion on the domain of sliding hyperplanes $\mathbf{s} = \mathbf{0}$. For example, a motion in which the estimation error of the stator current $\mathbf{e}_1$ is forced to be null. This also implies that $\dot{\mathbf{s}} = \dot{\mathbf{e}} = \mathbf{0}$ during the sliding motion.

To design the observer dynamic error $\mathbf{e}$ in the domain of which just above, is used a equivalent method of control ([83],[68]).

Then, from the equation:

$$\dot{\mathbf{s}} = \dot{\mathbf{e}} = \mathbf{C}\left[\mathbf{A}(\omega)\mathbf{e} + \mathbf{H}\mathbf{u}_{eq} + \mathbf{G}\mathbf{d} + \mathbf{T}\mathbf{v}\right] = 0 \tag{1.4.8}$$

of course:

$$\mathbf{C} = \begin{bmatrix} \mathbf{I} & \mathbf{0} \end{bmatrix}$$

we obtain the following expression of the equivalent control:

$$\mathbf{u}_{eq} = -\mathbf{H}_\alpha^{-1}\mathbf{C}\left[\mathbf{A}(\omega)\mathbf{e} + \mathbf{G}\mathbf{d} + \mathbf{T}\mathbf{v}\right] \tag{1.4.9}$$

and substituting the (1.4.9) in (1.4.7), we obtain:

$$\dot{\mathbf{e}} = \mathbf{P}\left[\mathbf{A}(\omega)\mathbf{e} + \mathbf{G}\mathbf{d} + \mathbf{T}\mathbf{v}\right] \tag{1.4.10}$$

$\mathbf{P}$ is given by:

$$\mathbf{P} = \mathbf{I}_4 - \mathbf{H}\mathbf{H}_\alpha^{-1}\mathbf{C}; \qquad \mathbf{I}_4 = diag(1,1,1,1)$$

P is the desired projection matrix.

From equation (1.4.10), it follows that, during sliding motion, the dynamic of observation error is divided into two independent parts.

The first one describes the estimation error of the stator current, according to the equation $\dot{\mathbf{e}} = \mathbf{0}$. The second part describes the estimation error of the rotor flux, according to the equation:

$$\dot{\mathbf{e}}_2 = \mathbf{A}_2(\omega)\mathbf{e}_2 + \mathbf{G}_1\mathbf{d} + \mathbf{T}_1\mathbf{v} \tag{1.4.11}$$

$$\mathbf{A}_2(\omega) = \mathbf{A}_{22} - \mathbf{H}_\beta\mathbf{H}_\alpha^{-1}\mathbf{A}_{12} \tag{1.4.12}$$

$$\begin{aligned} \mathbf{G}_1 &= \mathbf{G}_\beta - \mathbf{H}_\beta\mathbf{H}_\alpha^{-1}\mathbf{G}_\alpha \\ \mathbf{T}_1 &= \mathbf{T}_\beta - \mathbf{H}_\beta\mathbf{H}_\alpha^{-1}\mathbf{T}_\alpha \end{aligned} \tag{1.4.13}$$

1.4.1 Sliding Conclusion

The sliding motion exist if $\mathbf{s} = \mathbf{0}$. This condition depend only on the $\mathbf{H}_\alpha$. And for ease can choose this matrix with the following structure:

$$\mathbf{H}_\alpha = h_1\mathbf{I} + h_2\mathbf{J} \tag{1.4.14}$$

This matrix is not singular for each h_2 and h_1 strictly positive (as required).

This condition will be determined using the method of control hierarchy ([83],[68]).

Using this method, so that an sliding motion occurs on the surface $\mathbf{s}_1 = 0$, for the equation (1.4.7), is sufficient that:

$$\lim_{\mathbf{s}_1 \to \mathbf{0}^+} \dot{\mathbf{s}}_1 < 0; \qquad \lim_{\mathbf{s}_1 \to \mathbf{0}^-} \dot{\mathbf{s}}_1 > 0 \tag{1.4.15}$$

The previous conditions imply:

$$h_1 \leq h_\alpha - |h_2| \tag{1.4.16}$$

$$h_\alpha = a_{11}\,|e_{11}|_x - a_{13}\,|e_{21}|_x\,|d_1|_x - |d_3|_x - |v_1|_x - c_2\,|e_{22}|_x\,|\omega|$$

in this condition applies the convention that $|\cdot|_x$ denotes the max value of $|\cdot|$.

The equation (1.4.16) is satisfied for h_1 and $|h_2|$ belonging to the region on the left side of the straight line obtained assuming the equal sign in (1.4.16).

Finally, in order that a sliding motion exists on the surface $s_2 = 0$ for the system (1.4.7) projected on the surface $s_1 = 0$, is sufficient that:

$$\lim_{s_2\to 0^+} \dot{s}_2 < 0; \qquad \lim_{s_2\to 0^-} \dot{s}_2 > 0 \tag{1.4.17}$$

from which it has:

$$h_1^2 + h_2^2 \geq -h_c h_1 + h_b\,|h_2| \tag{1.4.18}$$

$$h_b = a_{11}\,|e_{11}|_x + a_{13}\,|e_{21}|_x + |d_1|_x + |d_3|_x + |v_1|_x + c_2\,|e_{22}|_x\,|\omega|$$

$$h_c = a_{13}\,|e_{22}|_x - a_{11}\,|e_{12}|_x + |d_2|_x + |d_4|_x + |v_2|_x + c_2\,|e_{21}|_x\,|\omega|$$

admitting that:

$$|e_{11}|_x = |e_{12}|_x; \quad |e_{21}|_x = |e_{22}|_x; \quad |d_1|_x = |d_2|_x; \quad |d_3|_x = |d_4|_x; \quad |v_1|_x = |v_2|_x$$

is achieved

$$h_c = -h_a$$

the corresponding sliding domain is in outside of the circumference obtained by assuming the equal sign in (1.4.18).

This implies that the region in which the sliding motion happens for $\mathbf{s} = 0$ is dependent on ω.

However, the the boundary shape of this region is independent on ω. Moreover if ω increases it moves on the left in the plane $h_1 - |h_2|$.

Choosing h_1 and h_2 in the sliding dominion and having $\mathbf{K}_0$, the matrix $\mathbf{H}_b$ can be calcu-

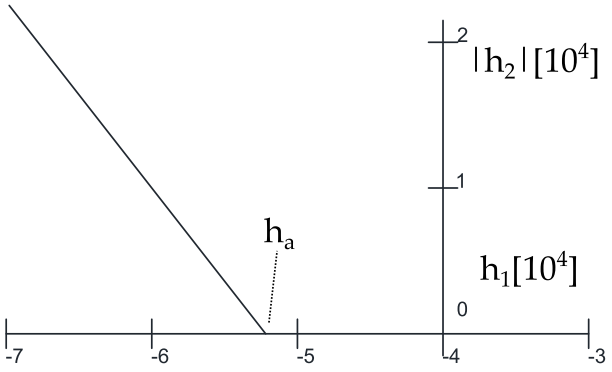

Figure 1.3: *Sliding dominion*

lated by the equation:

$$\mathbf{K}_0 = \mathbf{H}_b \mathbf{H}_a^{-1} \tag{1.4.19}$$

1.5 Nonlinear flux observer

If a magnetic circuit is assumed to be linear, the arguments for the design of the Luenberger and Sliding observer represent a powerful instrument for create a observer of the rotor state that ensures excellent performances. However, if we consider the effects of saturation, then we will have to deal with a nonlinear model. Thus, the results derived above should be modified. In this context, we must consider the model:

$$\begin{cases} \dot{x} = \mathbf{A}(|i_{mr}|)x + f(x) + g(x)u \\ y = \mathbf{C}x \end{cases} \tag{1.5.1}$$

where x, u and y are the state, the input and the output vector respectively defined as:

$$x = \begin{bmatrix} i_{s,\alpha} & i_{s,\beta} & i_{mr,\alpha} & i_{mr,\beta} \end{bmatrix}^T, \quad u = \begin{bmatrix} u_{s,\alpha} & u_{s,\beta} & \omega_r \end{bmatrix}^T, \quad y = \begin{bmatrix} i_{s,\alpha} & i_{s,\beta}, \end{bmatrix}^T \tag{1.5.2}$$

and $\mathbf{A}(|i_{mr}|)$, $f(x)$, $g(x)$ and $\mathbf{C}$ are defined as:

$$\mathbf{A}(|i_{mr}|) = \begin{bmatrix} -c_1 & 0 & c_3 & 0 \\ 0 & -c_1 & 0 & c_3 \\ a_{22}^* & 0 & -a_{22}^* & 0 \\ 0 & a_{22}^* & 0 & -a_{22}^* \end{bmatrix}, \; g(x) = \begin{bmatrix} f_1 & 0 & a_{21}T_r f_1 i_{mr,\beta} \\ 0 & f_1 & -a_{21}T_r f_1 i_{mr,\alpha} \\ 0 & 0 & -i_{mr,\beta} \\ 0 & 0 & i_{mr,\alpha} \end{bmatrix}, \; \mathbf{C} = \begin{bmatrix} 1 & 0 & 0 & 0 \\ 0 & 1 & 0 & 0 \end{bmatrix},$$

$$f(x) = \begin{bmatrix} \frac{c_2}{i_{mr,\alpha}^2 + i_{mr,\beta}^2}\left(2i_{s,\beta}^2 i_{mr,\alpha} - i_{s,\alpha}^2 i_{mr,\alpha} - 3i_{s,\alpha}i_{s,\beta}i_{mr,\beta}\right) + \frac{c_3 - a_{21}f_1}{i_{mr,\alpha}^2 + i_{mr,\beta}^2}\left(i_{s,\alpha}i_{mr,\beta}^2 - i_{s,\beta}i_{mr,\alpha}i_{mr,\beta}\right) \\ \frac{c_2}{i_{mr,\alpha}^2 + i_{mr,\beta}^2}\left(2i_{s,\alpha}^2 i_{mr,\beta} - i_{s,\beta}^2 i_{mr,\beta} - 3i_{s,\alpha}i_{s,\beta}i_{mr,\alpha}\right) + \frac{c_3 - a_{21}f_1}{i_{mr,\alpha}^2 + i_{mr,\beta}^2}\left(i_{s,\beta}i_{mr,\alpha}^2 - i_{s,\alpha}i_{mr,\alpha}i_{mr,\beta}\right) \\ \frac{c_2}{i_{mr,\alpha}^2 + i_{mr,\beta}^2}\left(i_{s,\alpha}i_{mr,\beta}^2 - i_{s,\beta}i_{mr,\alpha}\right) \\ \frac{c_2}{i_{mr,\alpha}^2 + i_{mr,\beta}^2}\left(i_{s,\beta}i_{mr,\alpha}^2 - i_{s,\alpha}i_{mr,\beta}\right) \end{bmatrix}$$

It's a linear time-varying part given by matrix A, and two nonlinear terms given by vector fields $\mathbf{G}u_3$ and $\mathbf{B}$. If $\mathbf{G}u_3$, then the result given in theorem 1 can be used. Indeed it can be shown that Theorem 1 continue to be valid if the coefficients in $\mathbf{A}$ are positive. Effectively, this happens. The time-variant coefficients contained in matrix $\mathbf{A}$ are positive for any value of $|i_{mr}|$. Moreover, for Theorem 1, the $g(x)$ terms does not induce any changes with regard to the convergence of the observer. This considerations are very important for the following result.

A design mode of an observer is to imitate the methods used in a linear system. That means that you are designing a model of the original system (1.5.1) and will force with the residual part.

$$e = y - \hat{y} = y - \mathbf{C}\hat{x}, \tag{1.5.3}$$

in the above equation have been used the convention that the symbol ˆ indicates the estimated variables. The equation of the observer becomes:

$$\dot{\hat{x}} = \mathbf{A}(|\hat{i}_{mr}|)\hat{x} + f(\hat{x}) + g(\hat{x})u + ke. \tag{1.5.4}$$

where k is a appropriately chosen gain.

Theorem 2. *Exists $\beta > 0$, such that the gain $k = \mathbf{K} = \begin{bmatrix} (\beta a_{22}^* - c_1) & a_{22}^* \end{bmatrix}^T \otimes I_2$ ensures the convergence of the nonlinear observer (1.5.4).*

1.6 Extended Kalman Filter

In this section is presented another approaches to design a rotor flux observers using the EKF (Extended Kalman Filter).

The the estimation error of the extended Kalman filter is mean square limited. For the development of the Extended Kalman Filter is used that illustrated in ([72]) whit the convergence conditions derived in ([77]).

Moreover, there is also an upper bound of the estimation error of the discrete time filter than that of the state of the model in continuous time calculated at the instants of sampling. An interesting behavior, evidenced in many works, is the loss of the property of observability of the state at low speed.

The Kalman Filter guarantees the optimal estimate for system models that are corrupted by uncorrelate additive white noise, both in the transient and the measurement systems. We will consider the stochastic discrete-time model, arising from (**??**) where the state and the output vectors are corrupted by the stochastic processes ζ_k and ξ_k:

1.6.1 Discrete-time mathematical model

A discrete time model corresponding to (0.6.4) can be obtained by using a first order Euler discretization. By choosing the stator current components as the system output, the discrete time model is given by:

$$\begin{aligned} \mathbf{x}_{k+1} &= \mathbf{A}_d\,\mathbf{x}_k + \mathbf{f}_d(\mathbf{x}_k) + \mathbf{B}_d\,\mathbf{u}_{s,k}\,, \\ \mathbf{y}_k &= \mathbf{C}_d\mathbf{x}_k\,, \end{aligned} \tag{1.6.1}$$

where matrices $\mathbf{A}_d$, $\mathbf{B}_d$, $\mathbf{C}_d$ and vector field $\mathbf{f}_d(\mathbf{x}_k)$ are:

$$\begin{gathered} \mathbf{A}_d = (\mathbf{I}_6 + T_s\,\mathbf{A}_c)\,,\quad f_d(\mathbf{x}_k) = T_s\,f_c(\mathbf{x}_k)\,, \\ \mathbf{B}_d = T_s\,\mathbf{B}_c\,,\quad \mathbf{C}_d = (\mathbf{I}_2, 0_{2\times 3}). \end{gathered} \tag{1.6.2}$$

T_s is the sampling time.

$$\begin{aligned} \mathbf{x}_{k+1} &= \mathbf{A}\,x_k + \mathbf{f}(x_k) + \mathbf{B}\,\mathbf{u}_{s,k} + \zeta_k\,, \\ \mathbf{y}_k &= \mathbf{C}\mathbf{x}_k + \xi_k\,, \end{aligned} \tag{1.6.3}$$

where ζ_k and ξ_k are the process and observation noises which are both assumed to be zero mean multivariate Gaussian noises with covariance Q_k and R_k respectively, which are assumed to be uncorrelated to each other and to other variables.

1.6.2 Structure of the filter

The Extended Kalman Filter designed for estimate the state $\mathbf{x}_k$ of the discrete time system (1.6.3), will be:

$$\hat{\mathbf{x}}_{k+1} = \mathbf{A}\,\hat{\mathbf{x}}_k + \mathbf{f}(\hat{k}) + \mathbf{B}\,\mathbf{u}_{s,k} + \mathbf{K}_k\,(\mathbf{y}_k - \mathbf{C}\,\hat{\mathbf{x}}_k)\ , \tag{1.6.4}$$

$\mathbf{K}_k$ is a gain matrix that must be appropriately updated in accordance with the following procedure.

The dynamics of the estimation error, $e_k = x_k - \hat{x}_k$, are determined by:

$$\mathbf{e}_{k+1} = \mathbf{A}\,\mathbf{e}_k + \mathbf{f}(\mathbf{x}_k) - \mathbf{f}(\hat{\mathbf{x}}_k) - \mathbf{K}_k\,\mathbf{C}\,\mathbf{e}_k + \zeta_k - \mathbf{K}_k\,\xi_k\,,$$

using the equation:

$$\mathbf{f}(\mathbf{x}_k) - \mathbf{f}(\hat{\mathbf{x}}_k) = \mathbf{J}(\hat{\mathbf{x}}_k)\,(\mathbf{x}_k - \hat{\mathbf{x}}_k) + \mathbf{h}(\mathbf{x}_k, \hat{\mathbf{x}}_k)\,, \tag{1.6.5}$$

then it follows that:

$$\mathbf{e}_{k+1} = (\mathbf{A}_k - \mathbf{K}_k\mathbf{C})\,\mathbf{e}_k + \mathbf{H}(\mathbf{e}_k)\,\mathbf{e}_k + \zeta_k - \mathbf{K}_k\,\xi_k \tag{1.6.6}$$

In this, $\mathbf{A}_k$ is determined at the state $\hat{\mathbf{x}}_k$ calculated by the Extended Kalman Filter. As usual, the covariance matrix of the error $\mathbf{e}_{k+1}$ can be obtained by omitting the nonlinear term $\mathbf{H}(\mathbf{e}_k)\,\mathbf{e}_k$ in(1.6.6), and it is thus given by:

$$\begin{aligned} \mathbf{P}_{k+1} &= (\mathbf{A}_k - \mathbf{K}_k\mathbf{C})\,\mathbf{P}_k\,(\mathbf{A}_k - \mathbf{K}_k\mathbf{C})^T + \mathbf{Q}_k + \\ &+ \mathbf{K}_k\mathbf{C}\mathbf{P}_k(\mathbf{A}_k - \mathbf{K}_k\mathbf{C})^T\,, \end{aligned} \tag{1.6.7}$$

$\mathbf{Q}_k$ is a positive definite matrix.

i.e. $\mathbf{Q}_k \geq \underline{q}\,I$, with $\underline{q} > 0$, for all time instants k, s.t.:

$$\mathbf{E}(\zeta_k\,\zeta_{k'}^T) = \mathbf{Q}_k\,\delta(k - k')$$

Minimizing $\mathbf{P}_{k+1}$ with respect to $\mathbf{K}_k$, the following expression for $\mathbf{K}_k$ is obtained:

$$\mathbf{K}_k = \mathbf{A}_k \mathbf{P}_k \mathbf{C}^T (\mathbf{C}\mathbf{P}_k \mathbf{C}^T + \mathbf{R}_k)^{-1}, \tag{1.6.8}$$

$\mathbf{R}_k$ is a positive definite matrix.

i.e. $\mathbf{R}_k \geq \underline{r}\,\mathbf{I}$, with $\underline{r} > 0$, for all time instants k, s.t.:

$$\mathbf{E}(\xi_k\, \xi_{k'}^T) = \mathbf{R}_k\, \delta(k - k')$$

Can be, therefore, take into account the following proposition:

Proposition 2. *The matrix* $\mathbf{A}_{s,k} = \mathbf{A}_k - \mathbf{K}_k\mathbf{C}$ *is bounded.*

i.e.:

$$||\mathbf{A}_{s,k}|| \leq S\,,$$

for all time instants k, where S is a positive real number.

1.7 Extended complex Kalman filter

In (1.6) was presented the Extended Kalman Filter, applied to a discrete time system, for estimating the state of an induction motor using the full order model.

In this section will be designed an Extended Complex Kalman Filter (ECKF) for estimating the state for a control system of an induction motor. Will be done exploiting the symmetries of the model and the complex version of the model (0.7.5)–(0.7.7).

For this reason a complex model (0.7.5)–(0.7.7) is taken.

This formulation allows a simpler observability analysis of the system and a more effective state estimation.

It is also shown that the complex implementation allows a reduction of the computation time with respect to the standard with real values. That is due at the lower dimensions of the matrices of the Extended Complex Kalman Filter respect the real-valued implementation. For the version complex of the extended Kalman filter no matrix inversion is required.

1.7.1 Filter derivation

To obtain an estimate of the discrete complex–valued state $\mathbf{x}$ of the nonlinear model (0.7.10), an extended complex Kalman filter has to be considered [70]. The filter has the same structure as a standard real EKF, except for the fact that the covariance matrix of the estimation error is Hermitian. in particular $\mathbf{P}_k = \mathbf{P}_k^H$, and the dynamical matrix of the underlying linearized model has complex-valued entries.

At first, a stochastic discrete-time model of the Induction Motor is obtained from (0.7.10), where the state and the output vectors are corrupted by the stochastic processes $\mathbf{w}_k$ and $\mathbf{v}_k$:

$$\begin{cases} \mathbf{x}_{k+1} = \mathbf{g}_k(\mathbf{x}_k, \mathbf{u}_k) + \mathbf{w}_k \,, \\ \mathbf{y}_k = \mathbf{h}_k + \mathbf{v}_k \,, \end{cases} \tag{1.7.1}$$

where $\mathbf{x}_k = (\mathbf{x}_{1,k}, \mathbf{x}_{2,k}, \mathbf{x}_{3,k})^T$, $\mathbf{w}_k$ and $\mathbf{v}_k$ are white Gaussian noise processes with covariance matrices given by $\mathbf{Q}_k$ and $\mathbf{R}_k$, respectively, and

$$h_k = x_{1,k} \,,$$

$$g_k = \begin{pmatrix} \tilde{a}_{11}\, x_{1,k} + \tilde{f}_1 (a_{22} - j\, x_{3,k})\, x_{2,k} + \tilde{f}_1\, u_k \\ \tilde{a}_{21}\, x_{1,k} + (1 - T_s\, a_{22} + j\, T_s\, x_{3,k})\, x_{2,k} \\ x_{3,k} \end{pmatrix} .$$

The processes $\mathbf{w}_k$ and $\mathbf{v}_k$ are assumed to be uncorrelated with each other and to the system state variables.

The Extended Complex Kalman Filter is described by the recursive algorithm involving *time* and *measurement update* phases.

$$\hat{\mathbf{x}}_{k+1|k} = \mathbf{g}_k(\hat{\mathbf{x}}_{k|k}, \mathbf{u}_k) \,, \tag{1.7.2}$$

During the k-th time update phase, estimates of the system state and of the error covariance matrix are computed as follows:

$$\mathbf{P}_{k+1|k} = \mathbf{F}_k\, \mathbf{P}_{k|k}\, \mathbf{F}_k^H + \mathbf{Q}_k \,, \tag{1.7.3}$$

where $\mathbf{F}_k$ is the dynamic matrix of the linearized model and is obtained by:

$$\mathbf{F}_k = \left.\frac{\partial \mathbf{g}_k(\mathbf{x}_k)}{\partial \mathbf{x}}\right|_{x=\hat{\mathbf{x}}_{k|k}} = \begin{pmatrix} \tilde{a}_{11} & \tilde{f}_1(a_{22} - j\,x_{3,k|k}) & -j\tilde{f}_1\,x_{2,k|k} \\ \tilde{a}_{21} & 1 - a_{22}\,T_s + j\,T_s\,x_{3,k|k} & j\,T_s\,x_{2,k|k} \\ 0 & 0 & 1 \end{pmatrix}.$$

During the k-th measurement update phase, a-posteriori estimates are computed as follows:

$$\hat{\mathbf{x}}_{k|k} = \hat{\mathbf{x}}_{k|k-1} + \mathbf{L}_k\left(\mathbf{y}_k - \mathbf{H}_k\,\hat{\mathbf{x}}_{k|k-1}\right), \tag{1.7.4}$$

$$\mathbf{P}_{k|k} = \mathbf{P}_{k|k-1} - \mathbf{L}_k\,\mathbf{H}_k\,\mathbf{P}_{k|k-1}, \tag{1.7.5}$$

where

$$L_k = P_{k|k-1}\,H_k^T\left(H_k\,P_{k|k-1}\,H_k^T + R_k\right)^{-1}, \tag{1.7.6}$$

and $\mathbf{H}_k$ is the output matrix of the linearized model and is given by:

$$\mathbf{H}_k = \left.\frac{\partial \mathbf{h}(\mathbf{x}_k)}{\partial \mathbf{x}}\right|_{\mathbf{x}=\hat{\mathbf{x}}_{k|k}} = \begin{bmatrix} 1 & 0 & 0 \end{bmatrix}.$$

The filter is initialized, at the instant $k = 0$, with $\hat{\mathbf{x}}_{0|0} = 0$ and $\mathbf{P}_{0|0} = \mathbf{P}_0$, where $\mathbf{P}_0 \in^{3\times 3}$ represents the initial estimate error covariance.

Remark 2. It is worth nothing that the following facts are the rational reasons for the processing time reduction:

1. The reduction of the order of the filter lead to a reduction of the number of operations as is shown in [37, Table 7.2], where the formulas presented demonstrate that the number of operations increase with the order of all the matrices involved.

2. No matrix inversion is required in the proposed Extended Complex Kalman Filter. Indeed in (1.7.6) the term $(\mathbf{H}_k\mathbf{P}_{k|k-1}\mathbf{H}_k^T + \mathbf{R}_k)$ is a scalar (it is a matrix in the 5^{th} order Extended Kalman Filter). Moreover this scalar is also real because $\mathbf{H}$ and $\mathbf{R}$ contain real elements and it is easy see that $\mathbf{P}$ matrix contains only real elements. The operation of matrix inversion that is necessary in the classic 5^{th} order Extended Kalman Filter is therefore translated in the inverse of a real number in the proposed Extended Complex Kalman Filter.

3. In the standard real-valued implementation the complexity of the model can be reduced taking into consideration that many elements of matrix **H** are zeros and manipulating the relations of the filter [43]. This fact is automatically included in the present complex formulation.

4. Matrices **Q**, **R**, $\mathbf{P}_{k|k}$, $\mathbf{P}_{k|k-1}$, $\mathbf{L}_k$ also have real elements in the complex form of the Extended Kalman Filter, while their order is 3 instead of 5, as in the standard real-valued implementation.

The problem of reducing the time of complexity of the estimation process has been treated by some authors, [44, 43]. In [43] a more efficient filtering process is proposed, which exploits the structural form of the Induction Motor model. In [44] an improvement of 25% is obtained by deriving a two-stage Extended Kalman Filter that is based on the procedure described in [51, 50] and uses suitable transformation matrices.

1.8 Robust Adaptive Kalman Filter

The Robust Adaptive Kalman Filter (RAKF) incorporates measurement and process noise covariance adaptation procedures (R and Q adaptation respectively) and utilizes adaptive factors in order to adjust itself against sensor/actuator faults. Thus the filter stands robust against the faults and even in case of sensor/actuator failure keeps providing accurate estimation results. In a single algorithm, the RAKF detects the fault, isolates it and applies the required adaptation process such that the estimation characteristic is not deteriorated. The performance of the proposed RAKF is investigated by simulations for the state estimation procedure of Induction Motor Control.

To remedy the inaccuracies of the model the descriptor form will be used [24, 5], because the terms of the physical parameters of the motor are expressed simply. For this reason we can take into account the uncertainties of the parameter of the motor. The model (0.6.4), expressed in terms of the "real" rotor flux, can be manipulated and expressed in the following descriptor form:

$$\sigma L_s \frac{i_{s,\alpha}}{dt} + \frac{L_r}{L_m}\frac{d\psi_{r,\alpha}}{dt} = -R_s i_{s,\alpha} + u_{s,\alpha}, \tag{1.8.1}$$

$$\sigma L_s \frac{i_{s,\beta}}{dt} + \frac{L_r}{L_m}\frac{d\psi_{r,\beta}}{dt} = -R_s i_{s,\beta} + u_{s,\beta}, \tag{1.8.2}$$

$$\frac{d\psi_{r,\alpha}}{dt} = \frac{L_m}{T_r} i_{s,\alpha} - \frac{1}{T_r}\psi_{r,\alpha} - \omega\psi_{r,\beta}, \tag{1.8.3}$$

$$\frac{d\psi_{r,\beta}}{dt} = \frac{L_m}{T_r} i_{s,\beta} - \frac{1}{T_r}\psi_{r,\beta} + \omega\psi_{r,\alpha}, \tag{1.8.4}$$

$$J_m \frac{d\omega_r}{dt} = -b_r\omega_r + k_t\left(\psi_{r,\alpha} i_{s,\beta} - \psi_{r,\beta} i_{s,\alpha}\right) - t_l, \tag{1.8.5}$$

$$z = \begin{bmatrix} i_{s,\alpha} & i_{s,\beta} \end{bmatrix}^T. \tag{1.8.6}$$

where $k_t = 2pL_m/(3L_r)$, and $z(t)$ is the output vector.

The coefficients appearing in the model (1.8.1)–(1.8.6), have simple expressions in terms of the physical parameters of the motor.

For example, looking at model (1.8.1)–(1.8.6), a variation in σLs produces variations in the first two terms of (1.8.1) and (1.8.2). Considering the usual model of the motor, the same variation in parameter σLs produces variations in all of the coefficients of the differential equations expressing the dynamics of the stator currents and in two terms of the equations expressing the dynamics of the rotor flux components. Moreover all the coefficients are functions of one or two electrical parameters, and for this reason the uncertainties of the model can easily be taken into consideration. This introduces robustness into the descriptor form compared to the conventional one.

1.8.1 Description of the model uncertainties

The model (1.8.1)–(1.8.6) is nonlinear, multi variable and affected by parametric uncertainties.

Moreover, the load torque t_l is unknown. For estimating speed, two approaches can be employed.

The first approach is based on the assumption that speed varies slowly in relation to the electromagnetic variables; this suggests that $\dot{\omega} = 0$ should substitute equation (1.8.5), thus obtaining the fifth-order model.

The second approach leads to a sixth-order model in which the load torque is assumed

as a slow variable and, consequently, the five-order state of the system (1.8.1)–(1.8.6) is augmented by the variable t_l whose dynamics are expressed by $\dot{t}_l = 0$.

The resulting model is nonlinear and requires an Extended Kalman Filter.

These two approaches are the ones followed in Sections 1.5 and 1.6 for designing the EKF ($\dot{t}_l = 0$) and the ECKF ($\dot{\omega} = 0$).

In this context we use an alternative approach for estimating the speed. This approach is based on the assumption that speed is a parameter in equations (1.8.3)–(1.8.4) of the model.

For this reason we consider only the model consisting of the linear equations (1.8.1)–(1.8.4) and (1.8.6) for designing the Robust Adaptive Kalman Filter.

The mathematical model (1.8.1)–(1.8.4) and (1.8.6) in the compact matricial form and including stochastic uncertainties, can be written in the following descriptor form:

$$\tilde{\mathbf{E}}\dot{\mathbf{x}}(t) = \tilde{\mathbf{F}}(t)\mathbf{x}(t) + \tilde{\mathbf{B}}\mathbf{u}(t) + \tilde{\mathbf{Q}}w(t), \tag{1.8.7}$$

$$\mathbf{z}(t) = \mathbf{H}\mathbf{x}(t) + \mathbf{R}v(t) \tag{1.8.8}$$

where $\mathbf{x}(t)$ and $\mathbf{u}(t)$ are the state and input vectors, which are the same as with the other conventional models used up to now; $w(t)$ and $v(t)$ are the system and measurement noises assumed zero-mean white noises uncorrelated with each other and with the other variables, having covariance matrices equal to I_4 and I_2, respectively, $\tilde{Q}$ and R are diagonal square matrices of suitable dimensions, and the matrices $\tilde{E}$, $\tilde{B}$, $\tilde{F}(t)$ and H are given by:

$$\tilde{\mathbf{E}} = \begin{bmatrix} \sigma L_s & 0 & \frac{L_r}{L_m} & 0 \\ 0 & \sigma L_s & 0 & \frac{L_r}{L_m} \\ 0 & 0 & 1 & 0 \\ 0 & 0 & 0 & 1 \end{bmatrix}, \quad \tilde{\mathbf{B}} = \begin{bmatrix} 1 & 0 \\ 0 & 1 \\ 0 & 0 \\ 0 & 0 \end{bmatrix},$$

$$\tilde{\mathbf{F}}(t) = \begin{bmatrix} -R_s & 0 & 0 & 0 \\ 0 & -R_s & 0 & 0 \\ \frac{L_m}{T_r} & 0 & -\frac{1}{T_r} & -\omega(t) \\ 0 & \frac{L_m}{T_r} & \omega(t) & -\frac{1}{T_r} \end{bmatrix}, \quad \mathbf{H} = \begin{bmatrix} 1 & 0 & 0 & 0 \\ 0 & 1 & 0 & 0 \end{bmatrix}.$$

Remark 3. The coefficients appearing in the model (1.8.1)–(1.8.4), and consequently in (1.8.7)–(1.8.8), have simple expressions in terms of the physical parameters of the motor. referring to

the model (1.8.1)–(1.8.4), a variation in σL_s produces variations in the first two terms of (1.8.1) and (1.8.2). Whereas when considering the usual model of the motor, the same variation in parameter σL_s produces variations in all of the the coefficients of the differential equations expressing the dynamics of the stator currents and in two terms of the equations expressing the dynamics of the rotor flux components. Although this introduces more robustness into the descriptor form of Kalman Filter compared to the conventional one. A robust descriptor of the Kalman Filter is designed for estimating the stator currents and the rotor flux.

Remark 4. The matrices $\tilde{\mathbf{B}}$ and $\mathbf{H}$ are not affected by uncertainties.

Remark 5. Matrix $\tilde{\mathbf{F}}(t)$ is time-varying because it depends on the speed $\omega(t)$. Matrix $\tilde{\mathbf{E}}$ is always non singular.

The following discrete-time stochastic model is obtained by using the Euler method, from the model (1.8.7)–(1.8.8):

$$\mathbf{E}x_{k+1} = \mathbf{F}_k x_k + \mathbf{B}u_k + \mathbf{Q}w_k, \tag{1.8.9}$$

$$\mathbf{z}_k = \mathbf{H}x_k + \mathbf{R}\mathbf{v}_k. \tag{1.8.10}$$

where $k := kT_s$ $(k \in \mathbb{Z})$ is the current discrete time. T_s is the sampling time, and $E = \tilde{E}$, $F_k = \tilde{E} + T_s\tilde{F}_k$, $\tilde{F}_k = \tilde{F}(kT_s)$, $B = T_s\tilde{B}$, $Q = T_s\tilde{Q}$.

The values of the electromagnetic parameters are different from the respective nominal values. Denoting the corresponding variations of matrices $\mathbf{E}$ and $\mathbf{F}_k$ with $\delta\mathbf{E}_k$ and $\delta\mathbf{F}_k$, the equation (1.8.9) becomes:

$$(\mathbf{E} + \delta\mathbf{E}_k)\,\mathbf{x}_{k+1} = (\mathbf{F}_k + \delta\mathbf{F}_k)\,\mathbf{x}_k + \mathbf{B}u_k + \mathbf{Q}w_k. \tag{1.8.11}$$

The equation (1.8.10) remains unchanged because $\mathbf{H}$ and $\mathbf{R}$ are constant. The matrices $\delta\mathbf{E}_k$ and $\delta\mathbf{F}_k$ are given by:

$$\delta\mathbf{E}_k = \begin{bmatrix} \delta(\sigma L_s) & 0 & \delta(\frac{L_r}{L_m}) & 0 \\ 0 & \delta(\sigma L_s) & 0 & \delta(\frac{L_r}{L_m}) \\ 0 & 0 & 0 & 0 \\ 0 & 0 & 0 & 0 \end{bmatrix},$$

$$\delta \mathbf{F}_k = \delta \mathbf{E}_k + T_s \delta \tilde{\mathbf{F}}_k,$$

where:

$$\delta \tilde{\mathbf{F}}_k = \begin{bmatrix} \delta(R_s) & 0 & 0 & 0 \\ 0 & \delta(R_s) & 0 & 0 \\ \delta(\frac{L_m}{T_r}) & 0 & \delta(\frac{1}{T_r}) & 0 \\ 0 & \delta(\frac{L_m}{T_r}) & 0 & \delta(\frac{1}{T_r}) \end{bmatrix}.$$

Usually, uncertainties for descriptor type models are represented in the following standard form:

$$\begin{bmatrix} -\delta \mathbf{F}_k & \delta \mathbf{E}_{k+1} \\ 0 & \delta \mathbf{H}_k \end{bmatrix} = \begin{bmatrix} \mathbf{M}_{f,k} & 0 \\ 0 & \mathbf{M}_{h,k} \end{bmatrix} \Delta_k \begin{bmatrix} -\mathbf{N}_{f,k} & \mathbf{N}_{e,k+1} \\ 0 & \mathbf{N}_{h,k} \end{bmatrix}, \tag{1.8.12}$$

where Δ_k is a bounded arbitrary contraction with $||\Delta_k||_\infty \leq 1$, and $\mathbf{M}_{f,k}$, $\mathbf{M}_{h,k}$, $\mathbf{N}_{f,k}$, $\mathbf{N}_{e,k+1}$ and $\mathbf{N}_{h,k}$ are known matrices. In our case, since $\delta \mathbf{H}_k = 0 \ \forall k \in \mathbb{Z}$, we have:

$$\mathbf{M}_{f,k} = \mathbf{I}_4, \ \ \mathbf{M}_{h,k} = \mathbf{I}_2, \ \ \mathbf{N}_{f,k} = \max_k ||\delta \mathbf{F}_k||,$$

$$\mathbf{N}_{e,k+1} = \max_k ||\delta \mathbf{E}_k||, \ \ \mathbf{N}_{h,k} = 0.$$

The dynamic model of the magnetizing current in a rotating reference frame (rotating at speed ω_0) can be derived from [80, Equations 6.1-17]:

$$\frac{di_{mr,d}}{dt} = \frac{1}{T_r^*} i_{s,d} - \frac{1}{T_r^*} i_{mr,d} + \frac{T_r}{T_r^*}(\omega_0 - \omega) i_{mr,q}, \tag{1.8.13}$$

$$\frac{di_{mr,q}}{dt} = \frac{1}{T_r^*} i_{s,q} - \frac{1}{T_r^*} i_{mr,q} - \frac{T_r}{T_r^*}(\omega_0 - \omega) i_{mr,d}, \tag{1.8.14}$$

where the modified rotor time constant T_r^* is:

$$T_r^* = T_r \frac{L}{L_m}, \tag{1.8.15}$$

while L is called dynamic magnetizing inductance and is equal to:

$$L = L_m + |i_{mr}| \frac{dL_m}{d|i_{mr|}}. \tag{1.8.16}$$

If the parameters a_{11}, a_{12}, a_{21} and a_{22} in (0.7.2) are rewritten replacing the rotor time constant

T_r with the modified rotor time constant T_r^* as follows:

$$a_{11}^* = \frac{R_s}{\sigma L_s} + \frac{1-\sigma}{\sigma T_r^*},\ a_{12}^* = \frac{1}{\sigma L_s T_r^*},\ a_{21}^* = L_s \frac{1-\sigma}{T_r^*},\ a_{22}^* = \frac{1}{T_r^*}, \tag{1.8.17}$$

then equations [80, Equations 6.1-11, 6.1-12] can be manipulated as follows, in order to obtain the two scalar equations of the two stator current components in the state-space form. In particular the two stator current equations can be written in a generic rotating reference frame (rotating at speed ω_0) as:

$$\begin{aligned}\frac{di_{s,d}}{dt} =& - c_1 i_{s,d} + (\omega_0 + c_2 T_r(\omega_0 - \omega))\, i_{s,q} + c_3 i_{mr,d} - ((c_3 T_r - a_{21}^* f_1 T_r^*)\, \omega_0 - c_3 T_r \omega)\, i_{mr,q} \\ & - c_2 \frac{i_{s,d}^2}{i_{mr,d}} + f_1 u_{s,d}, \end{aligned} \tag{1.8.18}$$

$$\begin{aligned}\frac{di_{s,q}}{dt} =& - c_1 i_{s,q} - (\omega_0 + c_2 T_r(\omega_0 - \omega))\, i_{s,d} + c_3 i_{mr,q} + ((c_3 T_r - a_{21}^* f_1 T_r^*)\, \omega_0 - c_3 T_r \omega)\, i_{mr,d} \\ & - c_2 \frac{i_{s,q}^2}{i_{mr,d}} + f_1 u_{s,q}, \end{aligned} \tag{1.8.19}$$

with:

$$c_1 = a_{11}^* + a_{12}^*(\Delta L - 2\Delta L^*), \tag{1.8.20}$$

$$c_2 = a_{12}^* \Delta L^*, \tag{1.8.21}$$

$$c_3 = a_{21}^* f_1 + a_{12}^*(\Delta L - \Delta L^*), \tag{1.8.22}$$

where $\Delta L = L - L_m$ and $\Delta L^* = \frac{L_{\sigma r}^2}{L_r^2} \Delta L$.

To avoid the formulation of problems that are too complex, it is convenient to analyze the parameter variations due to the increase in temperature and magnetic saturation. The changement of the temperature produces variation in rotor and stator resistances. However, rotor resistance also varies with the slip and consequently with load. For consider the magnetic saturation effects with accuracy, must be constructed more complex mathematical models (1.8.13)-(1.8.14) and (1.8.18)-(1.8.19). But these models generally lead to complex controllers. In usual cases, the saturation is considered assuming that it leads to a reduction of the mutual inductance L_m. Consequently, the saturation affects the values of the rotor and stator inductances given by:

$$L_r = L_{\sigma r} + L_m, \tag{1.8.23}$$

$$L_s = L_{\sigma s} + L_m. \tag{1.8.24}$$

where $L_{\sigma r} = \sigma_r L_m$ and $L_{\sigma s} = \sigma_s L_m$ are the rotor and stator leakage inductances, respectively, assumed to be constant because we are interested in the saturation of the flux main path. The values of the leakage inductances are small in relation to L_m, then we have $\delta(\sigma L_s) \ll \sigma L_s$, $\delta\left(\frac{L_m}{L_r}\right) \ll \frac{L_m}{L_r}$ and $\delta\left(\frac{L_m}{T_r}\right) \cong \frac{L_m}{L_r}\delta(R_r)$.

It follows that:

$$\mathbf{E} + \delta\mathbf{E}_k \cong \mathbf{E}, \;\; \mathbf{F}_k + \delta\mathbf{F}_k \cong \mathbf{E} + T_s(\tilde{\mathbf{F}}_k + \delta\tilde{\mathbf{F}}_k).$$

In order to set magnetic parameter variations, after the computation of $L_{\sigma r}$ and $L_{\sigma s}$ from the nominal values of the parameters, for a given percentage variation of L_m, the values of L_r and L_s are obtained using (1.8.23) and (1.8.24).

1.8.2 Problem formulation

For estimate the rotor flux components and the speed of an induction motor-load system, need to solving two linear least-squares subproblems. More precisely, assuming knowledge of the speed, denoted by $\hat{\omega}_k$, at instant k, the first subproblem is that of estimating the state of the model (1.8.9)–(1.8.10) by means of a descriptor Kalman filter, by solving the following minimization problem:

$$\min_{x_0} \left[||x_0||^2_{P_0^{-1}} + ||z_0 - Hx_0||^2_{R^{-1}} \right] \quad \text{for } k = 0 \tag{1.8.25}$$

$$\min_{x_k, x_{k+1}} \Big[||x_k - \hat{x}_{k|k}||^2_{P^{-1}_{k|k}} + ||Ex_{k+1} - (F_k x_k + Bu_k)||^2_{Q^{-1}} + ||z_{k+1} - Hx_k||^2_{R^{-1}} \Big] \quad \text{for } k > 0 \tag{1.8.26}$$

For the second subproblem, using the Eulero method, the last two equations of (1.8.9), expressing the dynamics of the rotor flux components, can be rewritten in the matrix form:

$$\begin{bmatrix} -T_s\psi_{r,\beta}(k) \\ T_s\psi_{r,\alpha}(k) \end{bmatrix} \omega_k = \begin{bmatrix} \psi_{r,\alpha}(k+1) - w_1\psi_{r,\alpha}(k) - w_2 i_{s,\alpha}(k) \\ \psi_{r,\beta}(k+1) - w_1\psi_{r,\beta}(k) - w_2 i_{s,\beta}(k) \end{bmatrix}, \tag{1.8.27}$$

where $w_1 = 1 - \frac{1}{T_r}T_s$ and $w_2 = \frac{L_m}{T_r}T_s$, and the values of the rotor flux components are given from the solution of the first subproblem (see next Section). From (1.8.27), the formulation

of the second subproblem is as follows:

$$\min_{\hat{\omega}_k} \|\hat{\Phi}_k \hat{\omega}_k - \hat{y}_k\|^2 \quad \text{for } k \geq 0, \tag{1.8.28}$$

where:

$$\hat{\Phi}_k = \begin{bmatrix} -T_s \hat{\psi}_{r,\beta}(k) \\ T_s \hat{\psi}_{r,\alpha}(k) \end{bmatrix},$$

$$\hat{y}_k = \begin{bmatrix} \hat{\psi}_{r,\alpha}(k+1) - w_1 \hat{\psi}_{r,\alpha}(k) - w_2 i_{s,\alpha}(k) \\ \hat{\psi}_{r,\beta}(k+1) - w_1 \hat{\psi}_{r,\beta}(k) - w_2 i_{s,\beta}(k) \end{bmatrix}.$$

Since the objective is to take into consideration the model uncertainties (cf. model (1.8.11)), we need to modify the formulation (1.8.25)–(1.8.26) into the following robust version:

$$\min_{x_0} \left[||x_0||^2_{P_0^{-1}} + ||z_0 - Hx_0||^2_{R^{-1}} \right] \quad \text{for } k = 0, \tag{1.8.29}$$

$$\min_{x_k, x_{k+1}} \max_{\delta \mathbf{F}_k, \delta \mathbf{E}_k} \Big[||x_k - \hat{x}_{k|k}||^2_{\mathbf{P}^{-1}_{k|k}} + ||(\mathbf{E} + \delta \mathbf{E}_k) x_{k+1} -$$

$$\big((\mathbf{F}_k + \delta \mathbf{F}_k) x_k + \mathbf{B} u_k\big)||^2_{\mathbf{Q}^{-1}} + ||\mathbf{z}_{k+1} - \mathbf{H} x_k||^2_{\mathbf{R}^{-1}} \Big] \text{ for } k > 0. \tag{1.8.30}$$

Equation (1.8.28) can be solved using least-squares methods (cfr. the following section).

1.8.3 Descriptor Kalman filter

Let us suppose ω_k is known and in (1.8.9)-(1.8.10) the matrix $\begin{bmatrix} \mathbf{E}^T & \mathbf{H}^T \end{bmatrix}^T$ is full column rank, the recursive filtered estimate $\hat{x}_{k|k}$ of the state x_k, solution of the problem (1.8.25)–(1.8.26), is given by the following algorithm [55].
At the instant $k = 0$ the algorithm is initialized with

$$\mathbf{P}_{0|0} = \left[\mathbf{P}_0^{-1} + \mathbf{H}^T \mathbf{R}^{-1} \mathbf{H} \right]^{-1}, \quad \hat{x}_{0|0} = \mathbf{P}_{0|0} + \mathbf{H}^T \mathbf{R}^{-1} z_0.$$

Then, at step k, update $\left\{ \hat{x}_{k|k}, \mathbf{P}_{k|k} \right\}$ to $\left\{ \hat{x}_{k+1|k+1}, \mathbf{P}_{k+1|k+1} \right\}$ as follows:

$$\mathbf{P}_{k+1|k+1} = \left[\mathbf{E}^T \left(\mathbf{Q} + \mathbf{F}_k \mathbf{P}_{k|k} \mathbf{F}_k^T \right)^{-1} \mathbf{E} + \mathbf{H}^T \mathbf{R}^{-1} \mathbf{H} \right]^{-1}, \tag{1.8.31}$$

$$\hat{x}_{k+1|k+1} = \mathbf{P}_{k+1|k+1}\left[\mathbf{E}^T\left(\mathbf{Q} + \mathbf{F}_k\mathbf{P}_{k|k}\mathbf{F}_k^T\right)^{-1}\left(\mathbf{F}_k\hat{x}_{k|k} + \mathbf{B}u_k\right) + \mathbf{H}^T\mathbf{R}^{-1}z_{k+1}\right]. \tag{1.8.32}$$

The algorithm (1.8.31)–(1.8.32) can be obtained as a solution of the following regularized least-squares problem:

$$\min_x = \left[x^T\mathbf{Q}x + (\mathbf{A}x - b)^T\mathbf{W}(\mathbf{A}x - b)\right], \tag{1.8.33}$$

where x^TQx is a regularization term, and $\mathbf{Q} = \mathbf{Q}^T > 0$ and $\mathbf{W} = \mathbf{W}^T \geq 0$ are weight matrices; $x \in \mathbb{R}^n$ is the unknown vector, $\mathbf{A} \in \mathbb{R}^{n\times n}$ is the data matrix and $b \in \mathbb{R}^{n\times 1}$ is the observation vector. The solution of (1.8.33), is:

$$\hat{x} = \left[\mathbf{Q} + \mathbf{A}^T\mathbf{W}\mathbf{A}\right]^{-1}\mathbf{A}^T\mathbf{W}b. \tag{1.8.34}$$

The problem (1.8.26) can be rewritten in the regularized least-squares form (1.8.33) with the following identifications:

$$\begin{gathered}
\mathbf{A} \leftarrow \begin{bmatrix} -\mathbf{F}_k & \mathbf{E} \\ 0 & \mathbf{H} \end{bmatrix}, \quad \mathbf{b} \leftarrow \begin{bmatrix} \mathbf{F}_k\hat{x}_{k|k} + \mathbf{B}\mathbf{u}_k \\ \mathbf{z}_{k+1} \end{bmatrix}, \\
\mathbf{W} \leftarrow \begin{bmatrix} -\mathbf{Q}^{-1} & 0 \\ 0 & \mathbf{R}^{-1} \end{bmatrix}, \mathbf{Q} \leftarrow \begin{bmatrix} -\mathbf{P}_{k|k}^{-1} & 0 \\ 0 & 0 \end{bmatrix}, \\
x \leftarrow \begin{bmatrix} -x_k - \hat{x}_{k|k} \\ x_{k+1} \end{bmatrix}.
\end{gathered} \tag{1.8.35}$$

Consequently, (1.8.34) with the identification (1.8.35) leads to the time and measurement-update of the Kalman filter (1.8.31)-(1.8.32).

1.8.4 Robust Descriptor Kalman filter

Consider the following robust version of the optimization problem (1.8.33):

$$\min_x \max_{\delta\mathbf{A},\delta\mathbf{b}} = \left[\|x\|_{\mathbf{Q}}^2 + \|(\mathbf{A} + \delta\mathbf{A})x - (\mathbf{b} + \delta\mathbf{b})\|_{\mathbf{W}}^2\right], \tag{1.8.36}$$

where $\{\delta\mathbf{A}, \delta\mathbf{b}\}$ are uncertainties modeled by:

$$\begin{bmatrix}\delta\mathbf{A} & \delta\mathbf{b}\end{bmatrix} = \mathbf{M}\Delta\begin{bmatrix}\delta\mathbf{N}_a & \delta\mathbf{N}_b\end{bmatrix}, \tag{1.8.37}$$

where $||\Delta||_\infty \leq 1$. The solution of (1.8.36) is given by:

$$\hat{x} = \left[\hat{\mathbf{Q}} + \mathbf{A}^T\hat{\mathbf{W}}\mathbf{A}\right]^{-1}\left[\mathbf{A}^T\hat{\mathbf{W}}\mathbf{b} + \hat{\lambda}\mathbf{N}_a^T\mathbf{N}_b^T\right], \tag{1.8.38}$$

where $\{\hat{\mathbf{Q}}, \hat{\mathbf{W}}\}$ are defined as follows:

$$\hat{\mathbf{Q}} = \mathbf{Q} - \hat{\lambda}^{-1}\mathbf{N}_a^T\mathbf{N}_a, \tag{1.8.39}$$

$$\hat{\mathbf{W}} = \mathbf{W} + \mathbf{W}\mathbf{M}\left(\hat{\lambda}\mathbf{I} - \mathbf{M}^T\mathbf{W}\mathbf{M}\right)\mathbf{M}^T\mathbf{W}, \tag{1.8.40}$$

$\hat{\lambda}$ is a non negative scalar parameter obtained by solving the following optimization problem [55]:

$$\hat{\lambda} = \arg\min_{\lambda \geq \|\mathbf{M}^T\mathbf{W}\mathbf{M}\|} G(\lambda), \tag{1.8.41}$$

where:

$$G(\lambda) = \|x(\lambda)\|_{\mathbf{Q}^2} - \lambda\|\mathbf{N}_a x(\lambda) - \mathbf{N}_b\|^2 + \|\mathbf{A}x(\lambda) - \mathbf{b}\|^2_{\mathbf{W}(\lambda)},$$

$$x(\lambda) := \left[\mathbf{Q}(\lambda) + \mathbf{A}^T\mathbf{W}(\lambda)\mathbf{A}\right]^{-1}\left[\mathbf{A}^T\mathbf{W}(\lambda)\mathbf{b} + \lambda\mathbf{N}_a^T\mathbf{N}_b\right],$$

$$\mathbf{Q}(\lambda) := \mathbf{Q} - \lambda^{-1}\mathbf{N}_a^T\mathbf{N}_a,$$

$$\mathbf{W}(\lambda) := \mathbf{W} + \mathbf{W}\mathbf{M}\left(\lambda\mathbf{I} - \mathbf{M}^T\mathbf{W}\mathbf{M}\right)\mathbf{M}^T\mathbf{W},$$

Now, the min-max problem (1.8.30) can be rewritten as problem (1.8.36) by means of the following identifications:

$$\mathbf{A} \leftarrow \begin{bmatrix}-\mathbf{F}_k & \mathbf{E} \\ 0 & \mathbf{H}\end{bmatrix}, \quad \mathbf{b} \leftarrow \begin{bmatrix}\mathbf{F}_k\hat{\mathbf{x}}_{k|k} + \mathbf{B}\mathbf{u}_k \\ \mathbf{z}_{k+1}\end{bmatrix},$$

$$\mathbf{W} \leftarrow \begin{bmatrix}-\mathbf{Q}^{-1} & 0 \\ 0 & \mathbf{R}^{-1}\end{bmatrix}, \quad \mathbf{Q} \leftarrow \begin{bmatrix}-\mathbf{P}_{k|k}^{-1} & 0 \\ 0 & 0\end{bmatrix},$$

$$\delta\mathbf{A} \leftarrow \begin{bmatrix} -\delta\mathbf{F}_k & \delta\mathbf{E} \\ 0 & 0 \end{bmatrix}, \ \delta\mathbf{b} \leftarrow \begin{bmatrix} \delta\mathbf{F}_k\hat{x}_{k|k} \\ 0 \end{bmatrix}, \tag{1.8.42}$$

$$\mathbf{N}_a \leftarrow \begin{bmatrix} -\mathbf{N}_{f,k} & \mathbf{N}_e \\ 0 & 0 \end{bmatrix}, \ \mathbf{N}_b \leftarrow \begin{bmatrix} \mathbf{N}_{f,k}\hat{x}_{k|k} \\ 0 \end{bmatrix},$$

$$\mathbf{M} \leftarrow \begin{bmatrix} -\mathbf{M}_f & 0 \\ 0 & \mathbf{N}_f \end{bmatrix}, \ x \leftarrow \begin{bmatrix} -x_k - \hat{x}_{k|k} \\ x^{k+1} \end{bmatrix}.$$

and the initial conditions are:

$$\mathbf{A} \leftarrow \mathbf{H}, \ \mathbf{b} \leftarrow \mathbf{z}_0, \ \delta\mathbf{A} \leftarrow 0, \ \delta\mathbf{b} \leftarrow 0, \ \mathbf{Q} \leftarrow \mathbf{P}_0^{-1},$$

$$\mathbf{M} \leftarrow \mathbf{M}_h, \ \mathbf{N}_a \leftarrow 0, \ \mathbf{N}_b \leftarrow 0.$$

From (1.8.38) and the identifications (1.8.42), the filtered robust optimum estimate $\hat{x}_{k|k}$ is obtained from the following recursive algorithm:

At instant $k = 0$ the algorithm is initialized with:

$$\mathbf{P}_{0|0} = \left[\mathbf{P}_0^{-1} + \mathbf{H}^T\hat{\mathbf{R}}^{-1}\mathbf{H}\right]^{-1},$$

$$\hat{x}_{0|0} = \mathbf{P}_{0|0} + \mathbf{H}^T\hat{\mathbf{R}}^{-1}z_0,$$

$$\hat{\mathbf{R}} = \mathbf{R} - \hat{\lambda}_{-1}^{-1}\mathbf{I}_2,$$

where $\hat{\lambda}_{-1}$ is obtained by minimizing the function $G(\lambda)$ (cf. (1.8.41)) with the identification (1.8.42) over the interval $\hat{\lambda}_{-1} > \lambda_l = \|\mathbf{R}^{-1}\|$.

Then, at step k, update $\left\{\hat{x}_{k|k}, \mathbf{P}_{k|k}\right\}$ to $\left\{\hat{x}_{k+1|k+1}, \mathbf{P}_{k+1|k+1}\right\}$ as follows:

$$\mathbf{P}_{k+1|k+1} = \left[\hat{\mathbf{E}}_{k+1}^T\left(\hat{\boldsymbol{\mathcal{Q}}}_k + \hat{\mathbf{F}}_k\mathbf{P}_{k|k}\hat{\mathbf{F}}_k^T\right)^{-1}\hat{\mathbf{E}}_{k+1} + \hat{\mathbf{H}}^T\hat{\boldsymbol{\mathcal{R}}}_{k+1}^{-1}\hat{\mathbf{H}}\right]^{-1}, \tag{1.8.43}$$

$$\hat{x}_{k+1|k+1} = \mathbf{P}_{k+1|k+1}\left[\hat{\mathbf{E}}_{k+1}^T\left(\hat{\boldsymbol{\mathcal{Q}}}_k + \hat{\mathbf{F}}_k\mathbf{P}_{k|k}\hat{\mathbf{F}}_k^T\right)^{-1}\left(\hat{\mathbf{F}}_k\hat{x}_{k|k} + \hat{\mathbf{B}}u_k\right) + \hat{\mathbf{H}}^T\hat{\boldsymbol{\mathcal{R}}}_{k+1}^{-1}\mathbf{z}_{k+1}\right], \tag{1.8.44}$$

where:

$$\hat{\mathbf{Q}}_k = \mathbf{Q} - \hat{\lambda}_k^{-1}\mathbf{I}_4, \ \hat{\boldsymbol{\mathcal{Q}}}_k = \begin{bmatrix} \hat{\mathbf{Q}}_k & 0 \\ 0 & \mathbf{I}_4 \end{bmatrix}, \ \hat{\mathbf{E}}_{k+1} = \begin{bmatrix} \mathbf{E} \\ \sqrt{\hat{\lambda}_k^{-1}}\mathbf{N}_e \end{bmatrix},$$

$$\hat{\mathbf{F}}_k = \begin{bmatrix} \mathbf{F}_k \\ \sqrt{\hat{\lambda}_k^{-1}}\mathbf{N}_{f,k} \end{bmatrix}, \quad \hat{\mathbf{H}} = \begin{bmatrix} \mathbf{H} \\ 0_{2\times 4} \end{bmatrix}, \quad \hat{\mathbf{B}} = \begin{bmatrix} \mathbf{B} \\ 0_{4\times 2} \end{bmatrix},$$

$$\hat{\mathbf{R}}_{k+1} = \mathbf{R} - \hat{\lambda}_k^{-1}\mathbf{I}_2, \; \hat{\boldsymbol{\mathcal{R}}}_{k+1} = \begin{bmatrix} \hat{\mathbf{R}}_{k+1} & 0 \\ 0 & \mathbf{I}_2 \end{bmatrix}. \tag{1.8.45}$$

and $\hat{\lambda}_k$ is obtained by minimizing the function $G(\lambda)$ (cf. (1.8.41)) with the identification (1.8.42) over the interval $\hat{\lambda}_k > \lambda_l = \left\| diag\{\mathbf{Q}^{-1}, \mathbf{R}^{-1}\} \right\|$.

Computation of $\hat{\lambda}_k$ can be carried out by means of the above described optimization procedure. However, in [75] the choice of $\hat{\lambda}_k$ as follows is proposed:

$$\hat{\lambda}_k = \hat{\lambda} = \begin{cases} (1+0,5)\lambda_l, & \text{for } \lambda_l \neq 0 \\ 0, & \text{for } \lambda_l = 0 \end{cases} \tag{1.8.46}$$

which allows the off-line computation of several of the above matrices, increasing the efficiency of the algorithm in terms of time consumption.

Remark 6. From (1.8.43) and (1.8.44), it is easy to verify that for descriptor systems without uncertainties ($\mathbf{M}_{f,k} = 0$, $\mathbf{M}_{h,k} = 0$, $\mathbf{N}_{f,k} = 0$, $\mathbf{N}_{e,k+1} = 0$, $\mathbf{N}_{h,k} = 0$) this algorithm collapses to DKF (1.8.31)–(1.8.32).

Remark 7. The main difference between the robust filter and the standard one is that in the robust algorithm, the new recursion operates on system and noise covariance matrices, modified in relation to the given nominal values. More precisely, the algorithm updates these matrices to the values necessary for obtaining robust estimation.

1.8.5 Speed estimation

The problem (1.8.28) could be solved by means of the OLS (ordinary least-squares) method as follows:

$$P_{\omega,k+1}^{-1} = \tau P_{\omega,k}^{-1} + \hat{\Phi}_k^T \hat{\Phi}_k, \tag{1.8.47}$$

$$\hat{\omega}_{k+1} = \hat{\omega}_k + P_{\omega,k+1}\hat{\Phi}_k^T \left(\hat{\Phi}_k \hat{\omega}_k - \hat{y}_k \right), \tag{1.8.48}$$

where $\tau < 1$ is the forgetting factor, and the algorithm is initialized with $P_{\omega,0} = P_0$ for some $P_0 > 0$ and $\hat{\omega}_0 = 0$.

Remark 8. The forgetting factor τ is introduced in (1.8.47), in order to avoid that for $\tau = 1$, $P_{\omega,k}^{-1}$ increases linearly, which implies that $P_{\omega,k}$ converges to zero for $k \to \infty$; this in turn implies that, during speed transients, the estimated speed tracks the actual one very slowly.

As is well known, the OLS algorithm assumes that $\hat{\Phi}_k$ is not affected by errors, and errors are confined to $\hat{y}_k$. However, this hypothesis does not correspond to our case, because estimation and modelling errors also cause errors in $\hat{\Phi}_k$. Therefore, in this application the use of TLS (Total Least-Squares) is better because it also takes into account errors in the data matrix. In fact, estimated rotor flux present in $\hat{\Phi}_k$ is affected both by modeling errors and noise, in a similar way to the observation vector. Consequently, instead of (1.8.28), a TLS problem is solved by minimizing the following modified cost function:

$$\min_{\hat{\omega}_k} \frac{\|\hat{\Phi}_k \hat{\omega}_k - \hat{y}_k\|^2}{1 + \hat{\omega}_k^2}. \tag{1.8.49}$$

The adaptation law that minimizes (1.8.49) is [18]:

$$\hat{\omega}_{k+1} = \hat{\omega}_k - \alpha_k \Gamma_k^T \hat{\Phi}_k + \alpha_k \hat{\Phi}_k^T \hat{\Phi}_k \hat{\omega}_k, \tag{1.8.50}$$

where α_k is a positive constant and Γ_k is given by:

$$\Gamma_k = \frac{\Delta_k}{1 + \hat{\omega}_k^2}, \quad \Delta_k = \hat{\Phi}_k \hat{\omega}_k - \hat{y}_k.$$

In [18] it is proved that the origin $\hat{\omega} = 0$ always belongs to the convergence domain of TLS. Hence, the use of null initial condition is the best choice if no prior information is given.

Chapter 2

Experimental Results

2.1 Introduction

This section shows the experimental results conducted by applying at the system to control the various types of observers of the rotor state analyzed in Chapter 1. Of them will be evaluated its strengths and weaknesses in the various operating conditions.

The complete diagram of the control system is shown in Figure 2.1. The control system is a field-oriented control (FOC). The control variable is the torque. The limitation of the voltage and the references of flux and torque are established in function of the bus-bar voltage.

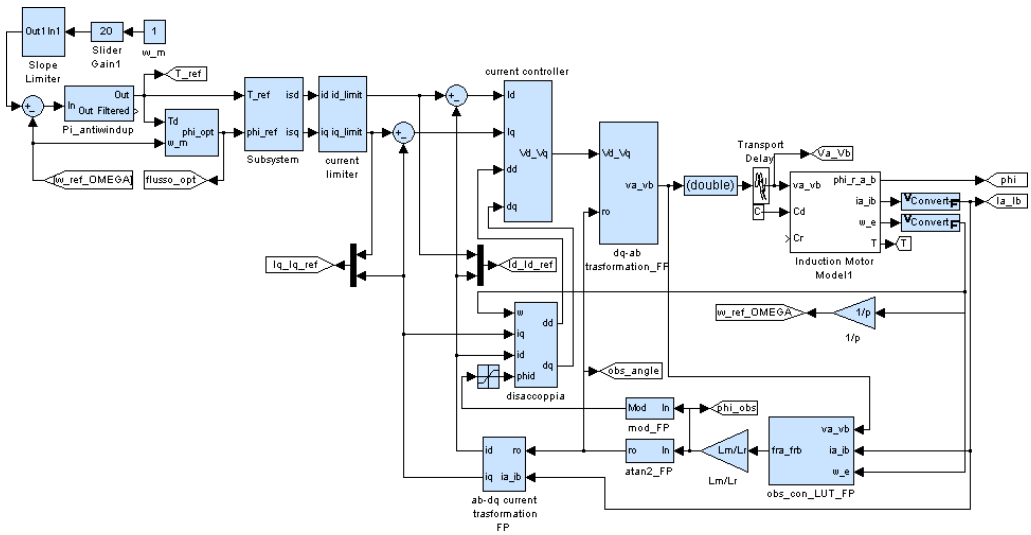

Figure 2.1: *Complete Scheme of the Control System*

2.2 Full Order and Reduced Order Luenberger Observer - Simulation and Experimental Results

The performances of the Full Order Luenberger Observer () have been evaluated using simulation implemented in MatLab®- Simulink®. The linear matrix inequality of the optimization problems have been solved using the free MatLab®toolbox YALMIP®. The Simulink®model includes observer (1.2.2) and the IM model (1.2.2), coupled with the mechanical equation. For the Induction Motor model and the observer, the parameters in Table 1 have been used. The Induction Motor used has a power of 0.75kW.

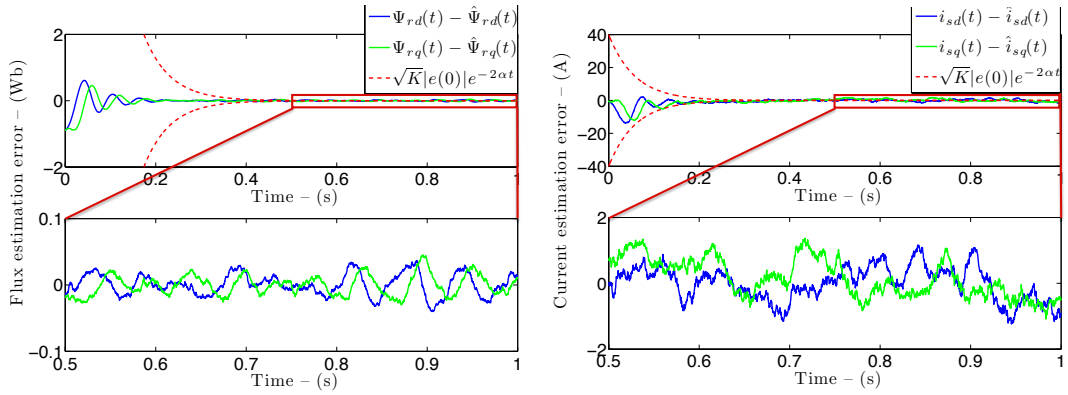

Flux error Current error

Figure 2.2: Test with observer gains computed from (**??**) without $\mathcal{L}_2$ optimization.

Figure 2.2 shows flux and current errors during a test where the current measurement, the input voltage and the speed measurement are corrupted by zero mean white noise with power spectral density equal to 10^{-4} for current and 10^{-3} for speed and voltage. The observer gains have been tuned fixing a convergence rate equal to $2a_{22}$ by means of selection (1.2.9) with $\eta = a_{22}$. These figures confirm the main result. In fact, the error variables, represented by the solid curves, depend by ω, and thus exhibit a peculiar time-varying transient. instead the upper bound of their norm, represented by the dashed curves, is a time-invariant function. In particular these dashed curves represent bounds (1.2.5) with $\sqrt{k} = 38.2$ which has been computed by solving (1.2.5) with $\alpha_l = 2a_{22}$.

The same test has been carried out through the tuning of the parameters of the observer with the $\mathcal{L}_2$ gain optimization (1.2.6) (with $\alpha_l = 2a_{22}$) in order to reduce the noise effects, obtaining the gain $\bar{L} = \left[\begin{smallmatrix} 9.5 \\ 5.3 \end{smallmatrix}\right]$. The results shown in Figure 2.3 highlight a significantly improved

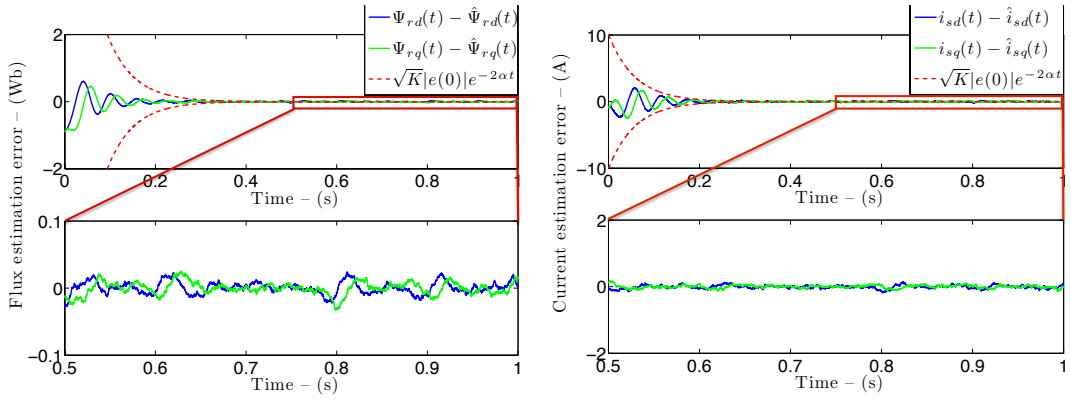

Flux error Current error

Figure 2.3: Test with observer gains computed by means of $\mathcal{L}_2$ optimization (1.2.6).

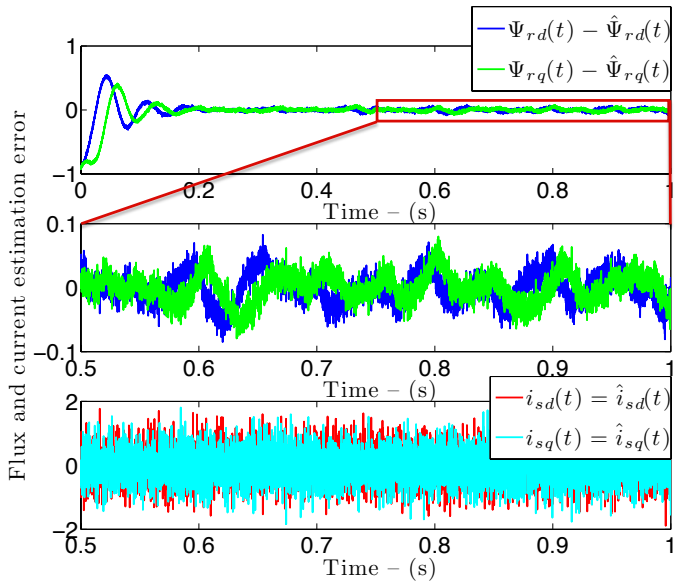

Figure 2.4: Flux error for the reduced order observer (**??**) (top two plots), and noise affecting the current measurement (lowest plot).

disturbance rejection at the steady state (see the lower curves). Once again, the bound (1.2.5) is represented by the dashed curves, where $\sqrt{k} = 10.1$ has been computed by solving (1.2.5) with $\alpha_l = 2a_{22}$.

Finally Figure 2.4 shows the behavior of the reduced order observer arising from the full order one in Figure 2.2. A comparison between Figure 2.2 and 2.4 clearly reveals the advantages of a full order solution, as commented on Remark 1. Indeed, the lower plots of Figure 2.2, respectively, compared to the two lowermost plots of Figure 2.4, show that the noise is more effectively filtered out by the full order solution.

2.2.1 literature notes

This chapter develops the problem of the estimation of the rotor flux in induction motors using a full order Luenberger observer. The literature presents several works regarding the design of observers for this purpose [81], [63], [80], [66]. The main problem to solve is that the Induction Motor dynamics are linear time-varying. Thus, becouse they depend linearly on the speed of rotation, so standard Linear Time Invariant techniques cannot be used. A typical approach is therefore apply a robust control, fixing a possible range of speed and set the observer gain for ensure stability when the speed is constant in this fixed set. i.e. the eigenvalues of the dynamic matrix are always with real part negative for all physical acceptable values of the rotor speed. In any case a empirical rule is to fix the speed of the error dynamics greater than the fastest state variable of the Induction Motor model [80], [63] to obtain time scale separation.

A different solution to overcome this problem is a time-varying gain in order to eliminate the effect of speed in the error dynamics. One important work that uses time-varying gain for flux estimation in Induction Motor is [81]. A other example is [48], which deals with the full-order flux observer design in encoderless Induction Motor drives and the gain chosen is time-varying as a function of the rotor speed. Moreover, for the same observer, [45] shows how to choose the gain using the linearized model, but it is also shown that the linearized model reveals potential instability problems. A reduced order version is also presented in [46]. In [39] it is shown that the observer gain selection is critical for the good behavior of the system, and a framework is developed, in which the properties of any gain selection can be easily assessed. Four candidate gain selections are considered, two of which do not use

the rotor speed in their equations (inherently encoderless schemes). The stability of these schemes are analyzed in [40] for different working conditions. A Lyapunov-based analysis of the stability of rotor flux observers for Induction Motor is proposed in [35] and [62], where it is shown how the observer gain is chosen such that the time derivative of the Lyapunov function, developed for the proposed observer, is negative and independent of the speed. Moreover, [62] carries out an analysis of the behavior when the speed signal is not correct. It is useful to underline that all these implementations, which use time-varying gains, have the problem that the speed signal, together with the model parameters, are not perfectly known, and the measured speed is also noisy and this leads to a further noise superimposed on the estimated variables.

Regarding the sensitivity to parameter variations, two main approaches can be found. In the first one, assuming nominal values for the motor parameters, the observer gain is designed in order to obtain satisfactory error dynamics and steady-state behaviour, even in the presence of motor parameter variations [1], [35], [61]. In [47] the equations of the parameter sensitivity of the rotor flux estimation are derived for a full-order flux observer, and based on the parameter sensitivity analysis, practical methods of designing robust observer gains are proposed. The same holds for [35], where the sensitivity analysis makes it possible to establish design criteria for a rotor flux reduced-order observer for the Induction Motor. The second approach considers online adaptation of the model parameters [63], [42], [67]. In particular the parameters adapted are those that vary during normal operation, i.e. stator and rotor resistances. For example in [63] a flux observer for an induction motor with an adaptive scheme is proposed. The parameters identified adaptively are stator and rotor resistance, which vary with motor temperature, and the stability is proved by Lyapunov's theorem. Furthermore, robustness of the induction motor drive system with the proposed flux observer is shown.

Recently, in [67] a novel local adaptive flux observer for induction motors is presented. Under persistence of excitation it estimates the motor fluxes and identifies the rotor resistance on-line.

Other works consider a more complex model, i.e. saturation effects, in order to have a more accurate estimate. For example [12] considers a nonlinear dynamic model of the Induction Motor that includes the effects of magnetic saturation and designs an observer–

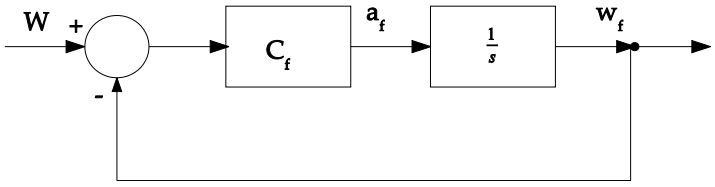

Figure 2.5: State Variable Filter

controller strategy that achieves semi-global exponential rotor position tracking. The flux estimate in this case is embedded in the control strategy.

2.3 Sliding Observer - Simulation and Experimental Results

The simulation experiments were carried out tacking into account both the ideal voltage waveforms given by the inverter, and the time delays connected to the implementation on microcomputer systems of the controller and the observer. Regarding to the sliding observer, this delay is equal to its sampling interval assumed equal to 25 ms. This observer has been tested in numerical simulation and, also, experimentally. The machine under test is a 7.5 kW induction motor, and has been considered having the following nominal parameters:

$$\begin{array}{llll} R_r = .19\Omega & L_r = .025H & L_m = .04107H & Rs = .45\Omega \\ L_s = .07712H & J = .2123Nms^2 & F = .015Nms & P = 2 \end{array}$$

With reference to the sliding observer, we have chosen:

$$h_2 = 0; \qquad h_1 = h_a$$

in order to compute h_a we have chosen $|v_1|_x$ and $|v_2|_x$ equal to the maximum value of the norm of $\underline{v}$ which is equal to $c_1 E_d$, where E_d is the DC voltage supplying the inverter, assumed equal to 513 V. The other quantities have been estimated using the rated values of the motor and the operating conditions of the closed loop system. We have obtained:

$$h_a = -(51639 + 119\,|w|)$$

The variables of interest shown later in the Figs. XXXXXXX are the speed error e_n, the per cent error e_m of the modulus of the rotor flux vector and the phase error e_f of the same

vector, defined as follows:

$$e_m = 100\left[\left(\phi_a^2+\phi_b^2\right)^{\frac{1}{2}} - \left(z_{21}^2+z_{22}^2\right)^{\frac{1}{2}}\right] / \left(\phi_a^2+\phi_b^2\right)^{\frac{1}{2}}$$

$$e_f = \tan^{-1}\left(\frac{\phi_b}{\phi_b}\right) - \tan^{-}1\left(\frac{z_{22}}{z_{21}}\right)$$

Some experimental tests have shown that considering the solution expressed by equations 1.3.27 and 1.3.28, the rotor flux estimation error increases indefinitely. Consequently, the tests discussed later have been carried out employing the solution given by equation 1.3.30. Moreover, these tests have been carried out assuming rotor and stator resistance variations equal to +50% of their nominal values.

Several tests have shown that the best results are obtained choosing $\rho = .23$ ($p_1 = .3$ and $p_2 = .7$) and $r = .002$ for $w \neq 0$ and $r = 0$ at zero speed. The value of r at zero speed allows to obtain a good behaviour of the observer also at zero speed. These tests have shown that for a certain value of ρ, if r diminishes starting from the above value corresponding to $w \neq 0$ the sliding observer is not able to track the actual rotor flux and the rotor flux estimation error increases. Moreover, the ripple present in the waveforms of e_m and e_f diminishes. If the value of r increases the mean value of both e_m and e_f diminishes but the above ripple increases. Now, for a fixed value of r, if ρ increases (p_1 increases and p_2 diminishes) the ripple present in e_m and e_f increases, the mean value of e_f diminishes and that of e_m increases. If ρ diminishes, the above ripple diminishes, the mean value of e_f increases and that of e_m diminishes. Finally, for fixed values of ρ and r, a reduction of the ripple present in e_m and e_f is obtained by diminishing the gains of the matrix Ha with respect to those computed using the sliding conditions.

The figure 2.9-2.11 show the waveform of e_n, e_m and e_f versus t corresponding to the values of ρ and r previously considered and to $h_1 = .1h_a$.

Regarding the reduced order observer we have carried out the same tests as for the sliding observer. These tests have shown that the same behavior previously described is obtained by varying ρ and r, except for the ripple which is negligible.

Other tests have shown that the behavior of the reduced order observer is not sensitive to possible commutation delays which cause equal variations of the instants T_1, T_2 and T_3.

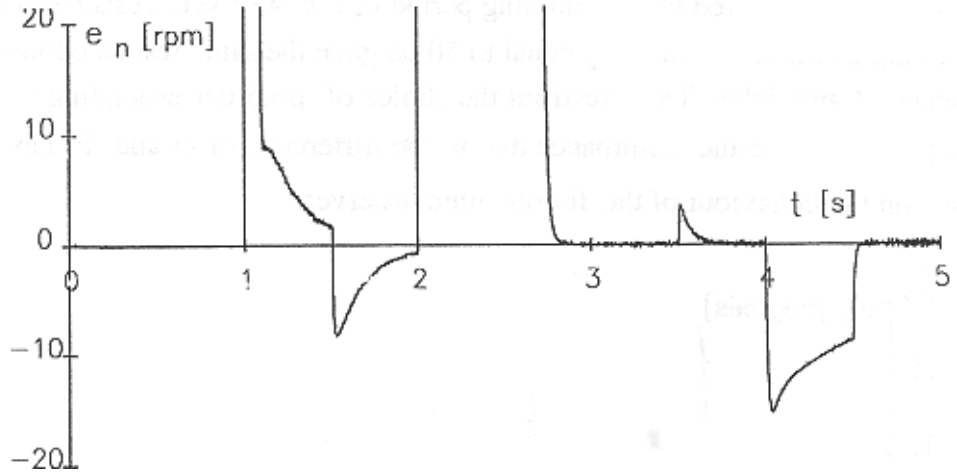

Figure 2.6: Waveform of e_n vs t: $c_r = 0$ and $n_r = 0$ for $t \in [0,1)$, $c_r = 40$ and $n_r = 200$ for $t \in [1,1.5)$, $c_r = 0$ and $n_r = 200$ for $t \in [1.5,2)$, $c_r = 0$ and $n_r = 2000$ for $t \in [2,3.5)$, $c_r = 20$ and $n_r = 2000$ for $t \in [3.5,4)$, $c_r = 0$ and $n_r = 2000 - 10000\,(t-4)$ for $t \in [4,4.5)$, $c_r = 0$ and $n_r = 1500$ for $t \in [4.5,5)$.

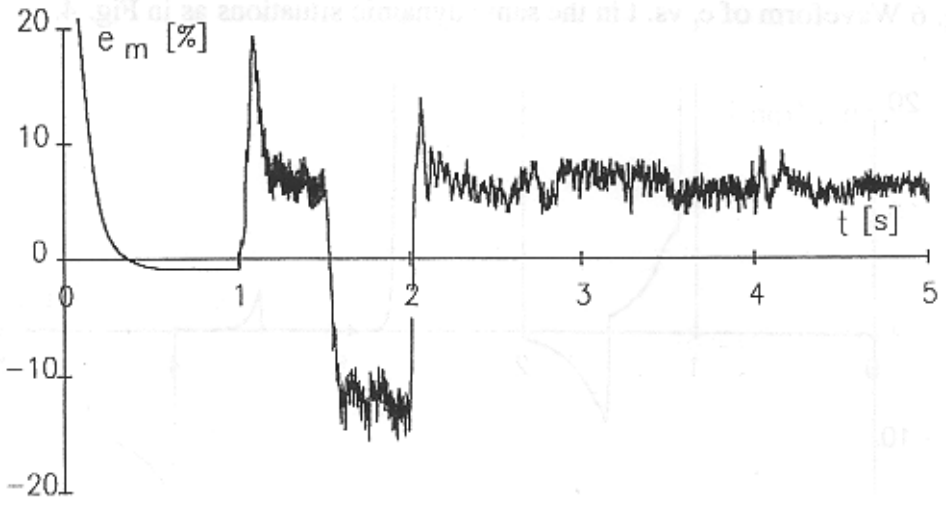

Figure 2.7: Waveform of e_m vs t in the same dynamic situations as in fig 2.6.

These variations have a negligible effect on the quantities u_{p1} and u_{p2} because the natural modes of the matrix $\mathbf{L}(w)$ at constant speed, choosing a value of r not very little, have a poor damping and a large period compared to the sampling period of the observer. Tests carried out assuming a commutation delay equal to 50 ms gave the same results obtained in absence of any delay. This justifies the choice of $\rho = .5$ corresponding to $p_1 = 1$ and $p_2 = 0$, because the disturbance due to the difference of $\underline{m}$ and $\underline{\tilde{m}}$ have not effect on the behavior of the discrete time observer.

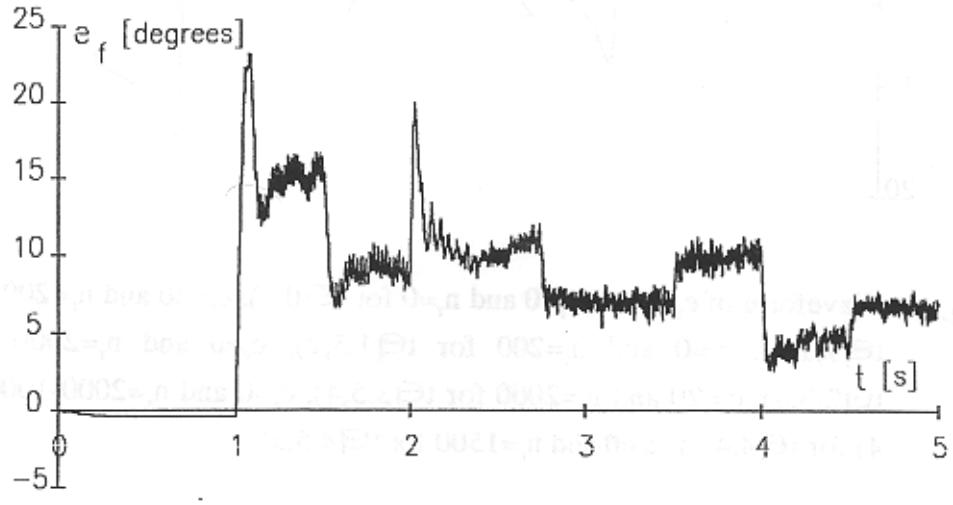

Figure 2.8: Waveform of e_f vs t in the same dynamic situations as in fig 2.6.

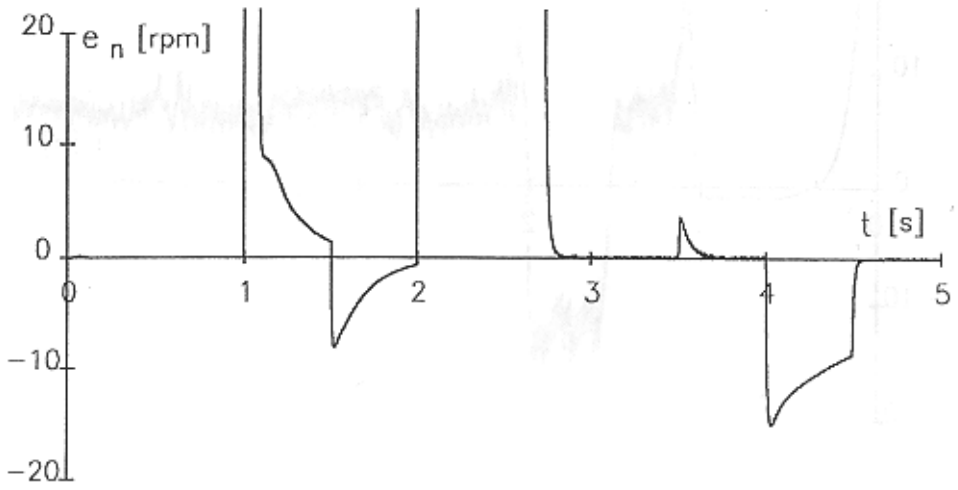

Figure 2.9: Waveform of e_n vs t in the same dynamic situations as in fig 2.6.

The Figures 2.9-2.11 show the waveforms of e_n, e_m and e_f in the same dynamic situations as in Figs. 2.6-2.8 assuming $\rho = .5$, for r the same values for the sliding observer and $c_f = .001$ (cf. Fig. 2.5).

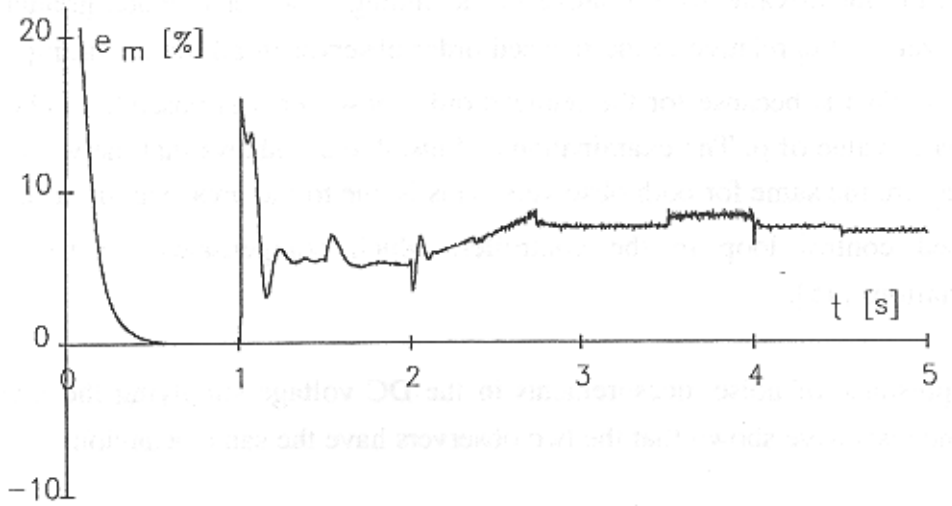

Figure 2.10: Waveform of e_m vs t in the same dynamic situations as in fig 2.6.

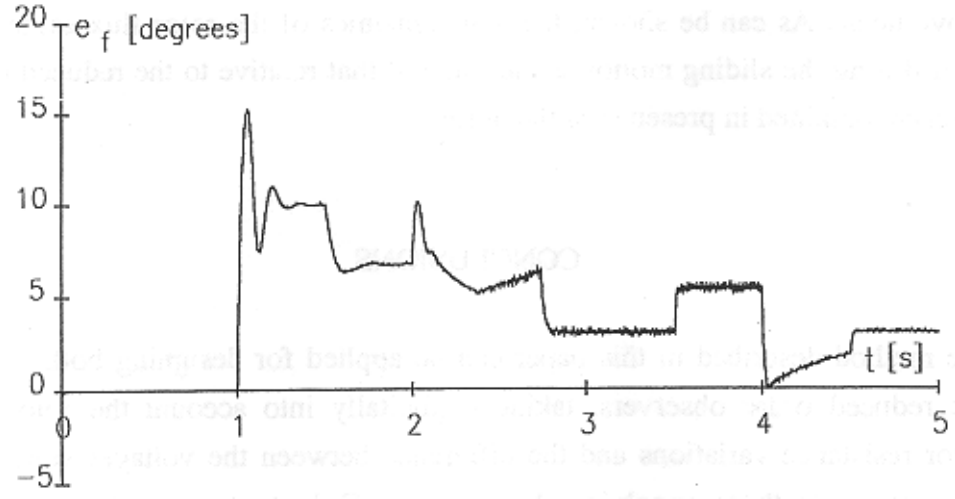

Figure 2.11: Waveform of e_f vs t in the same dynamic situations as in fig 2.6.

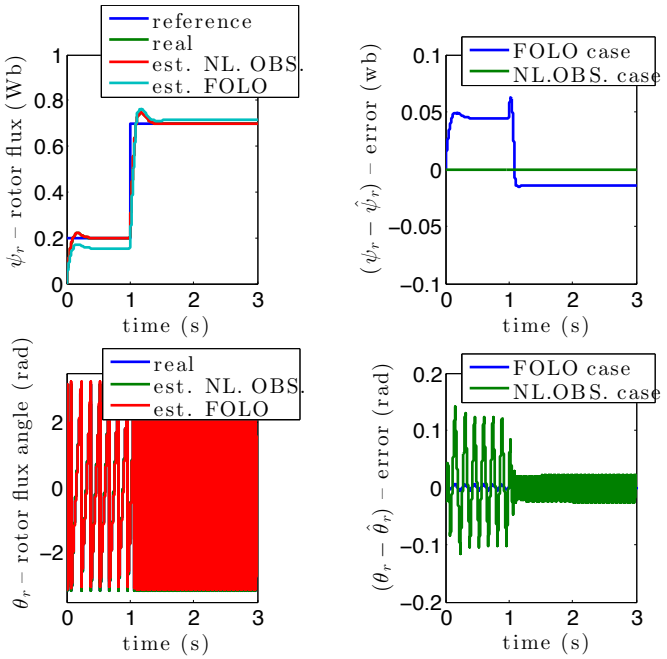

Figure 2.12: Amplitude and angle of the rotor flux in a simulation test during a contemporary speed, flux and torque step reference, $\omega_{rref} = 20 \rightarrow 100$ rad/s, $|\psi_{rref}| = 0.2 \rightarrow 0.7$ Wb $t_L = 2 \rightarrow 10$.

2.4 Nonlinear Flux Observer - Simulation and Experimental Results

This non-linear flux observer has been tested in numerical simulation and, also, tested experimentally. The machine under test is a 2.2 kW IM SEIMEC model HF 100LA 4 B5. The test system is equipped also with a torque controlled PMSM (Permanent Magnets Synchronous Motor) model Emerson Unimotor mechanically coupled to the Induction Motor, to implement an active load. The electromagnetic torque is measured on the shaft by a torque meter

The system has numerically simulated in Matlab®-Simulink®. In simulation stage, the Induction Motor it's been represented through his dynamic model of the Induction Motor, taking into consideration the magnetic saturation. It is the same dynamic model adopted for implementing the non-linear observer, but expressed in the rotor flux oriented reference frame. The simulated test has been performed twice, adopting the proposed non-linear observer taking into consideration the magnetic saturation, and adopting the classic Full Order Luenberger Observer. The classic Full Order Luenberger Observer has been tuned assuming constant electrical parameters of the Induction Motor. This electrical parameters are corresponding to the knee of the magnetization curve. As regard to the simulation test, a contem-

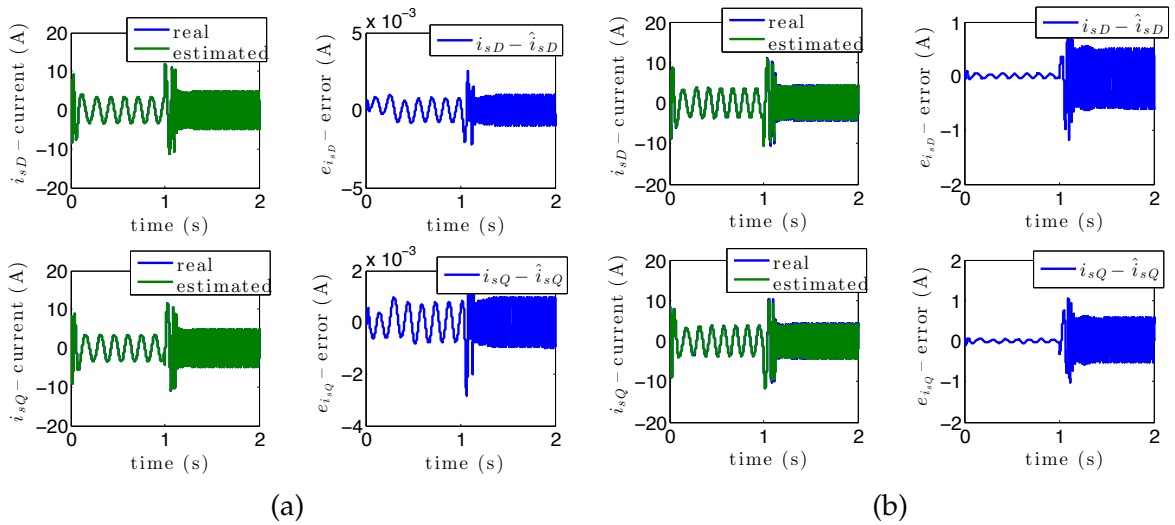

Figure 2.13: Simulation results during a contemporary speed, flux and torque step reference, $\omega_{rref} = 20 \rightarrow 100$ rad/s, $|\psi_{rref}| = 0.2 \rightarrow 0.7$ Wb $t_L = 2 \rightarrow 10$: (a) estimated and real $i_{s,\alpha}$, $i_{s,\beta}$ stator current components with nonlinear observer, (b) estimated and real $i_{s,\alpha}$, $i_{s,\beta}$ stator current components with FOLO.

porary step variation of the Induction Motor reference speed, rotor flux amplitude and load torque has been given the drive, of the type: $\omega_{rref} = 20 \rightarrow 100$ rad/s, $|\mathbf{\Psi}_{rref}| = 0.2 \rightarrow 0.7$ Wb $t_L = 2 \rightarrow 10$ Nm. In this context, the drive works at different speeds with different load torques and rotor flux levels: such a working condition emulates the behavior of the drive in optimal efficiency conditions. To display the behaviour of the observers, independently from the control action, both the non-linear observer and the Full Order Luenberger Observer have been tested in parallel with respect to the control system. To close the flux control loop has been feedback the real flux. Fig. 2.13. (a) shows the real rotor flux amplitude and the estimated one as well as its phase position, obtained with both the observers, as well as the corresponding estimation errors. It can be seen that, approaching the rated flux of the Induction Motor, in correspondence to which the parameters of the Full Order Luenberger Observer have been tuned, both observers work correctly with the estimated fluxes correctly tracking the real ones. Otherwise, at rotor flux equal to 0.2Wb, while the proposed non-linear observer is able to correctly estimate the real flux, the classic Full Order Luenberger Observer presents a very high estimation error, equal to about the 7% of the real flux. Even the rotor flux angle error, at 0.2Wb, is quite high with the Full Order Luenberger Observer around 7 degrees (0.13 rad), while it is negligible with the proposed non-linear observer. This is quite an important point, since the correct rotor flux angle estimation is responsible for the correct field orientation conditions and, thus, for the performance of the

entire control system. Fig.s 2.13.(b)-(c) show respectively the $i_{s,\alpha}$, $i_{s,\beta}$ real and estimated stator current components in the stator reference frame, as well as the instantaneous estimation error of both the observers. These figures clearly show that, while at the rated flux of the IM, in correspondence to which the parameters of the FOLO have been tuned, the observers tracking errors are very close to each other (as expected), for the lower value of the reference flux, the non-linear observer significantly overcomes the Full Order Luenberger Observer in terms of estimation accuracy. In particular it can be observed that the stator current estimation error is of the order 10^{-3} for the non-linear observer, while it is of the order unity for the Full Order Luenberger Observer, confirming the goodness of the proposed approach.

This is to be expected, since the non-linear observer has embedded the knowledge of the magnetic working condition of the Induction Motor. With regard to the experimental test, a set of contemporary step variation of the Induction Motor reference speed, rotor flux amplitude and load torque has been given the drive, of the type: $\omega_{rref} = 20 \rightarrow 40 \rightarrow 60 \rightarrow 80$ rad/s, $|\psi_{rref}| = 0.2 \rightarrow 0.4 \rightarrow 0.6 \rightarrow 0.8$ Wb $t_L = 2 \rightarrow 4 \rightarrow 6 \rightarrow 8$ Nm. Fig. 2.14.(a) shows the reference and measured speed under the above described test. Fig.s 2.14.(b)-(c) show respectively the $i_{s,\alpha}$, $i_{s,\beta}$ measured and estimated stator current components in the stator reference frame, as well as the instantaneous estimation error of both the observers. Like in the numerical simulation case, the test has been performed twice, adopting the proposed non-linear observer, and the Full Order Luenberger Observer. These figures confirm the simulation results and clearly show that, while approaching the rated flux of the Induction Motor, in correspondence to which the parameters of the Full Order Luenberger Observer have been tuned, the observers tracking errors are very close to each other (as expected), for low values of the reference flux (particularly 0.2 and 0.4 Wb), the non-linear observer significantly overcomes the Full Order Luenberger Observer in terms of estimation accuracy. The peak estimation error with the non-linear observer is about 0.5 A, while it overcomes 2 A (4 times) with the Full Order Luenberger Observer. As result, Fig. 2.14.(d) shows the waveform of the rotor magnetizing current amplitude, as obtained with both the observers, which is proportional to the rotor flux amplitude by $L_m(|i_{mr}|)$. It can be observed that, while approaching the rated flux of the Induction Motor, the $|i_{mr}|$ estimated by the two observers are very close to each other (as expected), for low values of the reference flux (particularly 0.2 and 0.4 Wb) they become quite different. In particular, at 0.2 Wb the $|i_{mr}|$ estimated by

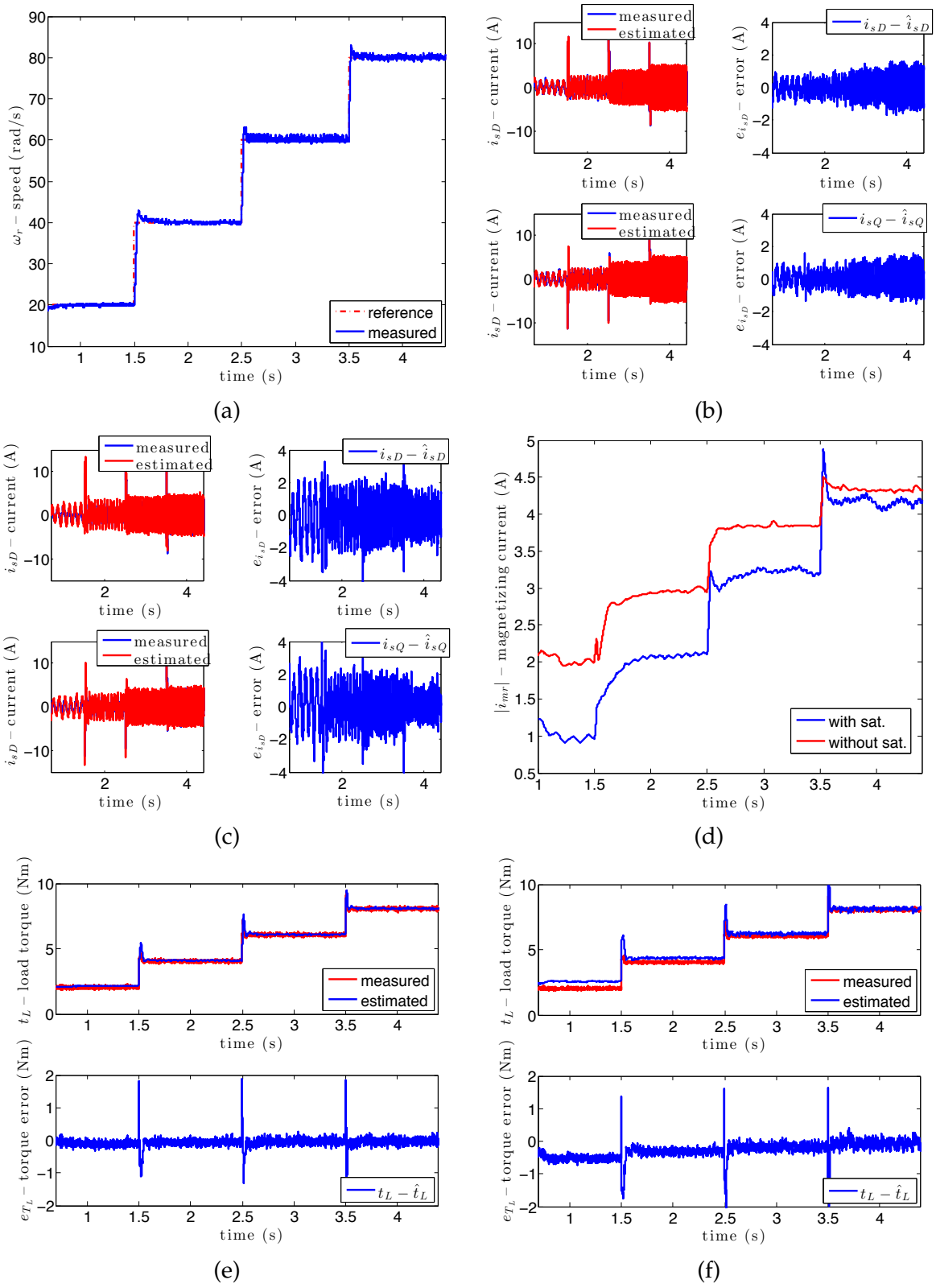

Figure 2.14: Experimental results during a contemporary speed, torque and flux step reference, $\omega_{rref} = 20 \rightarrow 40 \rightarrow 60 \rightarrow 80$ rad/s, $|\psi_{rref}| = 0.2 \rightarrow 0.4 \rightarrow 0.6 \rightarrow 0.8$ Wb $t_L = 2 \rightarrow 4 \rightarrow 6 \rightarrow 8$ Nm: (a) rotor speed, (b) estimated and measured $i_{s,\alpha}$, $i_{s,\beta}$ stator current components with nonlinear observer, (c) estimated and measured $i_{s,\alpha}$, $i_{s,\beta}$ stator current components with FOLO, (d) rotor magnetizing current (e), estimated and measured electromagnetic torque with nonlinear observer, (f) estimated and measured electromagnetic torque with Full Order Luenberger Observer.

the non-linear observer is much lower than that estimated with the Full Order Luenberger Observer, in fact in the linear region of the magnetizing curve the static magnetizing inductance is much higher. Since there are no flux sensors embedded in the Induction Motor, no direct comparison could be made between the estimated and the measured value of the rotor flux. However, an indirect confirmation of the accuracy of the flux estimation has been performed here comparing, with both the observers, the measured torque on the Induction Motor shaft (with the above described torque meter) with the estimated torque. The torque has been estimated, with both observers, on the basis of the torque equation. Since it depends on the estimated rotor flux and the measured stator current, the verification of the accuracy of the torque estimation is an indirect verification of the accuracy of the flux estimation. It should be remembered that, coherently with the adopted modelization of the two observers, the torque estimation based on the non-linear observer takes into consideration the variable parameters, while that based on the FOLO assumes constant parameters. Fig.s 2.14.(e)-(f) show the electromagnetic and load torques, respectively estimated with both the observers and measured. It can be observed that, while approaching the rated flux of the IM, the torque errors are very close to each other (as expected), for low values of the reference flux (particularly 0.2 and 0.4 Wb), the non-linear observer significantly overcomes the Full Order Luenberger Observer in terms of estimation accuracy. In particular, at 0.2 Wb the torque error becomes even about 25% with the Full Order Luenberger Observer, while it is almost null with the proposed non-linear observer. This is an indirect experimental confirmation of the better accuracy achievable in the rotor flux estimation with the proposed observer.

In conclusion the non-linear observer is based on the dynamic model of the Induction Motor considering the magnetic saturation, appropriately written in a state space form and expressed in the stationary reference frame. It belongs to the category of the non-linear observer characterized by a Lyapunov based convergence analysis. The proposed non-linear observer has been tested in numerical simulation and experimentally on a properly developed test. Its behaviour has been compared to that of a classic full-order Luenberger observer in variable flux working conditions, as well as the stator current components. Results clearly show the capability of such a non-linear observer to correctly estimate the rotor flux linkage amplitude and phase under flux varying conditions including strong variation of

the saturation of the iron path.

2.5 Extended Kalman Filter - Experimental results

The experiments have been performed with the aim of testing the control system with a observer of the rotor state designed with the use of the Extended Kalman Filter. The prototype constructed for this purpose consists of a induction motor with a power of 0,750kW and a powder brake system. The induction motor is driven by a source voltage inverter. A micro-controller DSpace 1103 is used to implement both the observer with the Extended Kalman Filter and the control law. In particular, the control law is designed according to a field-oriented approach, and consists in a cascade controller with four PI control loops, two inner current loops and two outer rotor flux and speed loops. A classic anti-wind-up scheme is designed for the speed control loop. The module of stator current and voltage vectors are constrained to $I_{s,MAX} = 7A$ in order to avoid damage to the machine, $V_{s,MAX} = 0,866V_{BUS}$. The measured variables are the two stator currents given by two Hall-effect transducers. All the above mentioned four control loops are closed through the proposed Extended Kalman Filter. In order to compare the estimated speed with the measured one, it must provide the system with a mechanical incremental encoder sensor with 1024 ppr. The whole controller, including the proposed estimator, is processed at 12 kHz.

Rated power	$750W$	Rated speed	$1410rpm$
Rated voltage	$380V$	Rated torque	$5Nm$
Rated frequency	$50Hz$	Pole pairs	2

Table 2.1: The rated data of the motor

L_s	$0.5236H$	J_m	$0.0056Nms^2$
L_e	$0.043H$	b_r	$1.68Nm$
R_s	15.68Ω	c_r	$0.0023Nms$
T_r	$0.0669s$	p	2

Table 2.2: The parameters of the motor.

The matrices **Q** and **R**, necessary for processing the Extended Kalman Filter, have been

obtained by means of a suitable preliminary experiment, so that the estimated stator currents produced by EKF correspond to those measured. The matrix $\mathbf{R}$ has been chosen equal to the identity matrix $\mathbf{I}_{2\times2}$, and $\mathbf{Q}$ has been parametrized as $\mathbf{Q} = diag\left(q_{11}\mathbf{I}_{2\times2}, q_{22}\mathbf{I}_{2\times2}, q_{33}, q_{44}\right)$, with $q_{11} = 8.149 \times 10^{-2}$, $q_{22} = 4.68 \times 10^{-5}$, $q_{33} = 2.619 \times 10^{-2}$ and $q_{44} = 11.363 \times 10^{-5}$.

The results of some experiments are shown in Figures 2.15-2.19. Figure 2.15 shows the waveforms of angular speed, stator currents, rotor flux and torque during a suitable test at a maximum speed of 100rad/s and rated load, while Figure 2.16 shows the waveforms of angular speed, stator currents, rotor flux and torque during a test at very low speed speed 3rad/s and rated load. In particular, Figure 2.15 shows the closed loop responses corresponding to a trapezoidal reference speed when the motor is fluxed at 0.8 Wb at $t = 0$, starts at $t = 0.5s$ with a step reference speed of $\omega_r = 100rad/s$, then at $t = 10s$ there is a speed reversal and finally the speed is put to zero by means of a ramp. A load torque of 4Nm is applied at 2s and removed at 8s. Figure 2.16 shows the closed loop responses corresponding to a very low speed test, which is a classic critical condition in all the model based observers/estimators for sensorless control of induction machines, when the motor is fluxed at 0.8Wb at $t = 0$, and then starts at $t = 0.5s$ with a step reference speed of $\omega_r = 3rad/s$. The load torque of 4Nm is applied at 2s and removed at 8s.

The Figure 2.17 is shown with the aim of verifying the observability conditions during the above two tests.

When the rotor flux vector is fixed in the reference stator frame, the rank condition is not satisfied and, consequently, nothing can be deduced about observability. However, it is useful to analyze the behavior of the system in the set of states in which the rank condition fails. This set contains the states corresponding to the operating situations in which the rotor flux vector is fixed in the reference stator frame, i.e. at zero stator frequency. This frequency $\dot{\rho}$, is given by:

$$\dot{\rho} = \omega + a_{21}\frac{i_{s,q}}{|\psi_r|},$$

where $i_{s,q}$ is the in-quadrature stator current in the frame rotating with the rotor flux, and its discrete-time version is:

$$\rho^{+} - \rho = T_s\left(\omega + a_{21}\frac{i_{s,q}}{|\psi_r|}\right), \tag{2.5.1}$$

in which ω, $i_{s,q}$ and $|\psi_r|$ are evaluated at the discrete-time instant k. The above set is then

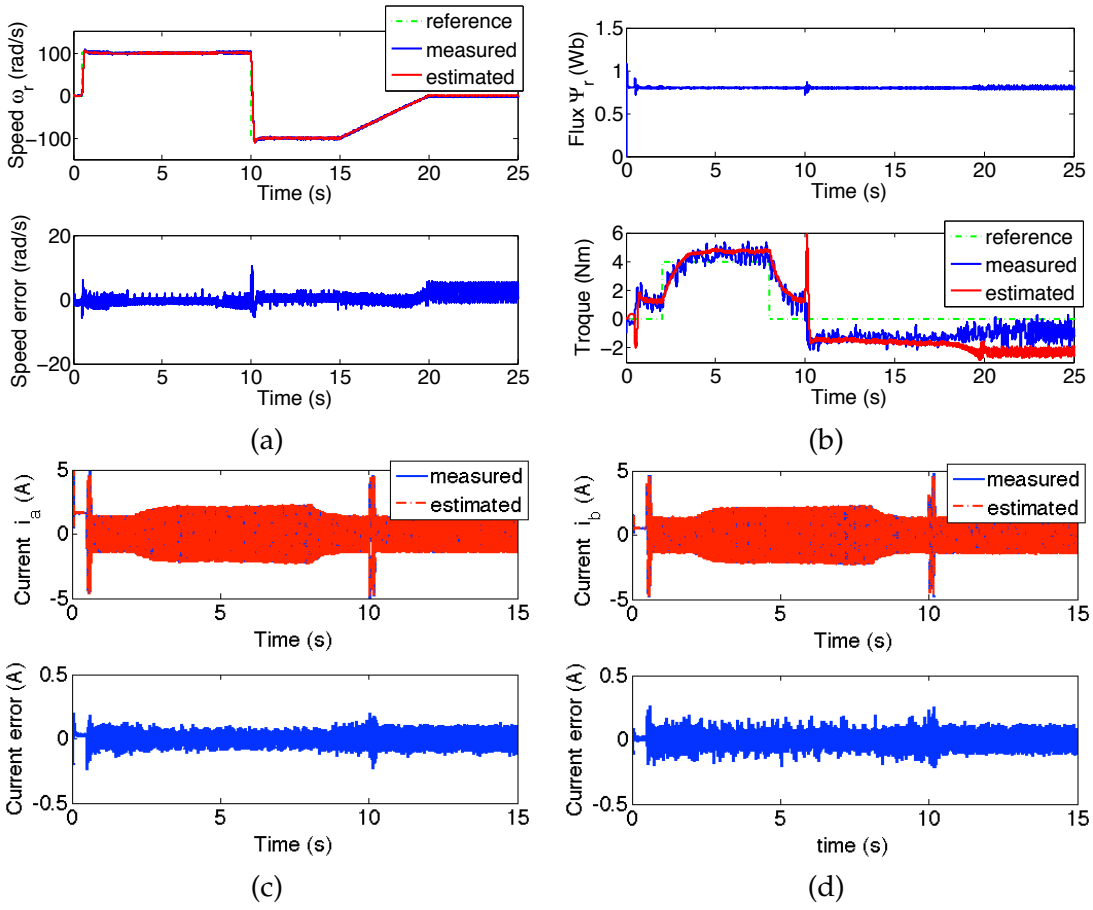

Fig. 2.15: Experimental waveform during a test at nominal speed and load, and with speed reversal.

obtained by putting $\rho^+ = \rho$, and is given by:

$$\omega + a_{21} \frac{i_{s,q}}{|\psi_r|} = 0. \tag{2.5.2}$$

During transients, it is more difficult to verify whether the rank condition is satisfied or not. From (2.5.1), if $x_5^+ \neq x_5$, the rank condition is not satisfied provided that:

$$\tan\left(\rho^+ - \rho\right) = \hat{f}_1 \, \hat{a}_{12} \, \frac{x_5 - x_5^+}{\hat{a}_{12}^2 + \hat{f}_1 \, x_5 \, x_5^+}. \tag{2.5.3}$$

Both members of (2.5.3) are computed on-line using the estimated variables instead of the actual ones. This corresponds to evaluating the observability property of the couple (A_k, C). In particular, in Figure 2.17.a and 2.17.b, the waveforms of the first and second members of (2.5.3) are shown corresponding to the tests of Figures 2.15 and 2.16, respectively.

From Figure 2.15-2.16 a good behavior of the estimator is shown, in all operating conditions. In fact, the observer is capable of tracking all state variables, and the controller with feedback from estimated variables is capable of coping with the disturbance very well.

The Figure 2.17.a shows that (2.5.3) is satisfied near to zero speed, before the starting with the machine fluxed ($t < 0.5s$), when the speed passes through zero during speed reversal (about $t = 10s$), and then when speed is forced again to zero ($t > 18s$). When the rank condition is lost, either in isolated instants or in a few instants of time, estimates given by EKF are correct, but when the rank condition is lost in several instants, the behavior of teh observer based on Extended Kalman Filter deteriorates. This is also shown in Figures 2.15.a-d, where the closed loop system, after a few instants in which it remains at rest, displays a speed oscillating from about $-0.5rad/s$ to about $2.5rad/s$, and there is also an error in the estimated load torque. For isolated instants, for example during speed reversal, the loss of rank does not represent a big problem. The Figure 2.17.b shows that even for very low speed, after a time interval before and at the beginning of the starting, in which (2.5.3) is satisfied, the system is capable of tracking the reference speed even in presence of the torque load.

From the above analysis, it is useful to note, that (2.5.3) represents a useful instrument to analyze when the observer, and therefore the whole control system, are working correctly.

In Figure 2.18, the set of values of $|A_k|$ are displayed, computed at the sampling instants, in the above discussed low and high speed experiments. The shape of the corresponding

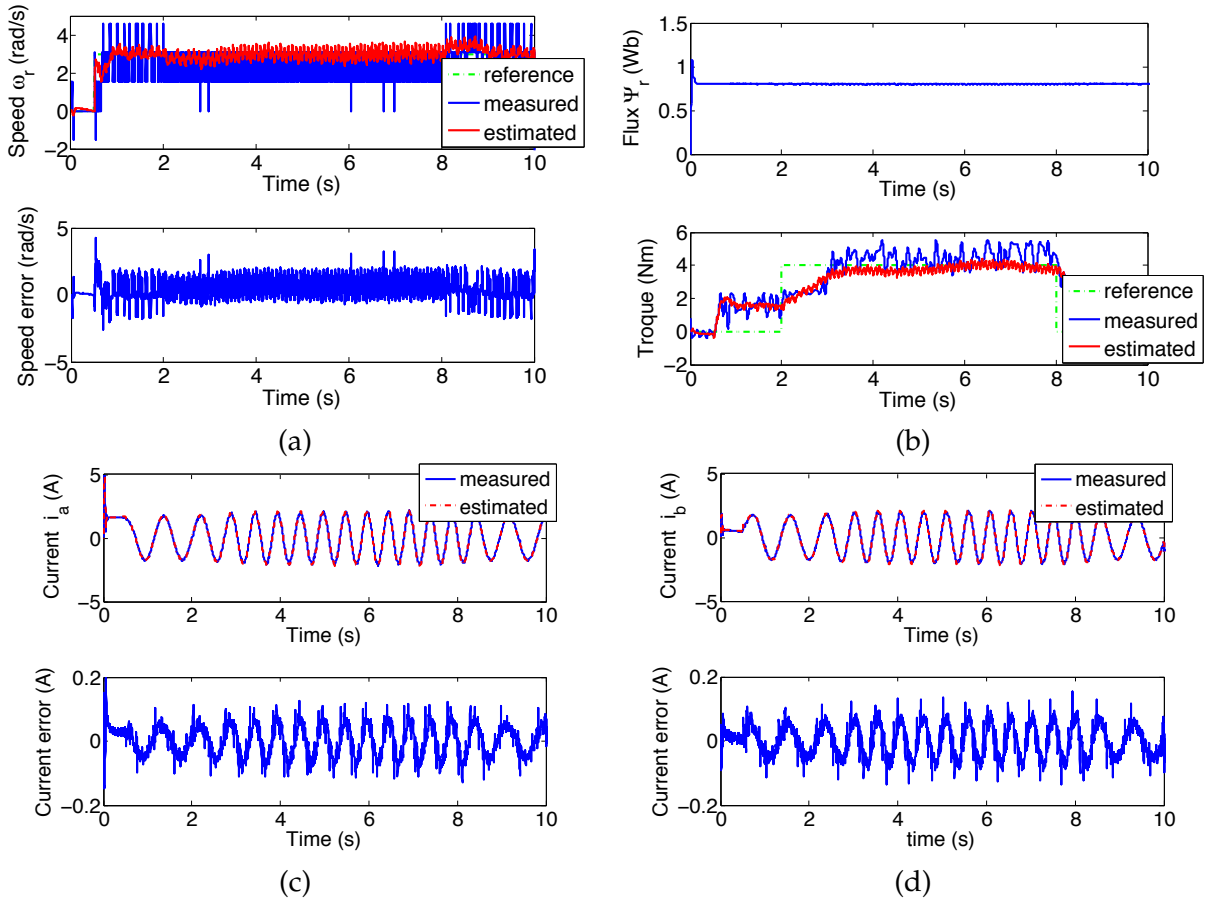

Fig. 2.16: Experimental waveform during a test at low speed and with nominal load.

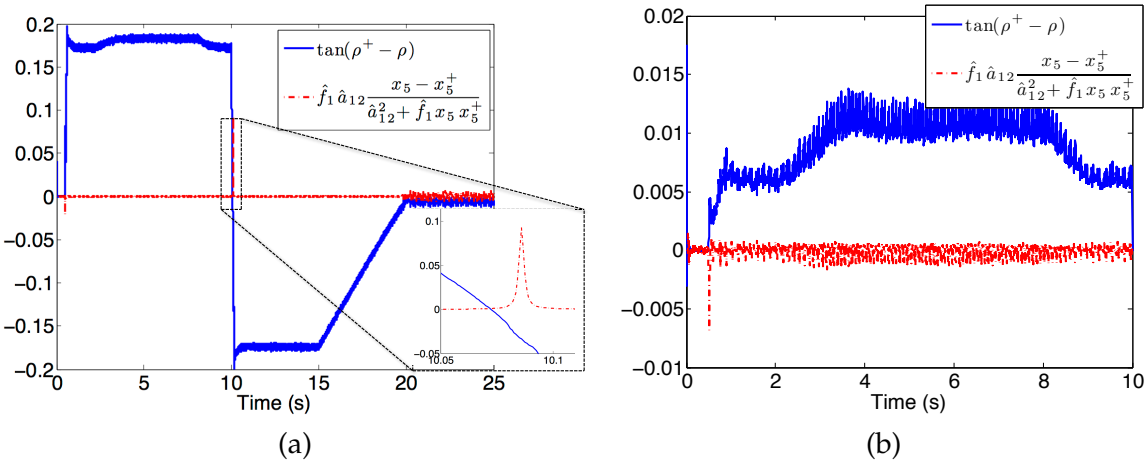

Fig. 2.17: Observability condition (2.5.3) computed at the sampling instants, for the test at Figure 2.15 (a) and for the test at Figure 2.16 (a).

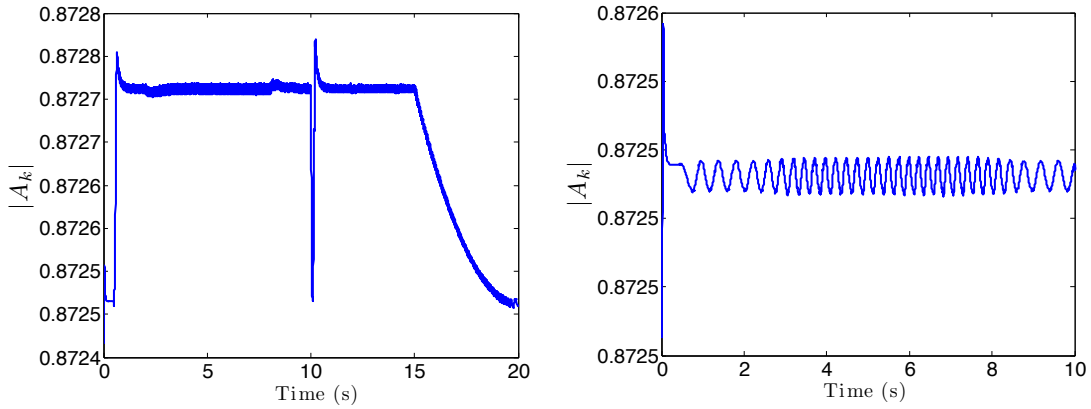

(a) (b)

Fig. 2.18: Set of values of $|A_k|$ computed at the sampling instants, for the test at Figure 2.15 (a) and for the test at Figure 2.16 (a).

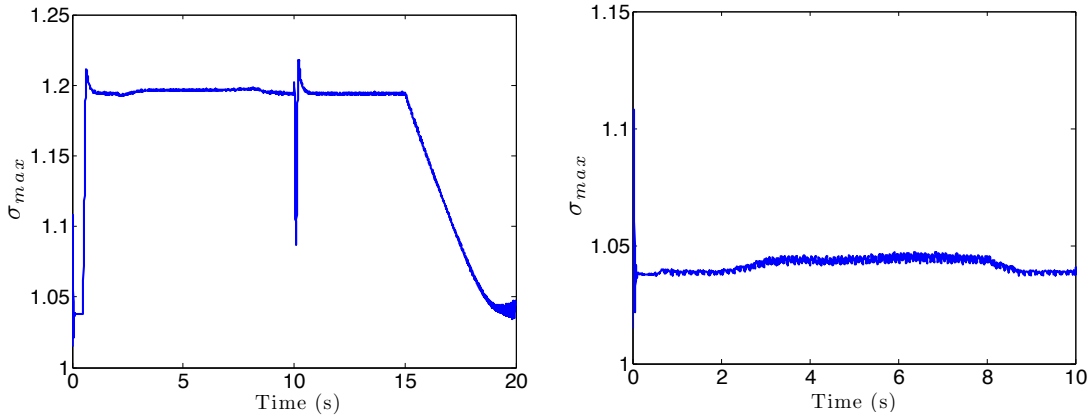

(a) (b)

Fig. 2.19: Set of values of the maximum singular value of A_k, $\sigma_{max}(A_k)$ computed at the sampling instants, for the test at Figure 2.15 (a) and for the test at Figure 2.16 (a).

waveforms shows that the matrix $\mathbf{A}_k$ is always non singular. In particular, it appears that the computed minimum value is greater than the term $-\hat{a}_{33}\,\mu_1$. This fact has been confirmed in many other experiments carried out in various operating conditions.

In Figure 2.19, the set of values of the maximum singular value of A_k, $\sigma_{max}(A_k)$, are displayed, computed at the sampling instants, in low and high speed experiments. As is well known $||\mathbf{A}_k|| = \sigma_{max}(\mathbf{A}_k)$ and, consequently, if $\sigma_{max}(\mathbf{A}_k)$ is bounded, it is possible to verify the first requirement of Assumption 2. From Figure 2.19, it appears that matrix $\mathbf{A}_k$ is bounded in norm, and the bound diminishes with the operative speed range.

2.6 Extended Complex Kalman Filter - Simulation results

The proposed ECKF estimator has been evaluated by means of simulations carried out in a MATLAB®/Simulink®environment. The Simulink®model includes the real–valued Induction Motor model (0.6.4), the ECKF estimator (1.7.2)-(1.7.6), and the controller. The nominal parameter for the Induction Motor model, are shown in tab. 2.2.

A field oriented vector controller has been realized, which involves four PI sub–controllers. The flux and speed loops have been closed by means of the proposed ECKF providing a full estimation of the Induction Motor's state. A frequency of $10kHz$ has been adopted for the execution of both the controller and the ECKF.

With regard to the tuning of the values of the covariance matrices $\mathbf{Q}$ and $\mathbf{R}$, in the majority of the papers in the literature, are preassigned or computed based on a "trial–and–error" procedure. This is the reason why different papers propose different values for the two matrices although they are determined for the same prototype. In [43, 44], a rule based on the minimization of the mean square error between the estimated variables and the actual ones is provided. Our approach was that of fixing the covariance matrix $\mathbf{R} = 1$ and then determining the covariance matrix $\mathbf{Q}$ by optimization based on genetic algorithm. This approach is theoretically justified by the known fact that only the ratios between the elements of $\mathbf{Q}$ and $\mathbf{R}$ affect the system behavior [14]. By doing this we have determined $\mathbf{Q} = \mathrm{diag}(1, 10^{-3}, 10)$.

2.6.1 Robustness Analysis

The robustness analysis for the proposed Extended Complex Kalman Filter is carried out by evaluating its ability to produce accurate state estimates even when the model parame-

ters are varied. A similar study is carried out in [35] for a reduced–order rotor flux optimal observer. The ECKF has been implemented with detuned parameters, while the Induction Motor model contains nominal parameters.

An initial study is carried out by analyzing the behavior of the Extended Complex Kalman Filter when the Induction Motor is operated at rated rotor speed and rated load. Figure 2.20 shows the steady–state estimation errors when the mutual inductance L_m, the rotor resistance R_r, and the rotor resistance R_s are varied. More precisely, Figures 2.20–a,b,c show the flux estimation error as mutual inductance is increased to up to 50% of its nominal value, the rotor resistance up to 300%, and stator resistance up to 50%, respectively (in the figures the modified values are indicated by the subscript m. Figures 2.20–d,e,f show results of the same analysis for the rotor speed estimation error. As can be seen, the influence of these parameters' variations is small, which shows a good robustness of the ECKF. Different behavior can be observed when the machine operates at low speed (Figure 2.21), when a small variation of the stator resistance produces a high error in the flux and speed estimates (cf. Figure 2.21–c and Figure 2.21–f). Moreover, it is worth noting that Figure 2.20–a also reveals that a variation of L_m up to 50% of its nominal value can produce a high flux estimation error of 40%, even at rated, low rotor speed.

From this analysis it is clear that the most critical condition is a variation of the stator resistance when the machine is operated at low speed. Therefore, an accurate R_s estimation is particularly important, which is not normally a problem, because it can be measured directly. Obviously the main source of variation is temperature, so in practical application R_s can be scheduled depending on motor temperature, but this is not trivial.

As for the sensitivity of the ECKF to noise measurement, Table 2.3 shows the mean and the standard deviations of the rotor speed and of the flux estimation errors, in the absence of noise and when a white noise is superimposed to the measured signal. As can be seen the ECKF is robust to noise, since both the means and the standard deviations of the estimation errors remain limited and small even in the presence of noise.

2.6.2 Experimental Results

In this section experimental results are presented validating the proposed 5–th order of the Extended Complex Kalman Filter. A closed loop control system has been made, which

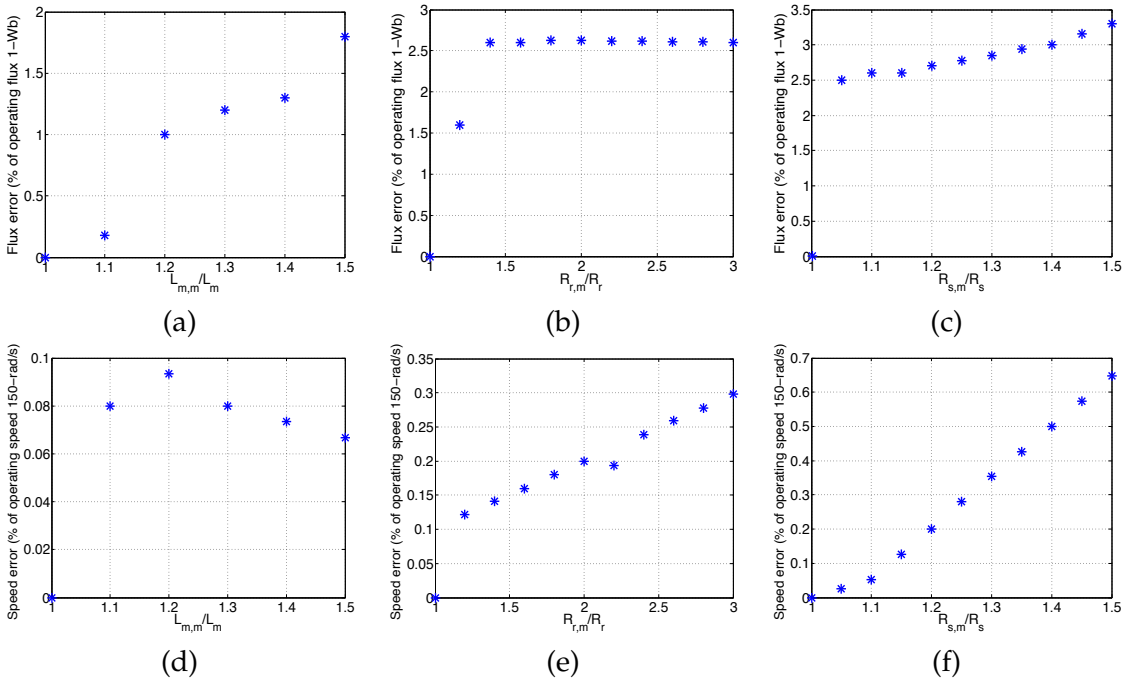

Figure 2.20: Simulation results at rated rotor speed (150 rad/s) and rated load, showing robustness performance of the ECKF: (a) flux error vs. L_m variation, (b) flux error vs. R_r variation, (c) flux error vs. R_s variation, (d) speed error vs. L_m variation, (e) speed error vs. R_r variation, (f) speed error vs. R_s variation.

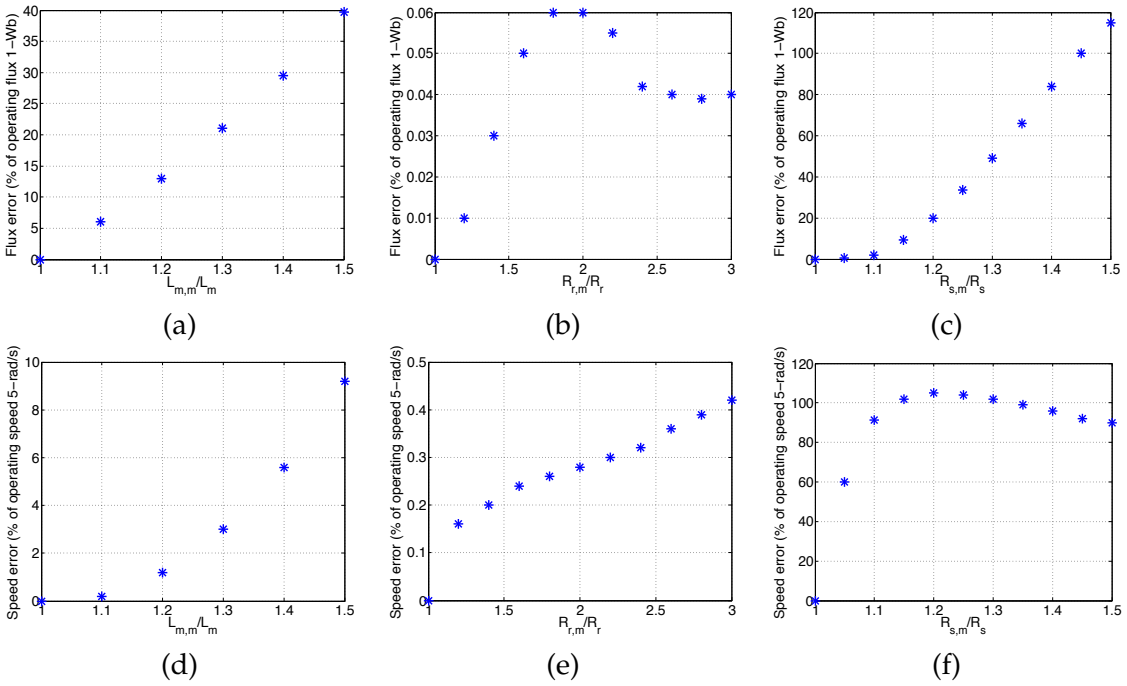

Figure 2.21: Simulation results at low rotor speed (5 rad/s) and rated load, showing robustness performance of the ECKF: (a) flux error vs. L_m variation, (b) flux error vs. R_r variation, (c) flux error vs. R_s variation, (d) speed error vs. L_m variation, (e) speed error vs. R_r variation, (f) speed error vs. R_s variation.

Table 2.3: Noise sensitivity of ECKF

	NO NOISY MEASURES	NOISY MEASURES
TEST AT 150 rad/s		
- standard deviation of the speed (rad/s)	0.05	0.7
- standard deviation of the flux estimate (Wb)	0.04	0.05
- mean error of the speed estimate (%)	0%	0%
- mean error of the flux estimate (%)	0%	0%
TEST AT 5 rad/s		
- standard deviation of the speed (rad/s)	0.06	0.5
- standard deviation of the flux estimate (Wb)	0.02	0.04
- mean error of the speed estimate (%)	0%	0%
- mean error of the flux estimate (%)	0%	0%

is composed of an Induction Motor, supplied by a voltage source inverter, a brake which applies the load t_l to the motor, a four–loop PI-type controller, and the proposed Extended Complex Kalman Filter which computes online state estimates that are used by the controller. The Induction Motor has been operated with a rotor flux of 1 Wb. Both the controller and the estimator Extended Complex Kalman Filter have been implemented on a platform involving dSPACE®dS1103®micro–controller, operating under a MATLAB®/Simulink®environment. The use of the dSPACE®platform is particularly important since it allows rapid prototyping of the control system and a real–time execution of it. The covariance matrices $\mathbf{Q}_k$ and $\mathbf{R}_k$ have been assumed to be constant and equal to $\mathbf{Q} = diag(1, 10^{-3}, 10)$ and $\mathbf{R} = 1$ (as in simulation tests). The Induction Motor has been fluxed during the first 0.5 s, and the stator currents have been measured by using two Hall–effect transducers.

Two experiments have been performed. the first experiment run at high rotor speed and with load (see Figure 2.22), and the other run at low rotor speed (Fig 2.23). The behavior of the system at high speed is satisfactory as discussed later. The rotor speed correctly tracks the reference speed, with relatively high error only during a first transient (cf. Figure 2.22–e and Figure 2.22–f), and reaches the steady–state operations without final error. In the presence of the load torque signal shown in Figure 2.22–d, whose value is 3 N.m, the speed tracking error is negligible. By applying a descended ramp reference speed, when the speed approaches zero, the tracking error initially increases to 4 rad/s, but then rapidly converges to zero. During steady–state operation at -150 rad/s, the load torque is removed (at $t = 13$ s) without speed error, whereas a speed error of about 9 rad/s occurs when the reference speed increases to lead the motor at the standstill. The rotor flux reaches a value of 1 Wb and remains almost constant during the entire duration of the experiment, except for op-

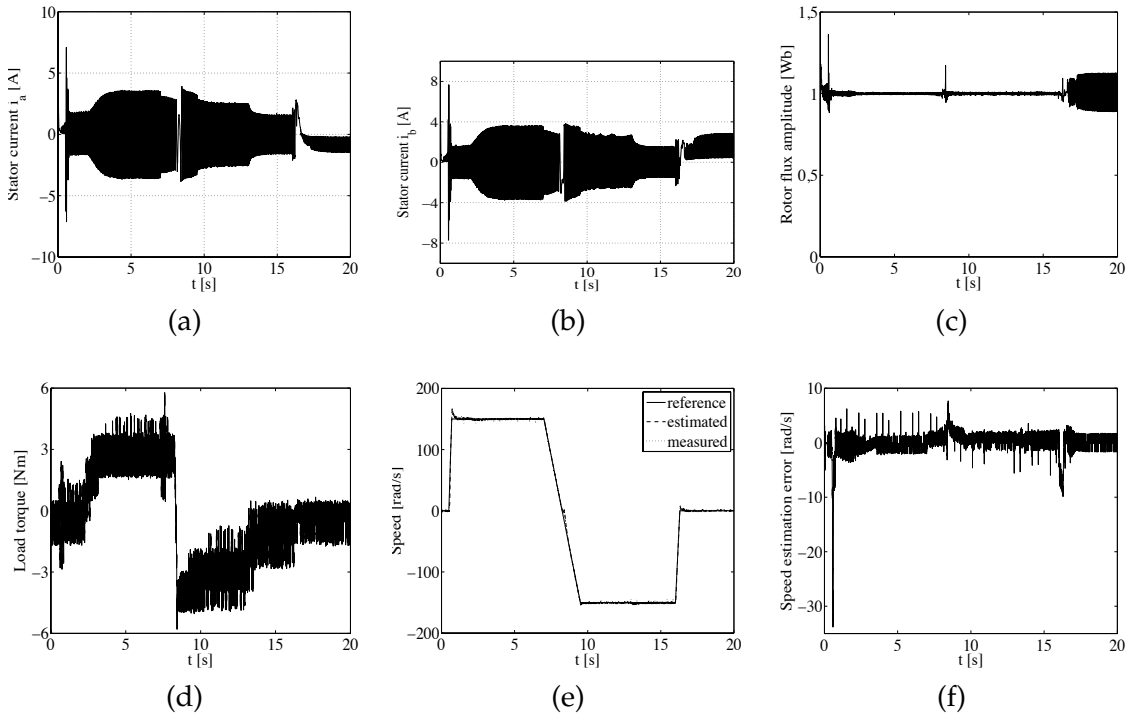

Figure 2.22: Experimental results at high rotor speed: (a) stator current along α–axis in fixed frame, (b) stator current along β–axis in fixed frame, (c) amplitude of the rotor flux vector, (d) applied load torque, (e) reference, estimated and actual speed, (f) speed estimation error $e_\omega = \omega_{r,k} - \hat{\omega}_{r,k}$.

erations at zero reference speed, when the rotor flux varies from 0.92 to 1.08. The stator currents are under the maximum allowed values under all the operating conditions. At low rotor speed the behavior of the system is also satisfactory up to a reference speed of 5 rad/s (see Figure 2.23–e). At 2 rad/s rotor speed a transient oscillation of the tracking error occurs, where a slow convergence to the steady state can be observed. The estimation of the rotor flux appears accurate during all the operating conditions. This fact can also be verified indirectly, by observing that the closed–loop system behaves nicely under all the above operating conditions.

A second experiment has been performed with the aim of analyzing the behavior of the real system respect to the observability conditions of Theorem **??**. The experiment starts by giving zero reference signal for the rotor speed and 1–Wb signal for the rotor flux reference in order to flux the Induction Motor. At the instant $t = 1$ s a 15–rad/s reference signal is applied for the rotor speed, and at the instant $t = 2$ s a load torque command of 2 Nm is applied to the motor by using the powder brake. Figure 2.24 gives the result of this experiment and shows that an accurate estimation of the rotor speed is obtained, even when the IM operates at low speed and with load torque. Furthermore, Figures 2.23–d and 2.23–e) show

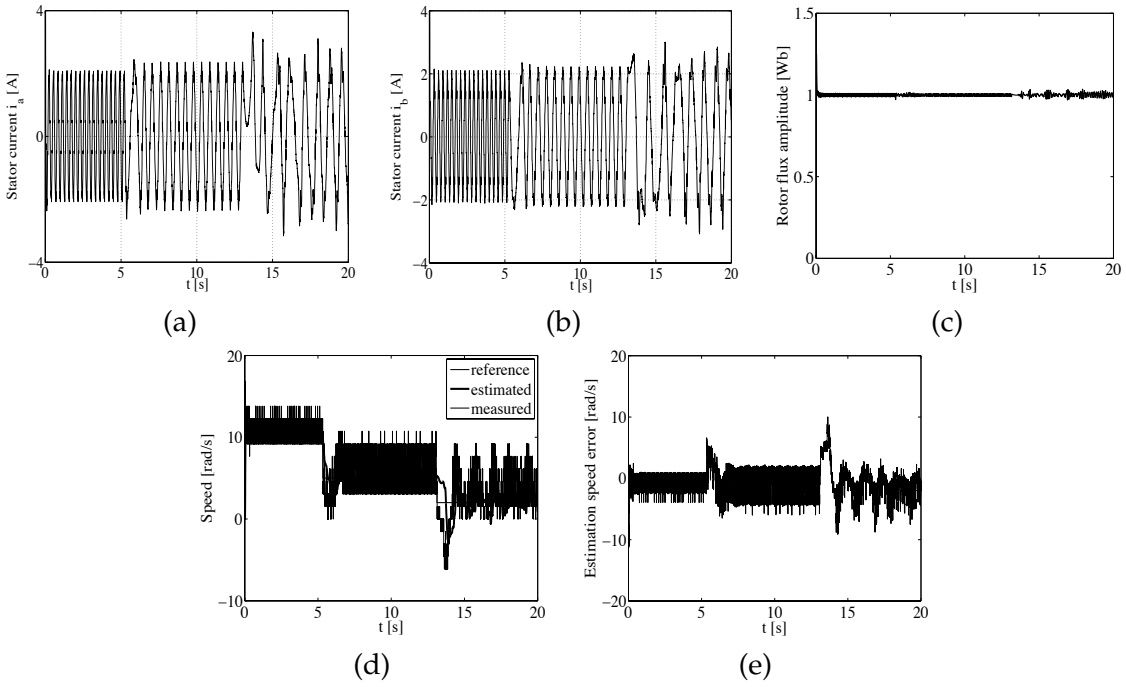

Figure 2.23: Experimental results at low rotor speed: (a) stator current along α–axis in fixed frame, (b) stator current along β–axis in fixed frame, (c) amplitude of the rotor flux vector, (d) reference, estimated and actual speed, (e) speed estimation error $e_\omega = \omega_{r,k} - \hat{\omega}_{r,k}$.

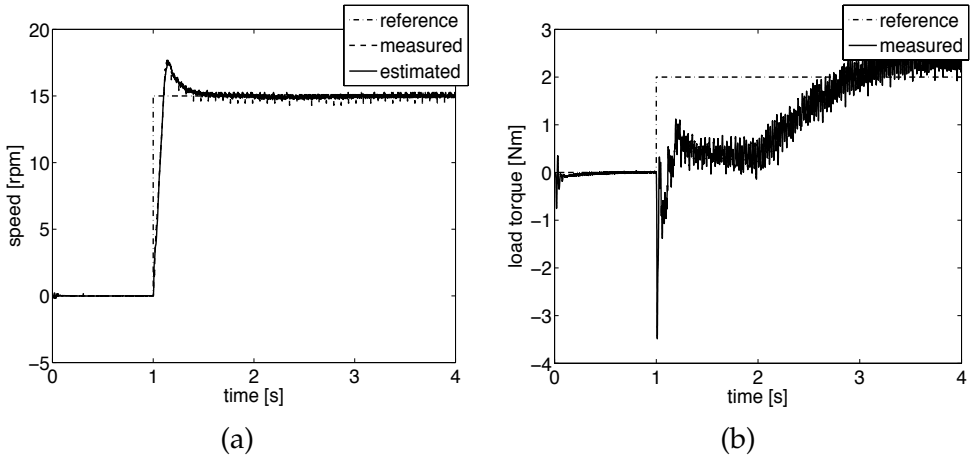

Figure 2.24: Experimental results at low rotor speed and load: (a) reference, estimated and measured speed, (b) applied load torque.

that when the rotor speed decreases down to 2 rad/s, the speed estimate degrades, as can be expected, because the Induction Motor is operating in the near of the region where the observability conditions are not satisfied. Similar behavior can be observed when the rotor speed reference signal is reversed from a positive to a negative value. As the real rotor speed approaches zero, the speed estimation error increases, but then it converges to zero again when the Induction Motor leaves the region where the observability conditions are not met (Figure 2.22–e and Figure 2.22–f). Finally, at zero reference speed, the filter only gives the correct speed only at zero load torque (see last time interval in Figure 2.22–e).

It should be said that the complex–valued model of the Induction Motor describes exactly the same behavior as the more traditional 5–th order model. Therefore, the proposed Extended Complex Kalman Filter produces exactly the same results as the corresponding more traditional Extended Kalman Filter, generated based on the 5–th order Induction Motor model under the hypothesis of constant speed (for example at $\dot{\omega} = 0$). While it is already apparent that the complex–valued model allows an easier and more compact observability analysis, its advantage is also related to the fact that the Extended Complex Kalman Filter requires lower computational effort. Processing both the proposed Extended Complex Kalman Filter and the conventional 5–th order Extended Kalman Filter , this being shaped by using Simulink®blocks and an ad–hoc 2×2 inversion algorithm, shows that a 35% reduction time is obtained with the Extended Complex Kalman Filter.

2.6.3 Literature notes

The estimation of the Induction Motor rotor speed can be performed by means of two types of method, both exploiting the information from stator current measurement. The former type of method is based on the recognition of the characteristics [49, 52] of the measured currents, whereas the latter is a model–based approach [80, 71]. The first type of method can be invasive if based on the superimposition of suitable signals on the standard ones [49], but also not invasive if based on spectral analysis of the stator currents [52]. They are also subject to interpretation errors of the above characteristics. The second type of method uses a–priori knowledge of the actual system and is not invasive since it involves only measured variables. Moreover, its sensitivity to variations of the model's parameters or poor knowledge of its values can be countered by using robust estimation techniques. Among these

model–based methods, MRAS–type [21, 76], Luenberger–type [19, 71], and sliding mode observers [87, 73, 34] are good examples of deterministic observers, whereas Kalman Filter [5] and extended Kalman Filter [3, 60, 80] are good examples of stochastic estimators.

Recently, variants of the Extended Kalman Filter have been proposed, as in [56], where the design and implementation of Unscented KFs (UKFs) for induction–motor sensorless drives is investigated. In [10], there is a description of the real-time implementation of a bi-input Extended Kalman Filter estimator, which deals with the estimation of the whole state of the Induction Motor together with stator and rotor resistances. To cope with the higher computational efforts required by these filters, alternative configurations based on Kalman filtering have been proposed [5, 24], where the complexity of the filter is reduced solving two linear least squares subproblems instead of a nonlinear one. Finally, different approaches that are not based on Kalman filtering [49, 82] could be followed.

Moreover the use of the Extended Kalman Filter, considered as a means to estimate the state of a sixth–order Induction Motor–load system model, has a double objective: firstly, to obtain filtered stator current components, which is essential for controlling the IM–load system; secondly, to estimate stator flux components and the speed for implementing sensorless state feedback control laws [25, 8]. The estimation of the load torque indirectly allows a better estimation of the speed, but it can also be used to implement control laws based on disturbance compensation.

2.7 Reduced Adaptive Kalman Filter - Experimental results

To validate the reduced Adaptive kalman Filter, a closed loop experiments are shown, which were carried out on a system consisting of the usual $0.750kW$ induction motor. The whole controller, including the proposed estimator, is implemented on a dSpace®DS1103®microcontroller that processes the control system at 12 kHz, and allows data acquisition of the measured variables and their visualization on the cockpit provided by dSPACE®software.

The measured variables are the speed computed starting from data acquired by means of a 1024 ppr incremental encoder that is useful for comparing estimated and measured speeds, which are filtered using a PLL scheme, and the two stator currents given by two Hall-effect transducers.

The rated data of the motor is shown in Table 2.1 and is the same used in the other

experimental tests presented (see the last chapter of this thesis for the details).

In order to analyze robustness, both Adaptive Kalman Filter and Reduced Adaptive Kalman Filter estimators are designed assuming the following uncertainties: 50% for R_r and R_s, and 30% for L_m. Note that neither cause nor rate of variation are needed for designing the estimator. Both estimators were initialized assuming $\mathbf{P}_0 = 50\mathbf{I}_4$, $x_0 = 0$, $\mathbf{R} = \mathbf{I}_2$, $\mathbf{Q} = diag\{2 \times 10^{-2}, 2 \times 10^{-2}, 2 \times 10^{-3}, 2 \times 10^{-3}\}$.

Figures 2.25–2.28 show the responses of the closed loop system in the presence of either robust or standard estimators, corresponding to a trapezoidal reference speed with a maximum speed of 150 rad/s, at no load and with speed reversal.

An examination of Figures 2.25 and 2.27 shows that both the estimators give good results. In fact, in both cases the speed tracks the reference one, the mean error is zero, and the maximum difference between measured and estimated speeds is less than $\pm 1 rad/s$. The spikes are due to the resolution of the encoder. Figures 2.26 and 2.28 show that both estimators are able to reproduce measured currents. Obviously, acting on the elements of matrix $\mathbf{Q}$, it is possible to conveniently filter these currents.

Figures 2.29–2.32 show the closed loop responses corresponding to a trapezoidal reference speed in the presence of a load torque of 5 Nm applied at 2 s and removed at 13 s. A comparison of Figures 2.29 and 2.31 shows that Reduced Adaptive Kalman Filter works better than Adaptive Kalman Filter at load; in fact, the maximum difference between measured and estimated speeds is in the interval $[-2.5, 0]\, rad/s$, with a mean displacement of about $-1 rad/s$ for Reduced Adaptive Kalman Filter, whereas it is in the interval $[-5, -3] rad/s$, with a mean displacement of about $-4 rad/s$ for Adaptive Kalman Filter. Looking at Figures 2.30–2.32, it appears that both estimators reproduce the measured currents very well. Figures 2.33–2.36 show the responses of the closed loop system at no load, during low speed tests ($3 rad/s$). Both estimators are able to track the reference speed with a mean speed equal to zero, but Reduced Adaptive Kalman Filter displays better dynamic properties and is slightly noisier than Adaptive Kalman Filter. Figures 2.37–2.40 show the responses at $3 rad/s$, with a $4 Nm$ step load torque applied at $2s$ and removed at $13s$. A comparison of Figures 2.37–2.39 shows that Reduced Adaptive Kalman Filter behaves well, both at load and not at load, with a maximum difference between measured and estimated speeds in the interval

$[-2, 2] rad/s$, with a mean displacement of about $-1 rad/s$. Also, in these difficult operating conditions, Reduced Adaptive Kalman Filter appears better from the dynamic point of view, but is also nosier than Adaptive Kalman Filter. Figures 2.41–2.42 show the speed responses of the system with feedback from Reduced Adaptive Kalman Filter and Adaptive Kalman Filter at step reference speed and no load. In this experiment only, both estimators are designed assuming the nominal resistances increased by 30%, and the mutual inductance decreased by 20%, compared to the values obtained with the previously described identification process. Examination of these figures shows that Reduced Adaptive Kalman Filter works better then Adaptive Kalman Filter for step reference speed variations, especially during transients.

Once again, we would like to point out that our experiments are carried out on an induction motor drive in which estimated variables are used for closing the control loops. In this study we show results at $3 rad/s$ at no load and load, even though we also reach lower speeds $(1 - 2 rad/s)$, but with a worse speed waveform. In our opinion, this is due to the non linear behavior of the brake, especially at low speed.

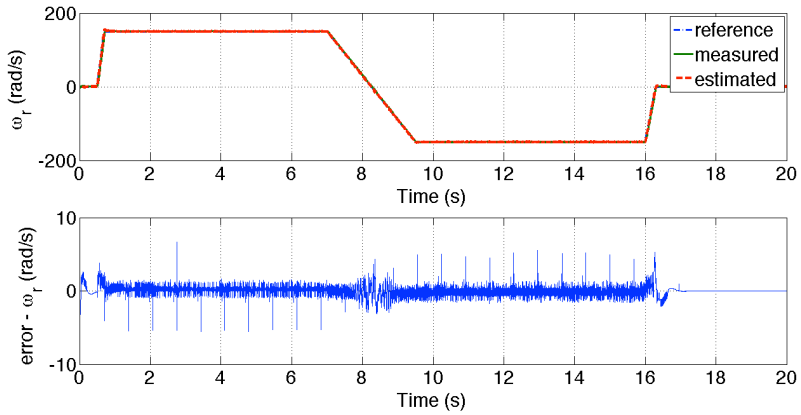

Figure 2.25: Speed response of the system with feedback from Reduced Adaptive Kalman Filter at high reference speed and no load. The machine is fluxed at zero reference speed up to 0.5 s , and then it is started with a trapezoidal reference speed of 150 rad/s.

2.7.1 Literature notes

Performance in the control of induction motor electrical drives are greatly affected by parameter uncertainty. Indeed the behavior of both controller and estimator, designed using a model-based approach, rapidly deteriorates in the presence of these uncertainties. Obviously, the behavior of the whole control system is particularly sensitive to that of the state

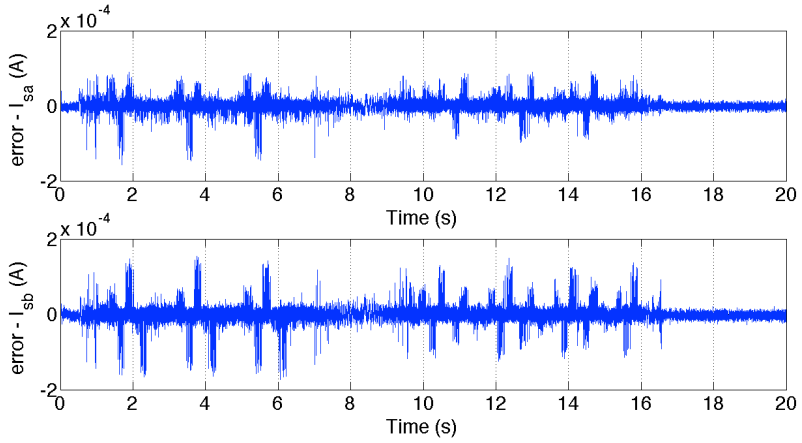

Figure 2.26: Current estimation error of the system with feedback from Reduced Adaptive Kalman Filter at high reference speed. Same conditions as Figure 2.25.

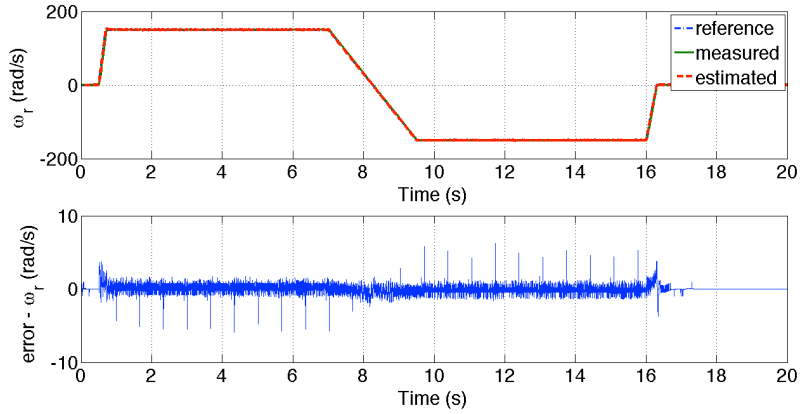

Figure 2.27: Speed response of the system with feedback from Adaptive Kalman Filter at high reference speed. Same conditions as Figure 2.25.

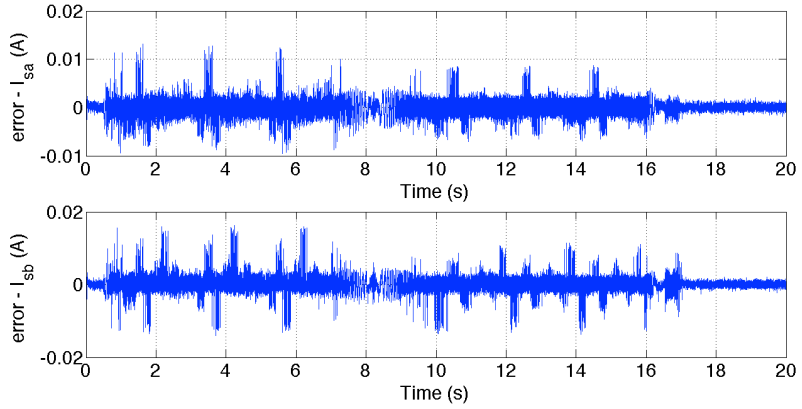

Figure 2.28: Current estimation error of the system with feedback from Adaptive Kalman Filter at high reference speed. Same conditions as Figure 2.25.

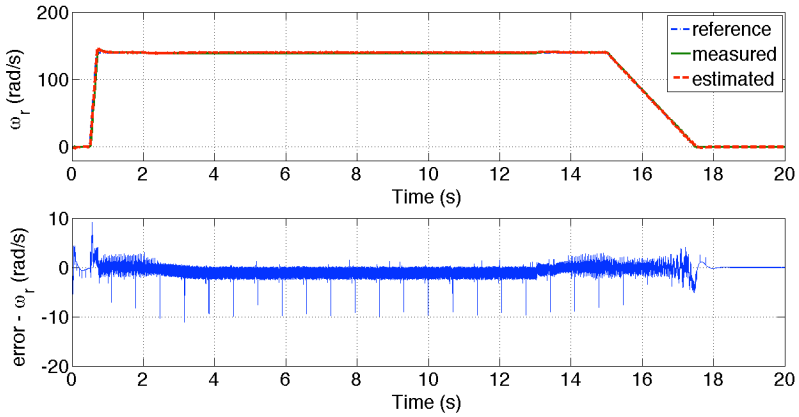

Figure 2.29: Speed response of the system with feedback from Reduced Adaptive Kalman Filter at high reference speed. A 5 Nm load torque is applied at 2 s and removed at 13 s.

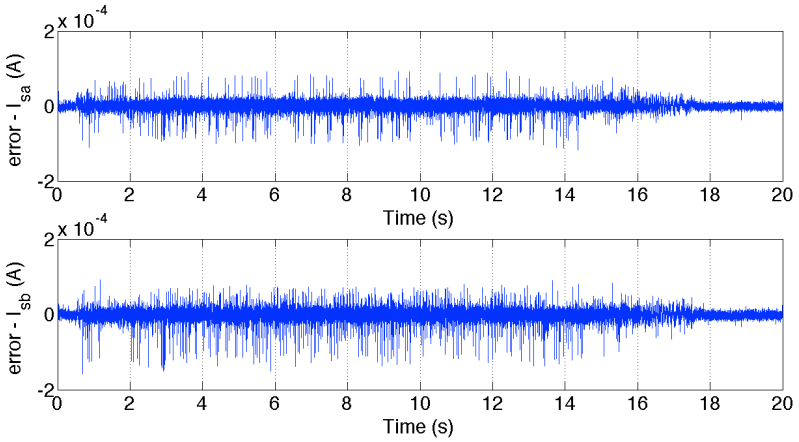

Figure 2.30: Current estimation error of the system with feedback from Reduced Adaptive Kalman Filter at high reference speed. Same conditions as Figure 2.29.

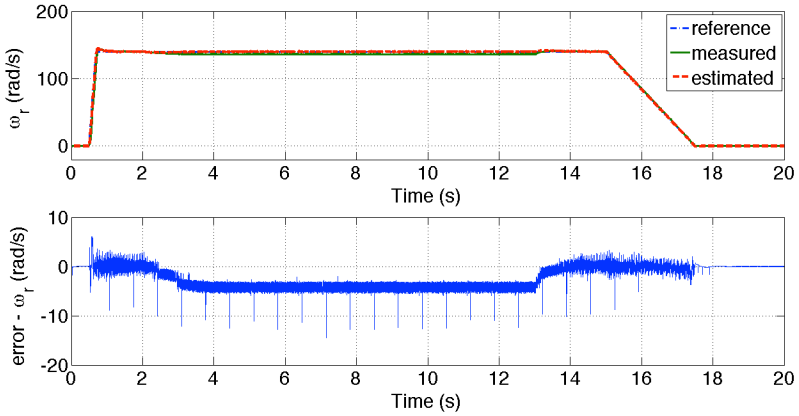

Figure 2.31: Speed response of the system with feedback from Adaptive Kalman Filter at high reference speed. Same conditions as Figure 2.29.

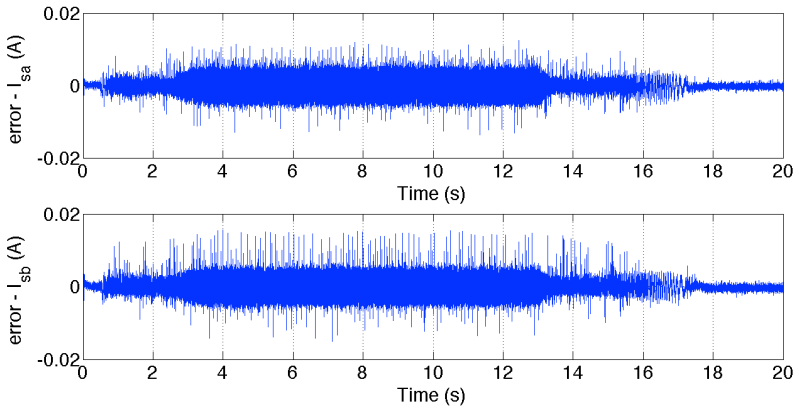

Figure 2.32: Current estimation error of the system with feedback from Adaptive Kalman Filter at high reference speed. Same conditions as Figure 2.29.

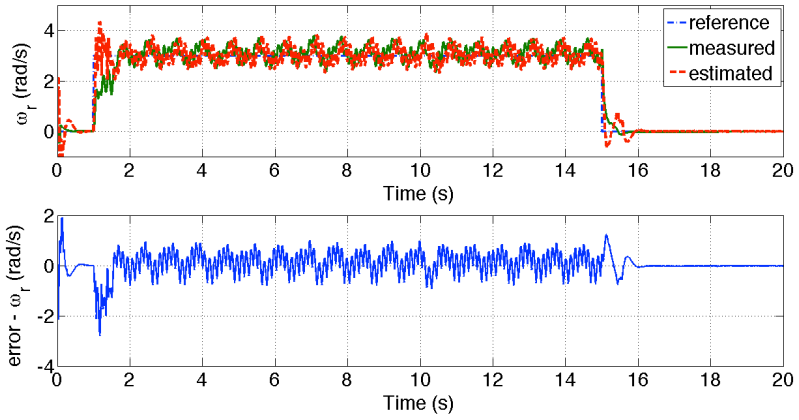

Figure 2.33: Speed response of the system with feedback from Reduced Adaptive Kalman Filter at no load and low reference speed. The machine is fluxed at zero reference speed. At 1 s, it is started with a step of 3 rad/s; and a further step of -3 rad/s, applied at 15 s, brings the reference speed to zero.

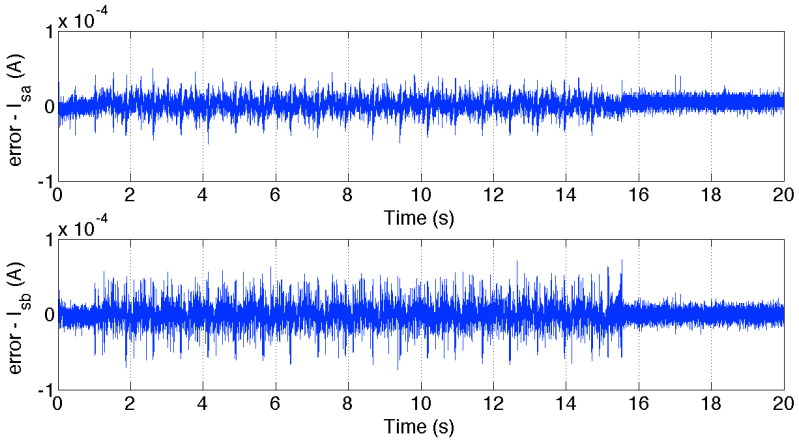

Figure 2.34: Current estimation error of the system with feedback from Reduced Adaptive Kalman Filter at low speed reference. Same operating conditions as Figure 2.33.

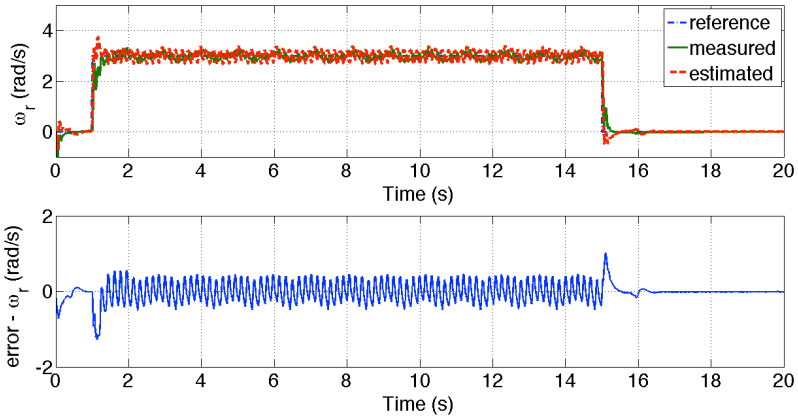

Figure 2.35: Speed response of the system with feedback from Adaptive Kalman Filter at low reference speed. Same operating conditions as Figure 2.33.

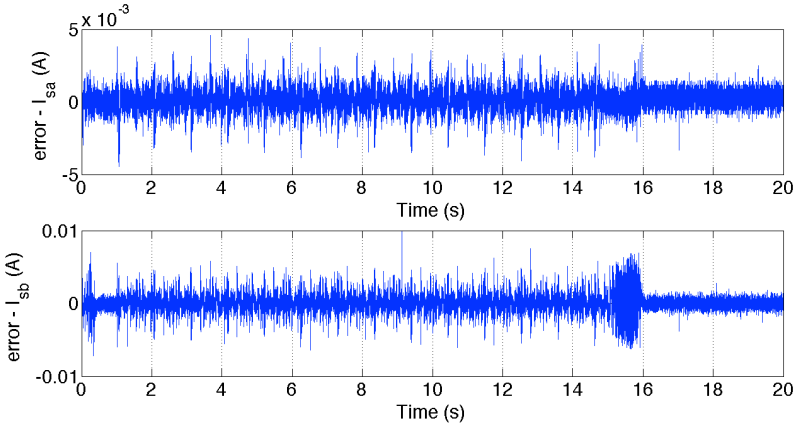

Figure 2.36: Current estimation error of the system with feedback from Adaptive Kalman Filter at low speed reference. Same operating conditions as Figure 2.33.

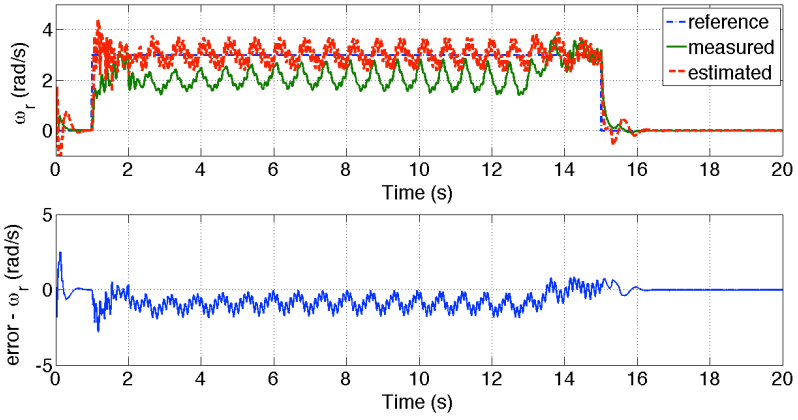

Figure 2.37: Speed response of the system with feedback from Reduced Adaptive Kalman Filter at low reference speed. The machine is fluxed at zero reference speed. At 1s, it is started with a step of 3rad/s; a load torque of 4Nm is applied at 2s, and removed at 13s.

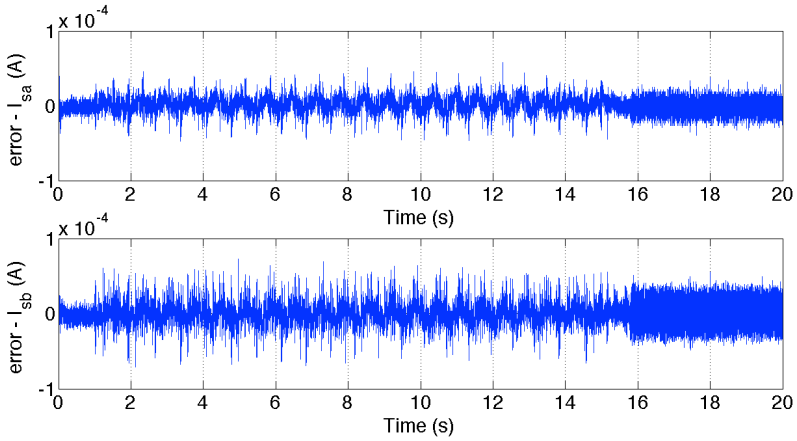

Figure 2.38: Current estimation error of the system with feedback from Reduced Adaptive Kalman Filter at low reference speed. Same operating conditions as Figure 2.37.

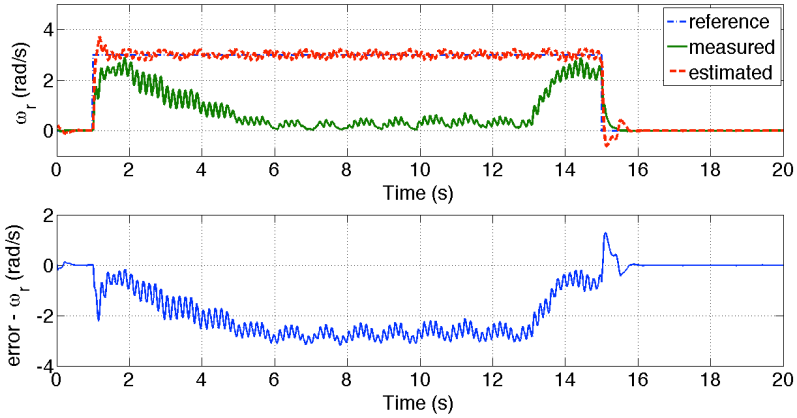

Figure 2.39: Speed response of the system with feedback from Adaptive Kalman Filter at low speed reference. Same operating conditions as Figure 2.37.

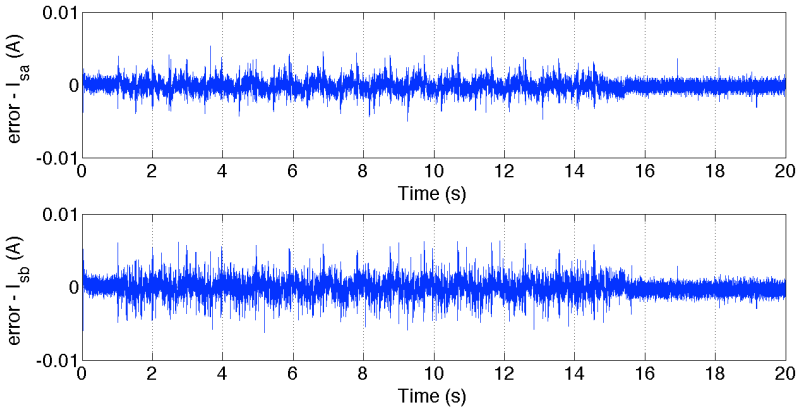

Figure 2.40: Current estimation error of the system with feedback from Adaptive Kalman Filter at low reference speed. Same operating conditions as Figure 2.37.

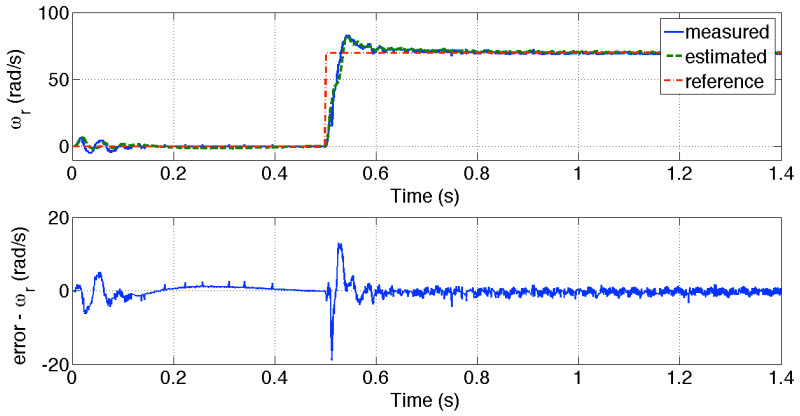

Figure 2.41: Speed response of the system with feedback from Reduced Adaptive Kalman Filter at step reference speed and no load. The machine is fluxed at zero reference speed. At 0.5 s, it is started with a step of 70 rad/s.

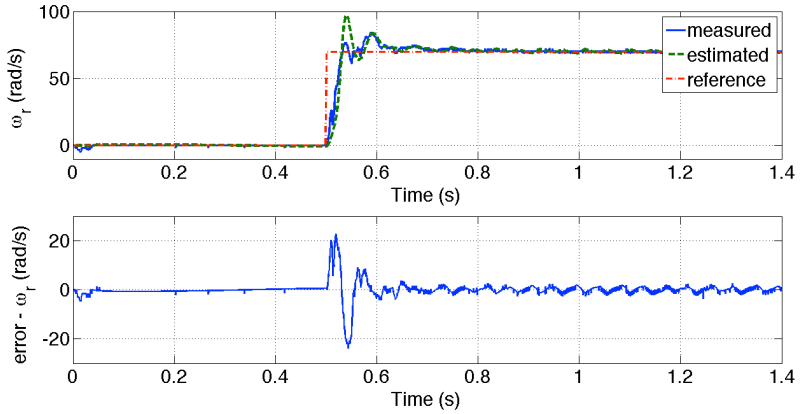

Figure 2.42: Speed response of the system with feedback from Adaptive Kalman Filter at step reference speed and no load. The machine is fluxed at zero reference speed. At 0.5s, it is started with a step of 70rad/s.

estimator. To cope with these uncertainties, on-line parameter identification and adaptive or robust design techniques can be employed for designing either the estimator or the controller, or both.

In [59] and [9] both rotor and stator resistances are estimated on-line using Neural Networks (NN) or two Extended Kalman Filters, respectively, whereas in [8] only stator resistance is estimated using an EKF; all of these works assume that stator, rotor and mutual inductances are well known. In [59] rotor and stator resistances are estimated by two different schemes involving two different NN that are constructed starting from a model of the induction motor, and speed is estimated using the same approach described in [64], in which the authors state that estimated speed is sensitive to noise, thereby requiring filtering. Experimental results obtained by processing data acquired from a closed loop drive show that in the presence of load torque, the speed does not track the measured one. In [9] rotor and stator resistances are estimated by two different seventh order Extended Kalman Filters that estimate the augmented state of the induction motor-load system, consisting of stator current and rotor flux components, speed, load torque and, alternatively, stator resistance and rotor resistance. However, the braided Extended Kalman Filter, consisting of two seventh order Kalman Filters, is too complex. Furthermore, in practical applications it is not possible to know the existence of the persistent excitation condition *a priori*, which is a mandatory condition for an exact parameter estimation. This appears clearly in the results shown in [9], aimed at proving the need to identify both rotor and stator resistances. [11] presents the real-time implementation of a bi input-extended Kalman filter (BI-EKF)-based estimator in order to overcome the simultaneous estimation problem of the variations in stator resistance and rotor resistance aside from the load torque and all states required for the speed-sensorless control of induction motors in the wide speed range. In [8] a conventional Extended Kalman Filter is studied and the corresponding results are given in the presence of various scenarios, but a sensitivity analysis in the presence of parameter variations is not carried out, whereas in [4] it is shown that EKF is sensitive to parameter variations, especially at low speeds. Moreover, the experimental results shown in works [9] and [8] are obtained by processing data acquired from V/f-controlled drives. Note that EKF is also applied for sensorless control of Synchronous AC drives [54].

An alternative solution to Extended Kalman Filter is presented in [57] where the de-

sign and implementation of unscented Kalman filters (UKFs) for induction motor sensorless drives is investigated. UKFs use nonlinear unscented transformations in the prediction step in order to preserve the stochastic characteristics of a nonlinear system. The advantage of using UTs is their ability to capture the nonlinear behavior of the system, unlike the Extended Kalman Filters that use linearized models. But in this work no reference was made to the parameter variation during operation.

In [64] rotor flux and stator currents are estimated by means of a Sliding Mode Observer (SMO), processed by the difference of the measured and observed stator currents. For those systems affine with respect to the input, the Sliding Mode observer is robust against all disturbances including parameter uncertainties that belong to the space generated by the column of the forcing matrix, but the estimates produced are affected by chattering, as shown in [64].

In [53], [21] and [20] model reference adaptive control techniques are proposed for designing observers, whereas in [78] the same techniques are employed for designing a controller. Other MRAS observers are described in the literature, and some of them are compared in [69].

From the control engineering point of view, the approach proposed in this study explicitly assumes the objective of the robustness of the estimator against variations of all the parameters of the motor, without the need to estimate some of them. A first step for reaching this objective is that of formulating the state estimation problem in two steps. In the first step, for a given speed, the rotor flux and stator currents are estimated by means of a linear fourth order Robust Descriptor Kalman Filter (RDKF), starting from measured stator currents and the supplied voltages computed by the controller; in the second step, the speed is estimated by solving a total least-squares problem starting from the dynamic equations of the rotor flux components (cf. also [21] and [20]). The descriptor form of the KF is used here because the coefficients of the model are functions of the physical electromagnetic parameters that are simpler than those appearing in the conventional form. Consequently, physical parameter variations can be directly translated into variations of the coefficients appearing in the model, and this intrinsically leads to a certain degree of robustness of the Descriptor Kalman Filter (DKF). Moreover, in order to explicitly take into account parameter uncertainties, a RDKF is designed according to [55] and [75].

The advantage of the procedure described is that the mechanical equation is not included in the state estimation procedure, thus avoiding the use of nonlinear estimation methods such as, for example, EKF, and the connected lack of observability properties of the model in certain operating conditions [15]; instead, only two linear least-squares problems must be solved for estimating the state of the system. Moreover, neither load torque estimation nor parameter estimation is required, guaranteeing, in any case, the robustness of the estimation. Finally, all of the parameter variations are simultaneously taken into account, and this occurs independently of the causes of their variation.

Conclusions

In this thesis the problem of designing observers and controllers for induction motors has been studied and thoroughly discussed using tools from the nonlinear system theory, both for analysis and control purposes. Useful techniques have been used to identify the machine parameters off-line.

In the Introduction was dealt the design a control system for a drive of asynchronous machines that uses a voltage source inverter to generate the currents and voltages which carry the drive by making use of an observer of the state rotor variables.

The used control algorithms is the *field oriented control* (FOC). The model of the asynchronous induction motor is described starting from the mechanical model, the electrical model through the Steinmetz equivalent electrical circuit that is the IEEE recommended equivalent circuit, the State Model of Asynchronous Motor and the mathematical model, completing with the discretization of the last model, realizing the Discrete time mathematical model.

In Chapter 1 several observer are taken in account in order to be able to compare their strengths and weaknesses. At first it's developed a (FOLO) Full Order Luemberger Observer and its Reduced Order version. Other observer that was considered it's the Sliding one. Then a version of Non linear Flux observer was synthesized in order to consider the effects of saturation which introduce a nonlinear effects. At last the (EKF) Extended Kalman Filter was considered, both in complex (ECKF) and the (RAKF) Robust Adaptive Kalman Filter version.

In Chapter 2 have been presented experimental and simulation results obtained by testing each of the previous algorithms. Excellent results were obtained by use of observer based

on Kalman Filter, and in particular, the Extended Complex Kalman Filter, because no matrix inversion is required. In fact the operation of matrix inversion that is necessary in the classic Extended Kalman Filter is therefore translated in the inverse of a real number in the proposed Extended Complex Kalman Filter.

In conclusion, a set of tools present in control theory have been applied successfully in motion control systems with induction motors. This work is certainly not a complete treatment, since many basic parts are omitted (only the references are given), and for this reasons is to be understood as completion of studies related to the subject matter.

Bibliography

[1] G. Figalli A. Bellini and G. Ulivi. "analysis and design of a microcomputer-based observer for an induction motor, vol.24 n.4". In *"Automatica"*, pages "549–555", "July 1988". (Quoted on pages 14 e 57)

[2] Y. A. Abramovich, C. D. Aliprantis, and O. Burkinshaw. Direct self-control of inverter.fed machine. *IEEE Trans. Power Elec.*, 3(4):420–429, "oct. 1988".

[3] F. Alonge and F. D'Ippolito. Extended kalman filter for sensorless control of induction motors. In *First Symposium on Sensorless Control for Electrical Drives (SLED)*, pages 107 –113, July 2010. (Quoted on page 81)

[4] F Alonge and F D'Ippolito. Robustness analysis of an extended kalman filter for sensorless control of induction motors. In *Industrial Electronics (ISIE), 2010 IEEE International Symposium on*, pages 3257–3263. IEEE, 2010. (Quoted on page 90)

[5] F Alonge, F D'Ippolito, and A Sferlazza. Sensorless control of induction motor drive based on robust kalman filter and adaptive speed estimation. *Industrial Electronics, IEEE Transactions on*, 61(3):1444–1453, 2014. (Quoted on pages 39 e 81)

[6] F. Alonge and T. Raimondi. "design of a reduced order observer for induction motors". In *"Proc. 7th Int. Conf. on Control Systems and Computer Science"*, volume "1", pages "46–55", "Bucharest", "May 1987". (Quoted on page 14)

[7] Gennaro Figalli Armando Bellini. *Il Motore Asincrono negli Azionamenti Industriali*. Universit di Torino, UniTor, Torino, 1993.

[8] M. Barut, S. Bogosyan, and M. Gokasan. Speed–sensorless estimation for induction motors using extended kalman filters. 54(1):272–280, February 2007. (Quoted on pages 81 e 90)

[9] Murat Barut, Seta Bogosyan, and Metin Gokasan. Experimental evaluation of braided ekf for sensorless control of induction motors. *Industrial Electronics, IEEE Transactions on*, 55(2):620–632, 2008. (Quoted on page 90)

[10] Murat Barut, Ridvan Demir, Emrah Zerdali, and Remzi Inan. Real-time implementation of bi input-extended kalman filter-based estimator for speed-sensorless control of induction motors. *Industrial Electronics, IEEE Transactions on*, 59(11):4197–4206, 2012. (Quoted on page 81)

[11] Murat Barut, Ridvan Demir, Emrah Zerdali, and Remzi Inan. Real-time implementation of bi input-extended kalman filter-based estimator for speed-sensorless control of induction motors. *Industrial Electronics, IEEE Transactions on*, 59(11):4197–4206, 2012. (Quoted on page 90)

[12] Aman Behal, M Feemster, Darren M Dawson, and A Mangal. Partial state feedback control of induction motors with magnetic saturation: elimination of flux measurements. *Automatica*, 38(2):191–203, 2002. (Quoted on page 57)

[13] Armando Bellini. *Controllo Diretto della Coppia negli Azionamenti con Motore Asincrono*. Automazione e Strumentazione, Torino, "Luglio-Agosto 2000".

[14] Sergio Bittanti and Sergio M Savaresi. On the parametrization and design of an extended kalman filter frequency tracker. *Automatic Control, IEEE Transactions on*, 45(9):1718–1724, 2000. (Quoted on page 74)

[15] C Canudas De Wit, A Youssef, JP Barbot, Ph Martin, and F Malrait. Observability conditions of induction motors at low frequencies. In *Decision and Control, 2000. Proceedings of the 39th IEEE Conference on*, volume 3, pages 2044–2049. IEEE, 2000. (Quoted on page 92)

[16] Yoichi Hori Cao-Minh Ta. Convergence improvement of efficiency optimization control of induction motor drives. *IEEE Transactions on Industry Applications*, 37(6), 2001.

[17] S.I.Seleme Jr." "C.Canudas de Wit. *"Robust Torque Control Design for Induction Motor: the Minimum Energy Approach"*, volume "33, 1". "Automatica", 1997.

[18] Giansalvo Cirrincione, Maurizio Cirrincione, Jeanny Herault, and Sabine Van Huffel. The mca exin neuron for the minor component analysis. *Neural Networks, IEEE Transactions on*, 13(1):160–187, 2002. (Quoted on page 51)

[19] M. Cirrincione, M. Pucci, G. Cirrincione, and G.-A. Capolino. An adaptive speed observer based on a new total least-squares neuron for induction machine drives. 42(1):89–104, jan.-feb. 2006. (Quoted on page 81)

[20] Maurizio Cirrincione, Marcello Pucci, Giansalvo Cirrincione, and G-A Capolino. An adaptive speed observer based on a new total least-squares neuron for induction machine drives. In *Industry Applications Conference, 2004. 39th IAS Annual Meeting. Conference Record of the 2004 IEEE*, volume 2, pages 1350–1361. IEEE, 2004. (Quoted on page 91)

[21] Maurizio Cirrincione, Marcello Pucci, Giansalvo Cirrincione, and G-A Capolino. A new tls-based mras speed estimation with adaptive integration for high-performance induction machine drives. *Industry Applications, IEEE Transactions on*, 40(4):1116–1137, 2004. (Quoted on pages 81 e 91)

[22] A.Tani D.Casadei, G.Serra. Implementation of a direct torque control algorithm for induction motor based on a discrete space vector modulation. *IEEE trans. on Power Electronics*, 14(4), "July 2000".

[23] G.Grandi G.Serra A.Tani D.Casadei. Effects of flux and torque hysteresis band amplitude in direct torque control of induction machine. *Conf. Proc. of 1994 IEEE.IECON*, pages 299–304, 1994.

[24] Filippo D'Ippolito, Francesco Alonge, and Antonino Sferlazza. Descriptor-type robust kalman filter and neural adaptive speed estimation scheme for sensorless control of induction motor drive systems. In *Robust Control Design*, volume 7-1, pages 51–56, 2012. (Quoted on pages 39 e 81)

[25] T. Du, P. Vas, and F. Stronach. Design and application of extended observers for joint

state and parameter estimation in high-performance ac drives. *IEE Proceedings on Electric Power Applications*, 142(2):71–78, March 1995. (Quoted on page 81)

[26] M. Koyama et al. Microprocessor-based vector control system for induction motor drives with rotor time constant identification function. *IEEE Trans. Ind. Appl.*, IA-22(3):453–459, "May/June 1986". (Quoted on page 14)

[27] S.Sangwongwanich et al. Design of sliding observer for robust estimation of rotor flux of induction motors. *"Proc. IPEC-Tokio Conf."*, "2":1235–1242, "april 1990". (Quoted on page 27)

[28] "F.Alonge and T.Raimondi". *"Sliding and Reduced Order Observer for Flux Estimation of Induction Motor: Analysis and Design"*. "Istituto di Automatica e Sistemistica - Universit di Palermo", "Viale delle Scienze, Palermo", 2000.

[29] F.Alonge and T.Raimondi. "an estimator of rotor flux of induction motors". In *"Proc. 6th Conf. on Power Electronics and Motion Control Vol.2, Budapest"*, pages 494–499, "October 1990". (Quoted on pages 14 e 20)

[30] F.D'Ippolito F.M.Raimondi F.Alonge and A.Urso. Least squares and genetic algorithms for parameters identification of induction motor. *"Control Engineering Practice"*, "9/6":647–657, "giugno 2001".

[31] Y. Funahashi. Stable state estimator for bilinear systems. *Int. J. Control*, 29(2):181–188, 1979. (Quoted on page 10)

[32] R. Gabriel and W. Leonhard. "microprocessor control of induction motor". In *"Proc. Int. Semiconductor Power Converter Conf., Orlando"*, pages 385–396, "May 1982". (Quoted on page 14)

[33] G.Giardina. *Controllo Robusto di Azionamenti con Motore a Induzione: realizzazione di un prototipo e implementazione di un controllore su DSP*. Universit di Palermo, Dipartimento di Ingegneria Automatica e Sistemistica, 1999.

[34] Malek Ghanes and Gang Zheng. On sensorless induction motor drives: sliding-mode observer and output feedback controller. *Industrial Electronics, IEEE Transactions on*, 56(9):3404–3413, 2009. (Quoted on page 81)

[35] Francesco Alonge Filippo D'Ippolito Giuseppe Giardina and Tonino Scaffidi. Design and low-cost implementation of an optimally robust reduced-order rotor flux observer for induction motor control. *IEEE Transactions on Industrial Electronics*, 54(6):3205–3216, dec 2007. (Quoted on pages 57 e 75)

[36] R.M. Stephan e E.H. Watanabe G.O.Garcia, J.C.Mendes Lus. "fast efficiency maximizer for adjustable speed induction motor drive". In *"IEEE Proc. of the 1992 International Conference on Power Electronics and Motion Control - Vol.1"*, pages "37–42", "Tokio", 1992.

[37] Mohinder S Grewal and Angus P Andrews. *Kalman filtering: theory and practice using MATLAB*. Wiley. com, 2011. (Quoted on page 38)

[38] S. Hara and K. Furuta. Minimal order state observers for bilinear systems. *Int. J. Control*, 24(5):705–718, 1976. (Quoted on pages 8 e 10)

[39] Lennart Harnefors. Design and analysis of general rotor-flux-oriented vector control systems. *Industrial Electronics, IEEE Transactions on*, 48(2):383–390, 2001. (Quoted on page 56)

[40] Lennart Harnefors and Marko Hinkkanen. Complete stability of reduced-order and full-order observers for sensorless im drives. *Industrial Electronics, IEEE Transactions on*, 55(3):1319–1329, 2008. (Quoted on page 57)

[41] Lennart Harnefors and Marko Hinkkanen. Stabilization methods for sensorless induction motor drives-a survey. *Industrial Electronics, IEEE Transactions on*, In Press.

[42] Masaru Hasegawa. Robust-adaptive-observer design based on γ-positive real problem for sensorless induction-motor drives. *Industrial Electronics, IEEE Transactions on*, 53(1):76–85, 2006. (Quoted on page 57)

[43] M Hilairet, F Auger, and C Darengosse. Two efficient kalman filters for flux and velocity estimation of induction motors. In *Power Electronics Specialists Conference, 2000. PESC 00. 2000 IEEE 31st Annual*, volume 2, pages 891–896. IEEE, 2000. (Quoted on pages 39 e 74)

[44] Mickaël Hilairet, François Auger, and Eric Berthelot. Speed and rotor flux estimation of

induction machines using a two-stage extended kalman filter. *Automatica*, 45(8):1819–1827, 2009. (Quoted on pages 39 e 74)

[45] Marko Hinkkanen. Analysis and design of full-order flux observers for sensorless induction motors. *Industrial Electronics, IEEE Transactions on*, 51(5):1033–1040, 2004. (Quoted on page 56)

[46] Marko Hinkkanen, Lennart Harnefors, and Jorma Luomi. Reduced-order flux observers with stator-resistance adaptation for speed-sensorless induction motor drives. *Power Electronics, IEEE Transactions on*, 25(5):1173–1183, 2010. (Quoted on page 56)

[47] Marko Hinkkanen and Jorma Luomi. Parameter sensitivity of full-order flux observers for induction motors. *Industry Applications, IEEE Transactions on*, 39(4):1127–1135, 2003. (Quoted on page 57)

[48] Marko Hinkkanen and Jorma Luomi. Stabilization of regenerating-mode operation in sensorless induction motor drives by full-order flux observer design. *Industrial Electronics, IEEE Transactions on*, 51(6):1318–1328, 2004. (Quoted on page 56)

[49] Joachim Holtz. Sensorless control of induction motor drives. *Proceedings of the IEEE*, 90(8):1359–1394, 2002. (Quoted on pages 80 e 81)

[50] Chien-Shu Hsieh. General two-stage extended kalman filters. *Automatic Control, IEEE Transactions on*, 48(2):289–293, 2003. (Quoted on page 39)

[51] Chien-Shu Hsieh and Fu-Chuang Chen. Optimal solution of the two-stage kalman estimator. *Automatic Control, IEEE Transactions on*, 44(1):194–199, 1999. (Quoted on page 39)

[52] Kevin D Hurst and Thomas G Habetler. Sensorless speed measurement using current harmonic spectral estimation in induction machine drives. *Power Electronics, IEEE Transactions on*, 11(1):66–73, 1996. (Quoted on page 80)

[53] Matteo Felice Iacchetti. Adaptive tuning of the stator inductance in a rotor-current-based mras observer for sensorless doubly fed induction-machine drives. *Industrial Electronics, IEEE Transactions on*, 58(10):4683–4692, 2011. (Quoted on page 91)

[54] Lahoucine Idkhajine, Eric Monmasson, and Amira Maalouf. Fully fpga-based sensorless control for synchronous ac drive using an extended kalman filter. *Industrial Electronics, IEEE Transactions on*, 59(10):3908–3918, 2012. (Quoted on page 90)

[55] João Y Ishihara, Marco H Terra, and José CT Campos. Robust kalman filter for descriptor systems. *Automatic Control, IEEE Transactions on*, 51(8):1354–1354, 2006. (Quoted on pages 46, 48 e 91)

[56] Saeed Jafarzadeh, Cristian Lascu, and M Sami Fadali. State estimation of induction motor drives using the unscented kalman filter. *Industrial Electronics, IEEE Transactions on*, 59(11):4207–4216, 2012. (Quoted on page 81)

[57] Saeed Jafarzadeh, Cristian Lascu, and M Sami Fadali. State estimation of induction motor drives using the unscented kalman filter. *Industrial Electronics, IEEE Transactions on*, 59(11):4207–4216, 2012. (Quoted on page 90)

[58] M.Ghaneei J.Faiz, S.H.Hossieni and A.Keyhani A.Proca. *Direct Torque Control of Induction Motor for Electric Propulsion System*. Electric Power Systems Research, 1998.

[59] Baburaj Karanayil, Muhammed Fazlur Rahman, and Colin Grantham. Online stator and rotor resistance estimation scheme using artificial neural networks for vector controlled speed sensorless induction motor drive. *Industrial Electronics, IEEE Transactions on*, 54(1):167–176, 2007. (Quoted on page 90)

[60] Young-Real Kim, Seung-Ki Sul, and Min-Ho Park. Speed sensorless vector control of induction motor using extended kalman filter. 30(5):1225 –1233, sep-oct 1994. (Quoted on page 81)

[61] Hossein Madadi Kojabadi and Liuchen Chang. Comparative study of pole placement methods in adaptive flux observers. *Control engineering practice*, 13(6):749–757, 2005. (Quoted on page 57)

[62] C Korlinchak and M Comanescu. Sensorless field orientation of an induction motor drive using a time-varying observer. *IET electric power applications*, 6(6):353–361, 2012. (Quoted on page 57)

[63] K Kubota, Kouki Matsuse, and Takayoshi Nakano. New adaptive flux observer of induction motor for wide speed range motor drives. In *Industrial Electronics Society, 1990. IECON'90., 16th Annual Conference of IEEE*, pages 921–926. IEEE, 1990. (Quoted on pages 56 e 57)

[64] Cristian Lascu, Ion Boldea, and Frede Blaabjerg. Very-low-speed variable-structure control of sensorless induction machine drives without signal injection. *Industry Applications, IEEE Transactions on*, 41(2):591–598, 2005. (Quoted on pages 90 e 91)

[65] W. Leonhard. "control of ac machines with the help of microelectronics". In *"Proc. 3rd IFAC Symp. on Control in Power Electronics and Electrical Drives, Survey Paper, Lausanne"*, pages 35–58, "September 1983". (Quoted on page 14)

[66] Riccardo Marino, Patrizio Tomei, and Cristiano M Verrelli. *Induction motor control design*. Springer, 2010. (Quoted on page 56)

[67] Riccardo Marino, Patrizio Tomei, and Cristiano Maria Verrelli. A new flux observer for induction motors with on-line identification of load torque and resistances. In *18th IFAC World Congress, Milano, Italy*, volume 18, pages 6172–6177, 2011. (Quoted on page 57)

[68] G.Bertoni M.E.Penati. La sintesi del controllo sliding mode nei sistemi a struttura variabile. In *"6° incontro su Identificazione, Controllo e Ottimizzazione dei sistemi dinamici, L'Aquila"*, "September 1989". (Quoted on pages 29 e 30)

[69] Kazuhiro Ohyama, Greg M Asher, and Mark Sumner. Comparative analysis of experimental performance and stability of sensorless induction motor drives. *Industrial Electronics, IEEE Transactions on*, 53(1):178–186, 2006. (Quoted on page 91)

[70] I.R. Petersen and A.V. Savkin. *Robust Kalman filtering for signals and systems with large uncertainties*. Birkhäuser Boston, 1999. (Quoted on page 37)

[71] K. Rajashekara, A. Kawamura, and K. Matsuse. *Sensorless control of AC motor drives: speed and position sensorless operation*. IEEE press New York, 1996. (Quoted on pages 80 e 81)

[72] K. Reif, S. Gunther, E. Yaz, and R. Unbehauen. Stochastic stability of the discrete–time extended kalman filter. *tac*, 44(4):714–728, April 1999. (Quoted on page 34)

[73] M. Rodic and K. Jezernik. Speed-sensorless sliding-mode torque control of an induction motor. 49(1):87–95, February 2002. (Quoted on page 81)

[74] Gary L. Skibinski Russel. J. Kerkman and David W. Schlegel. Ac drives: Year 2000 (y2k) and beyond. *"IEEE APEC '99"*, "March 14-18,1999".

[75] Ali H Sayed. A framework for state-space estimation with uncertain models. *Automatic Control, IEEE Transactions on*, 46(7):998–1013, 2001. (Quoted on pages 50 e 91)

[76] H. Tajima and Y. Hori. Speed sensorless field-orientation control of the induction machine. 29(1):175–180, jan-feb 1993. (Quoted on page 81)

[77] Tzyh-Jong Tarn and Y. Rasis. Observers for nonlinear stochastic systems. *tac*, 21(4):441–448, August 1976. (Quoted on page 34)

[78] AV Ravi Teja, Chandan Chakraborty, Suman Maiti, and Yoichi Hori. A new model reference adaptive controller for four quadrant vector controlled induction motor drives. *Industrial Electronics, IEEE Transactions on*, 59(10):3757, 2012. (Quoted on page 91)

[79] Takahashi T.Naguchi, I. A new quick-response and high-efficiency control strategy of an induction motor. *IEEE Trans. Ind. App.*, "IA-22":820–827, "sept-oct 1986".

[80] P. Vas. *Sensorless Vector and Direct Torque Control*. Oxford Science Publication, 1998. (Quoted on pages 43, 44, 56, 80 e 81)

[81] G. C. Verghese and S.R. Sanders. Observers for flux estimation in induction machines. *IEEE Trans. on Ind. Electron.*, 35(1):"85–94", "Feb. 1988". (Quoted on pages 14, 21 e 56)

[82] R Vieira, C Gastaldini, R Azzolin, and H Grundling. Sensorless sliding mode rotor speed observer of induction machines based on magnetizing current estimation. *Industrial Electronics, IEEE Transactions on*, In Press. (Quoted on page 81)

[83] V.I.Utkin. Variable structure systems with sliding modes. *"IEEE Trans. Automat. Contr., Survey paper"*, "AC-22 no.2":212–222, "06 jan 2003". (Quoted on pages 29 e 30)

[84] D.A. Wismer and R. Chattergy. *Introduction to NonLinear Optimization*. New York: North Holland, 1978. (Quoted on page 25)

[85] W.Leonhard. *Control of Electrical Drives*. Springer-Verlag, 1985.

[86] Y.A.Chapuis and D.Roye. Direct torque control and current limitation method in startup of an induction machine. *in Proc. IEEE Conf. Power Electronics and Variable Speed Drives*, pages 451–455, "sept. 1998".

[87] Zhang Yan, Changxi Jin, and V. Utkin. Sensorless sliding-mode control of induction motors. 47(6):1286 – 1297, dec 2000. (Quoted on page 81)